Fibre Interferometry for Differential Measurements

Martin Dignan Smith

A dissertation submitted for the degree of Doctor of Philosophy

Heriot-Watt University

School of Engineering and Physical Sciences

October 2015

Abstract

This thesis investigates the use of interferometry as an interrogation technology for the measurement of differential length at two widely separate locations. Differential length measurements are essential and can have many applications in industrial processes, therefore accurate measurements can be a critical. Such differential length measurements can be applied to aspects of differential pressure. Using an all optical fibre approach, the research utilises the effects of light interference for both low coherent and high coherent light sources for the determination of a differential length between individual sensing cavities separated by up to 10's of meters.

The construction of the differential length interrogation system makes use of two Fabry-Perot cavities arranged in a tandem configuration, as a means of determining the differential length between them. Such an arrangement provides a common path through which an optical broadband light source at a central wavelength of 1550 nm can propagate. As a consequence of this configuration, differential lengths are made simply using one single measurement, removing the need to determine each individual length. An additional benefit of this common optical path prevents environmental factors such as temperature and air pressures from affecting the measurement length in question.

Using a scanning reference Michelson interferometer to induce an optical path change, low coherence interference effects are present when the optical path length of the differential Fabry-Perot cavities is equal to the optical path length difference in the Michelson interferometer. Using a separate DFB laser light source to illuminate the reference interferometer high coherence interference fringes, present when the optical path length of one interferometer arm is changing due to a piezo fibre stretcher, can be analysed to provide an accurate length determination. Taking into consideration the noise within the system the interrogation technique has a length measurement resolution of 27.43 nm. Demonstrations show that a differential length of 82.539 µm could be measured with an uncertainty of 41.00 nm.

Through the characterisation of a deformable silicon diaphragm, it would be possible to construct a sensing system capable of measuring a differential pressure of 1 Pa in 100 kPa. This however would require a 9.13 mm thick diaphragm, with a radius of

0.35 m. Such a diaphragm would be out of the question and so further investigation into reducing the length measurement resolution would need to be carried out.

For my mum

In memory of my dad

Acknowledgements

Firstly I would like to thank my primary supervisor Dr Robert Maier for guiding me with patience and expertise throughout the duration of my PhD. I am forever grateful for him for giving me the opportunity to carry out the work described in this thesis and for the encouragement he has shown me.

I would also like to thank my second supervisor Dr William MacPherson for training me in all aspects of this project. Without his guidance and support I would not have achieved most of the results detailed in this thesis.

I would like to thank Dr Richard Carter for his assistance in the lab and for the numerous times he has help solve errors within Labview. My thanks go to all the other members of the applied optics and photonics group both past and present for insightful discussions and support throughout the duration of my studies.

Special thanks go to my office companions Wojciech Gora, Dr Frank Albri and Dr Jun Li for their insightful conversations and encouragements throughout my PhD duration. Particular thanks go to Wojciech not only for his help in MatLab, but for our numerous football conversations providing a nice distraction now and again.

I am also grateful to my friends, in particular Dr Ashleigh Barron whom I am fortunate to have had the support of throughout my entire university career.

Thanks goes out to my fiancée Louise Wanstall for her continued support throughout the final years of my PhD and for picking me up when times were bad.

More than a thank you is owed to my family, in particular my parents Kim and Andrew for encouragement and support throughout not only my PhD but in every aspect of my life. I wouldn't be where I am today without them. Thanks also to my sister Emma, brother-in-law Bryan, and the newest member of our family, my wee nephew Mark. I couldn't have done this without you all.

ACADEMIC REGISTRY
Research Thesis Submission

Name*:*	Martin Dignan Smith		
School/PGI:	School of Engineering and Physical Sciences / IPAQS		
Version: *(i.e. First, Resubmission, Final)*	Final	Degree Sought (Award **and** Subject area)	Ph.D Physics

Declaration

In accordance with the appropriate regulations I hereby submit my thesis and I declare that:

1) the thesis embodies the results of my own work and has been composed by myself
2) where appropriate, I have made acknowledgement of the work of others and have made reference to work carried out in collaboration with other persons
3) the thesis is the correct version of the thesis for submission and is the same version as any electronic versions submitted*.
4) my thesis for the award referred to, deposited in the Heriot-Watt University Library, should be made available for loan or photocopying and be available via the Institutional Repository, subject to such conditions as the Librarian may require
5) I understand that as a student of the University I am required to abide by the Regulations of the University and to conform to its discipline.

* *Please note that it is the responsibility of the candidate to ensure that the correct version of the thesis is submitted.*

Signature of Candidate*:*		Date:	

Submission

Submitted By *(name in capitals):*	MARTIN DIGNAN SMITH
Signature of Individual Submitting:	
Date Submitted:	

For Completion in the Student Service Centre (SSC)

Received in the SSC by *(name in capitals):*			
Method of Submission *(Handed in to SSC; posted through internal/external mail):*			
*E-thesis Submitted (**mandatory for final theses)***			
Signature:		Date:	

Contents

List of Tables

List of Figures

List of Abbreviations

OPL	Optical Path Length
DFB	Distributed Feed-Back
LVDT	Linear Variable Differential Transformer
NA	Numerical Aperture
FBG	Fibre Bragg Grating
UV	Ultra Violet
FSR	Free Spectral Range
FFT	Fast Fourier Transform
HeNe	Helium Neon
LED	Light Emitting Diode
SLED	Super Luminescent Diode
FWHM	Full Width Half Maximum
InGaAs	Indium Gallium Arsenide
ASE	Amplified Spontaneous Emission
OSA	Optical Spectrum Analyser
GRIN	Gradient Index
HCN	Hydrogen Cyanide
RC	Resistor-Capacitor
CWT	Continuous Wavelet Transform
DWT	Discrete Wavelet Transform

List of Publications

Conference contributions

M. D. Smith, W. N. MacPherson and R. R. J. Maier, "Differential length measurement using low coherence coupled tandem interferometry," Proc. SPIE 8774, *Optical Sensors 2013*, Prague, Czech Republic (2013).

M. D. Smith, W. N. MacPherson and R. R. J. Maier, "Low coherence tandem interferometry for the measurement of differential length sensing at two widely separated locations," Proc. SPIE 8924, *Fourth Asia Pacific Optical Sensors Conference*, Wuhan, China (2013).

Chapter 1: Introduction

1.1. Motivation

Pressure comes in all shapes and forms, from the pressure of writing a Ph.D thesis, to the hot water pressure from your shower in the morning. In most industrial applications of pressure measurement, accuracy is a key factor. In some cases more than others, measurement resolutions of 1 in 100,000 can be pivotal.

Differential pressure measurements are essential in a wide range of industrial processes. The main goal of this research is for the development of an interrogation technology through which the differential length of two individual sensing cavities can be measured and thus used for the determination of a differential pressure. The problem of measuring the differential pressure of two separate locations, at distances up to 10's of meters apart, is an issue which can exist within a complex pipe work series.

Being able to measure differential pressure with an absolute pressure in the order of 100 kPa and a requirement for a differential pressure resolution in the order of 1 Pa, remains a challenge for existing sensors. Currently such measurements are carried out by using long liquid or gas filled pipes, bringing the pressures to a single differential pressure gauge which has a sufficiently large dynamic range and resolution. Unfortunately this approach does not achieve the required finesse because of the pressure gradients and other practical complications that can exist within the piped connection.

It is for this reason that this thesis presents an all optical fibre approach of determining the differential length of two independent sensors, which could be applied to applications of pressure measurements. The configuration will be such that the interconnecting fibre optic leads are a passive element in the application and insensitive to the surrounding area, even when separated by the distances previously mentioned. The use of fibre optics also has advantages over free space optics such as flexibility, integration and compact nature.

1.2. Differential Length Measurement Application

A possible application in which the measurement of differential length can be utilised is in the determination of differential pressure and flow rate measurements. Pipe work, for the delivery of liquid, can have many bends, turns, and interior obstacles which may affect the liquid flow, especially over long lengths. Being able to measure the change in flow from one position to another would help in the structuring of the pipe work in order to optimise the arrangement and maintain a healthy and steady flow. Figure 1.1 shows a typical pipe system and the change in pressure which may result due to a restriction in the form of a valve, extended or narrowed pipe, or multiple bends.

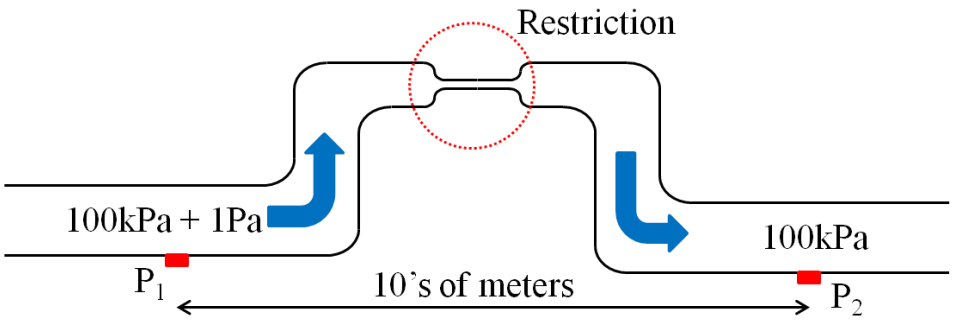

Figure 1.1: Schematic of a typical pipe work system showing the change in pressure due to restrictions which occur within the flow.

There are currently a number of conventional methods which are commercially available for pressure measurement. In some practical systems in which a measurement resolution of 1 Pa is desirable, against large background pressures up to 100 kPa, with temperature variations up to 130 °C, differential sensors capable of reading within the desired pressure range have their limitations in the form of accuracy (typically 2%). In Chapter 2 a more detailed analysis of current conventional methods and their limitations will be given however a few examples will be briefly discussed below.

Pressure measurements are capable of being made via a variety of electrical methods, including piezoresistive and capacitive sensors, which will be discussed more detailed in Chapter 2. Other techniques include the use of manometers. Electronic differential manometers are commercially available (1) however in most cases the resolution (0.05%) is inadequate. These devices also require additional interconnecting tubes to

carry the liquid to the manometer device for measurement which may contain bends and twists as it leads from the measurement area to the manometer. These bends, along with environmental factors such as temperature changes, may result in pressure changes along the tubes, and could therefore alter the measurement of interest. It may also be a requirement for measurements of liquid pressure, due to the occurrence of air bubbles, to bleed the interconnecting tubes to avoid inaccuracies of the measured pressure.

It is possible to measure flow directly within the pipe using devices such as an ultrasonic flow meter (2) or an impeller flow meter (3). An ultrasonic flow meter monitors the average velocity of a fluid, using ultrasonic transducers, by averaging the difference in measured transit time between the pulses of ultrasound propagating into and against the direction of the flow. These flow meters however can be affected by changes in the fluid temperature, density, and viscosity, and can even be affected by suspended particles within the fluid. An impeller flow meter probe is equipped with lightweight helical impellers mounted on double sapphire bearings. The impellers contain magnets which actuate Hall-effect switches within the probe to detect impeller rotation. The main shortcoming of impeller-type flow meters is the lack of sensitivity to low-velocity flow and the need to be inserted into the path of the liquid. This would most likely have an influence of the flow rate due to the obstruction it would create.

It is partially for these reasons that the desired interrogation system be an optical fibre sensing configuration, utilising the effects of interferometry. Such an interrogation system would be small in size allowing for multiple measurement position to be placed within close proximity to one another and also allow for data analysis to be carried out at far locations away from the measurement position. Fibre optic sensors are primarily immune to electromagnetic radiation due to the dielectric nature of the fibre making them prime candidates for the use in noisy electromagnetic environments where conventional electric sensors may not be possible. Further details regarding fibre optics and the sensing techniques that can be implemented will be given in the remainder of this chapter with a more in depth analysis given in Chapter 2.

1.3. Interferometry

Interferometry utilises the wave nature of electromagnetic radiation making use of the principle of superposition to combine waves. The resultant wave combination therefore

has a meaningful property that is a diagnostic of the original state of the waves. This works because when two waves of identical frequency (or wavelength) combine, the resulting pattern is determined by the phase difference between the two waves. As illustrated in Figure 1.2, waves that are in phase will undergo constructive interference while waves that are out of phase will undergo destructive interference. For the two waves to interfere and produce a stable pattern as illustrated, they must have the same frequency. A more complete analysis of interferometry is provided in Chapter 3.

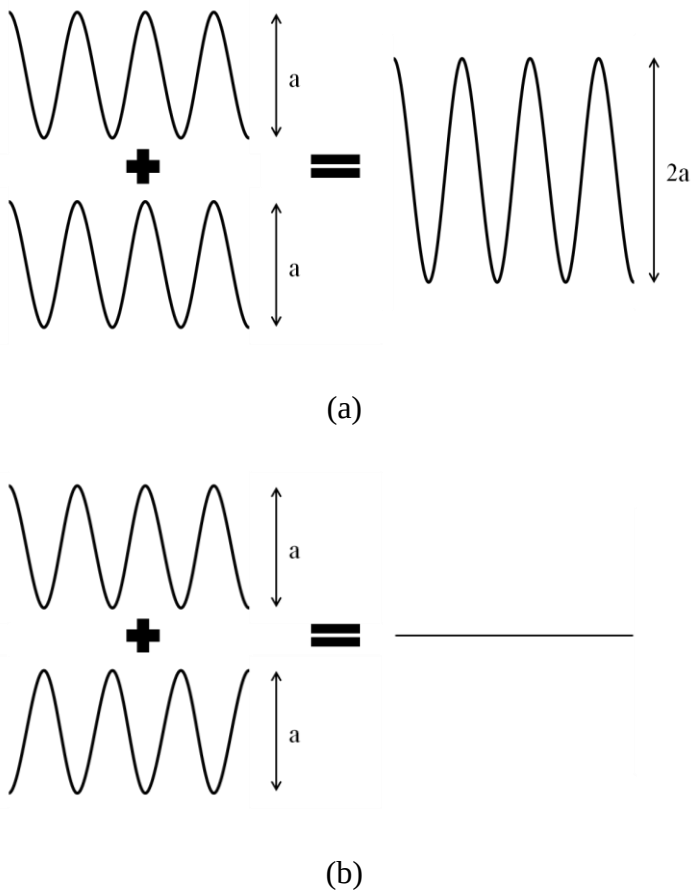

Figure 1.2: Superposition of waves showing (a) constructive and (b) destructive interference effects.

If the sources are both "white light" or broadband sources however, the corresponding wavelengths of each source will interfere and the overlapping monochromatic patterns will produce a white light interference pattern. If a white light source is used in a two beam interferometer such as a Michelson interferometer, details of which will be provided in Chapter 2, when the optical path length (OPL) difference of the two

interferometer paths is within the coherence length of the source, an interference pattern, illustrated in Figure 1.3, is observed. It is within this region that the light waves superimpose coherently.

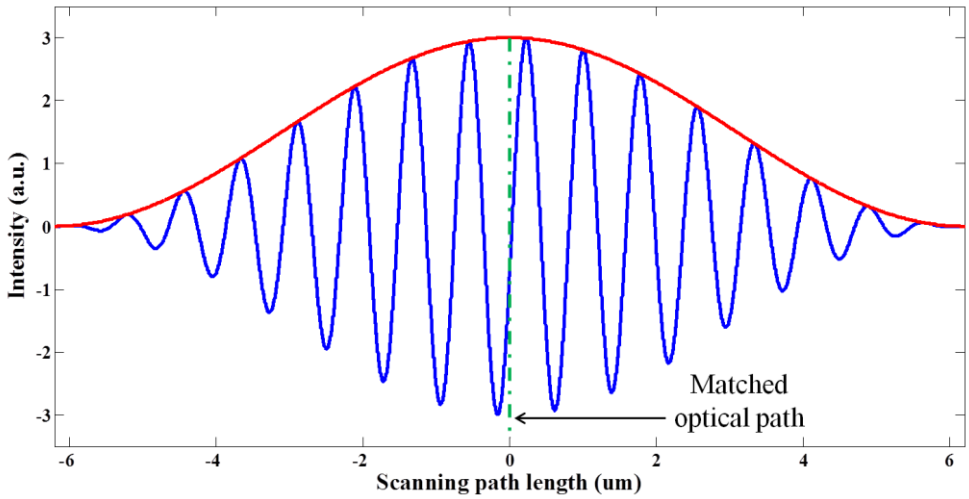

Figure 1.3: White light interferogram generated as a result of a matched optical path length (OPL) of two interferometer paths within the coherence length of the light source. This image was modelled using a broadband light source centred at 1550 nm with a spectral width of 263.93 nm.

It is possible to define the absolute length of an optical path through scanning of the other optical path because interference fringes are only observed when the path lengths match.

Interferometry making use of light or some other form of electromagnetic wave has become one of the most widely used techniques of distance measurement following pioneering experiments to determine the speed of light in 1881 by Michelson (4). Optical systems that make use of interferometry as a means of measuring the change in interference of two light beams, where one beam has been perturbed by the measurand, are known as interferometers. The most commonly known and used interferometers are the Michelson (5), Mach-Zender (6), Sagnac (7), and Fabry-Perot (8). A detailed illustration and description of each interferometer arrangement will be provided in Chapter 2. More advanced interferometric systems are based on tandem interferometry using broadband, or low coherent, light sources, in which length measurements are

made when compared to a second ‘reference’ distance of known length. Further details on how these interferometric systems operate and how they are used in sensing techniques will be discussed in Chapter 2. Interferometers have been extensively used for precision metrology as changes in the OPL difference or phase of the interferometer can be measured to within a fraction of the wavelength of light. It should be noted that the accuracy is related to the accuracy and stability of the source wavelength.

1.4. Fibre Optic Sensors

Fibre optic sensors have become a solution for the monitoring of environmental parameters such as strain (9), temperature (10) and pressure (11) due to the numerous advantages they hold over conventional sensors. The overall size of fibre optics allows for the development of small, lightweight sensors which can have numerous applications in industry. The advantage of some form of fibre optic sensors ability to be multiplexed on a large scale along a single fibre also helps in keeping the size and weight to a minimum (12). As mentioned in section 1.2, a further advantage of fibre optic sensors is their immunity to electromagnetic radiation. They can also be used in potentially dangerous environments such as flammable or explosive environments (13) as they are intrinsically safe due to their electromagnetic passivity, and can be integrated into composite materials to form smart structures (14).

Material properties of optical fibres are a key element in their advantages over conventional sensors. Standard communications fibre (Corning SMF-28) (15) is the most widely used single mode optical fibre and is commonly used at wavelengths in the 1310 nm to 1550 nm regions. This fibre exhibits low attenuation within these wavelength ranges, typically <0.35 dB/km at 1310 nm and <0.22 dB/km at 1550 nm, and is therefore capable of transferring data from the sensing region to the interrogation system for use in remote operations without the loss of vital information over distances up to 30 km (16). The material strength of an optical fibre is high, in particular the tensile strength; however this strength is reduced with the formation of cracks along on surface which could form when the fibre is under tension. Use of a protective coating on the fibre is a means of preventing these surface cracks, and maintaining the long term stability of the fibre.

Optical fibre sensors have been extensively researched for use in numerous industrial applications as replacements for conventional sensors. The fibre gyroscope (17), for precise rotational measurement due to cross axis insensitivity to vibration and shock, has become an established and widely used fibre sensor serving a particular use in inertial navigation. With no moving parts, as are found in the mechanical spinning mass gyroscope, the fibre optic alternative doesn't rely on inertial resistance to movement making it a more stable and reliable solution. Further established fibre sensors include the optical fibre hydrophone for measuring under water acoustic signals (18) which takes advantage of the multiplexing feature of optical fibre sensors by integrating over one hundred sensors per fibre cable, and sensors for medical uses, including imagery, illumination, and light beam delivery (19). Despite the many advantages that fibre optic sensors have, they have not been extensively commercialised due to the developed and established technological competition of conventional sensors. A successful fibre optic sensor must offer advantages that cannot be achieved with a conventional sensor.

1.5. Differential Length Measurement

Optical fibre sensors can be constructed in such a way as to measure one parameter, through which a second parameter can be determined. For example a pressure sensor based upon a flexible diaphragm can provide a measure of pressure via a measure of diaphragm deflection. In the case of this research differential pressure measurements between two separate locations will be determined with the use of a differential length measurement interrogation system. This can be achieved using independent Fabry-Perot sensing cavities constructed such that the reflective surface of the cavity end face will be in the form of a deformable diaphragm. When an external pressure is exerted on this diaphragm deformation will result in a change in the cavity length. Knowing the characteristics of this deformable diaphragm, the applied pressure can be determined through measurement of the change in the differential length being calculated due to the change in the diaphragm central deflection.

This thesis outlines the approach and techniques used in achieving the goal of measuring differential length, with applications in the use of pressure measurements. The differential length will be between two widely separated independent Fabry-Perot cavities formed using a cleaved fibre optic end and a reflective surface.

In order to make differential length measurements between the two independent Fabry-Perot sensing cavities, these will be arranged in a tandem configuration. Although the interconnecting fibre leads between the sensing cavities may experience environmental factors such as temperature and pressure changes, using such an arrangement, these factors should not influence the measurement signal and desired outcome. The Fabry-Perot cavities are in turn connected to a scanning, reference Michelson interferometer, used as a calibration tool for length measurements. This provides an all fibre optic configuration, making use of both low and high coherence interferometry techniques as will be shown in Chapter 4.

The technique uses an OPL difference scan, passing through zero OPL difference in order to recover the interferogram, similar to that shown in Figure 1.3. One method to allow such a scan whilst keeping an all optical fibre arrangement would be to use a piezo electric cylinder, calibrated using a distributed feed-back (DFB) laser. Problems such as birefringence and polarisation mode dispersion introduced using such a method will be discussed in Chapters 2 and 5. Techniques such as the Hilbert transform, peak detection, and fringe counting are employed as a means of determining the desired length.

1.6. Thesis layout

Chapter 2 of this thesis reviews conventional and electrical sensing techniques for making differential length and pressure measurements, and why these particular components would not be a viable solution to the overall goal. There is also an overview of the fundamentals of fibre optics and how their properties have made them ideal candidates for sensing. The different fibres available are discussed, and the formations of birefringence in optical fibres and why it is important to consider this. Optical measurement techniques are also considered, forming the foundation of why the particular technique was chosen, and also examples of some current fibre sensors are shown.

Chapter 3 investigates the theory behind the Michelson interferometer and how this simple, yet important, configuration can be used in optical metrology. Chapter 3 continues by looking at Fabry-Perot cavities and the theory of extrinsic cavities formed between the fibre end and an external reflective surface. Investigations into the

reflectivity and transitivity of the cavity boundaries reveal how the cavity visibility can be altered and how this affects the optical transfer function. The theory of interference for both high and low coherent light sources is considered in this chapter, as both sources are considered for use in this project. The Hilbert transform is investigated as well as how this technique can be used as a means of obtaining the envelope of a particular wave packet.

With the interrogation technique of differential length measurement having an application in the measurement of pressure, the theory behind deformable diaphragms, which could possibly be used as the reflective surfaces of the Fabry-Perot sensing cavities, is also discussed in Chapter 3.

The individual aspects of the interrogation scheme used for making differential measurements is considered in Chapter 4, as is the implementation of the interrogation scheme as a whole. The methods used in devising the individual components and sub sections of the working system is discussed and why those particular methods over alternative techniques were chosen and the advantages of doing so.

Chapter 5 includes analysis and performance of the optical components and light sources used and the details of the selection choice. Noise within the system is discussed and how this has an effect on the experimental arrangement and on the measurement accuracy. The effect of a changing temperature on the interconnecting fibre leads between the sensing heads is considered and its effect, if any, on the measurements.

Chapter 6 describes the possible sensing configuration of a diaphragm based pressure sensor for use in the developed differential length measurement system. Diaphragm fabrication and material choice are discussed in order to optimise the sensing configuration.

Finally, in Chapter 7, a brief summary of the thesis is provided along with the conclusions based on the research carried out. Future work is also suggested in this chapter.

1.7. References

1. Omega Engineering inc. Manometers www.omega.co.uk2003-2015. Available from: http://www.omega.com/subsection/manometers.html.
2. Omega Engineering inc. Introduction to Ultrasonic Doppler Flowmeters 2003-2015. Available from: http://www.omega.com/prodinfo/ultrasonicflowmeters.html.
3. Robertson Geologging Ltd, Impeller Flowmeter 1979-2015. Available from: http://www.geologging.com/slimhole-logging/impeller-flowmeter/.
4. Michelson AA. The relative motion of the Earth and the Luminiferous ether. American Journal of Science. 1881;22:120-9.
5. Yuan L, Yang J, Zhou L, Jin W, Ding X. Low-coherence Michelson interferometric fiber-optic multiplexed strain sensor array: a minimum configuration. Applied Optics. 2004;43(16):3211-6.
6. Yu Y, Jiang L, Wang S, Yang J, Li B, editors. Strain-insensitive optical fiber Mach-Zehnder interferometric temperature sensor. International Conference on Optical Instruments and Technology: Optical Sensors and Applications; 2011.
7. Fu HY, Tam HY, Shao L-Y, Dong X, Wai PKA, Lu C, et al. Pressure sensor realized with polarization-maintaining photonic crystal fiber-based Sagnac interferometer. Applied Optics. 2008;47(15):2835-9.
8. Chen J, Zhao J, Huang X, Huang Z. Extrinsic fiber-optic Fabry-Perot interferometer sensor for refractive index measurement of optical glass. Applied Optics. 2010:5592-6.
9. Yuan L, Ansari F. White-light interferometric fiber-optic distributed strain-sensing system. Sensors and Actuators A-Physical. 1997;63(3):177-81.
10. Lebid SY, Fitio VM, Bobitski YV, Wiecek T, editors. Fiber-optic temperature sensor1999.
11. Gander MJ, MacPherson WN, Barton JS, Reuben RL, Jones JDC, Stevens R, et al. Embedded micromachined fiber-optic Fabry-Perot pressure sensors in aerodynamics applications. IEEE Sensors Journal. 2003:102-7.
12. Kersey AD, Berkoff TA, Morey WW. Multiplexed fiber Bragg grating strain-sensor system with a fiber Fabry-Perot wavelength filter. Optics Letters. 1993;18(16):1370-2.
13. MacPherson WN, Gander MJ, Barton JS, Jones JDC, Owen CL, Watson AJ, et al. Blast-pressure measurement with a high-bandwidth fibre optic pressure sensor. Measurement Science and Technology. 2000;11(2):95.
14. Udd E. Fiber optic smart structures. Proceedings of the IEEE. 1996;84(1):60-7.
15. Corning inc. SMF 28e Optical Fiber Product Information. In: Incorporated C, editor. 2002.
16. Matsumoto H, Hirai A, editors. Remote Measurements of Lengths by Excess-Fraction Method Using Optical Fiber Networks and Tandem Interferometer. Optical Fiber Communication Conference and National Fiber Optic Engineers Conference; 2009 2009/03/22; San Diego, California: Optical Society of America.
17. Lefevre HC, editor Fundamentals of the interferometric fiber optic gyroscope1996.
18. Cranch GA, Nash PJ, Kirkendall CK. Large-scale remotely interrogated arrays of fiber-optic interferometric sensors for underwater acoustic applications. Sensors Journal, IEEE. 2003;3(1):19-30.
19. Tearney GJ, Brezinski ME, Bouma BE, Boppart SA, Pitris C, Southern JF, et al. In Vivo Endoscopic Optical Biopsy with Optical Coherence Tomography. Science. 1997;276(5321):2037-9.

Chapter 2: Review

2.1. Introduction

As stated in Chapter 1, this research focuses on the development of an interrogation technology for measuring the differential pressure between two independent and potentially widely separated sensing cavities. Such a measurement will be determined in terms of the differential length measurement of the two Fabry-Perot cavities. The main purpose of this chapter is to first review conventional state-of-the-art measurement systems capable of providing pressure and length measurements, and secondly to provide an introduction and review on optical fibres as an alternative and how they can be integrated as sensors to measure such parameters. Optical fibre interferometric sensors will be reviewed in a more detailed manner as this is the approach the research will focus on, however other fibre optic sensor techniques such as intensity and polarisation based sensors will be discussed, as well as the use of Fibre Bragg Gratings. A more complex interferometric system in the form of a tandem configuration will be reviewed, as will the effects of birefringence within optical fibres when used in an interferometric system.

2.2. Introduction to Pressure

Pressure is the ratio of force to the area over which that force is distributed. Measurements of pressure can be carried out in two forms: absolute, measuring one individual pressure; and differential, the difference between two or more separate pressures. A pressure gauge is commonly used to describe an instrument used for measuring pressure. Commonly used pressure gauges include the manometer (1), a liquid filled tube in a U-shape form, which when exposed to pressure from one end will result in the rise or fall of the internal fluid. Measures of the change in liquid can determine the external pressure applied.

Other measures of determining the extent of a pressure force include the monitoring of material properties. When this force is exerted upon a material surface, deformation of that surface may arise due to the material properties and design. Such techniques for pressure sensing include the use of Bourdon tubes (2), bellows (3), and diaphragms (4).

Diaphragms are of particular interest in the use for pressure measurements due to the flexibility of the design parameters and the possibility of mounting electrical components on the surface.

In the context of many optical fibre sensors, diaphragm based pressure sensors are based on an extrinsic Fabry-Perot interferometer, as illustrated in Figure 2.1. The interferometer cavity is formed between the reflective surface of the deformable metallic diaphragm and the Fresnel reflection from the cleaved fibre end used to carry light to and from the cavity. A further explanation of the measurement capabilities of such an arrangement and the deformation properties of a diaphragm will be covered in the remainder of this chapter and in Chapter 3.

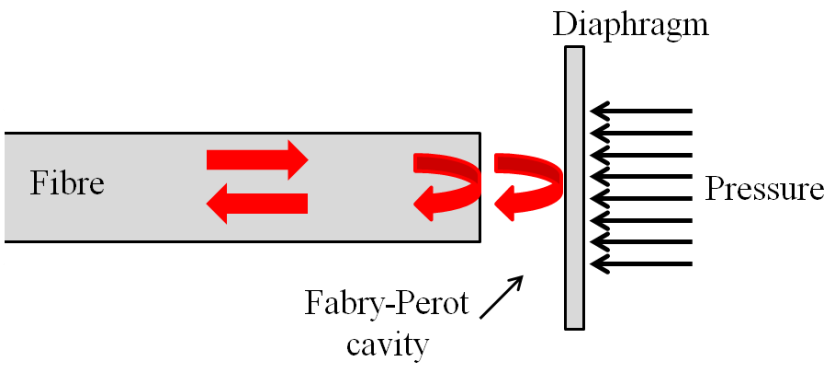

Figure 2.1: Diaphragm Fabry-Perot pressure sensing cavity.

The optical path length of the Fabry-Perot cavity is measureable through the Free Spectral Range (FSR) technique, more details of which will be provided in section 2.5.5. Changes in the optical path length of the cavity due to deflections in the diaphragm can be monitored, thus through knowledge of the diaphragm properties or when calibrated against a standard diaphragm, the applied pressure which induces deformation can be calculated.

2.3. Conventional Sensing Techniques

There exist many suitable techniques for the measurement of length or pressure. In the case of this work, measurements will be based on differential length or pressure.

Generally, pressure measurements are made by measuring the force that is applied to a known area. Alternatively, measurements can be made by determining the effect that a pressure may have on a sensing element in terms of the stress or strain applied to this particular element. This is then used to determine the actual pressure and is the general principle which many electrical sensors adopt.

The most commonly used electrical pressure sensor makes use of piezoresistive materials as the sensing element. Piezoresistive materials provide a way to convert an applied strain to an electrical signal. Embedding a piezoresistive material onto a sensing element, for example a deformable diaphragm, allows for stress changes to be monitored when deformation of the diaphragm occurs. Strain in the diaphragm results in a change in the material resistance which can be electronically measured. Typically the piezoresistive material is used as one of the arms of a Wheatstone bridge circuit, illustrated in Figure 2.2, as a means of measuring applied strain.

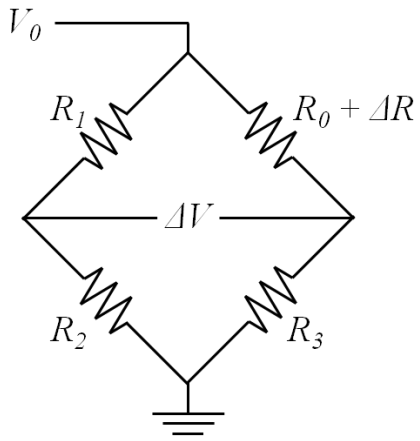

Figure 2.2: Wheatstone bridge construction.

Through changes in the output voltage ΔV, as a result of the changing resistance ΔR, the mechanical stress of the diaphragm can be determined. This fabrication is based on standard semiconductor processing techniques. Packaged transducers or unpackaged semiconductor chips are available commercially.

Differential pressure sensors can be manufactured which cover large pressure ranges with high measurement accuracy, over a wide temperature range. For example Honeywell (5) have developed a series of differential pressure sensors with

measurement accuracy ranging from 0.1% to 0.2%, with a maximum operating pressure from 3.4 kPa to 68.9 MPa. These sensors operate on the above mentioned piezoresistive effect. Figure 2.3 shows typical examples of such sensors.

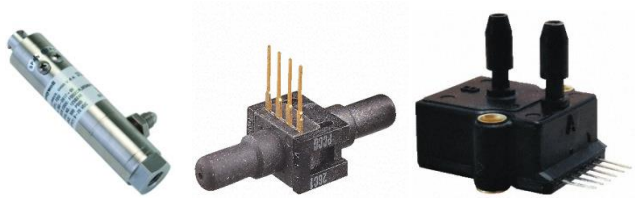

Figure 2.3: Honeywell series of differential pressure sensors (5)

An alternative electrical sensor, this time based upon parallel plate capacitors, is a capacitive sensor. These sensors primarily use a deformable diaphragm for pressure detection where the sensing element is a pair of parallel plates to form the capacitor. In most cases the deformable diaphragm is one of the capacitive plates. Upon contact with pressure, this plate will flex, whilst the other plate, attached with a rigid seal to a ceramic substrate, remains insensitive to pressure. As the pressure changes and the diaphragm flexes, the spacing between the capacitor plates changes, resulting in the measurement of the applied pressure. This design produces a highly reliable and stable variable capacitance.

Mechanical methods are also commercially available for the measurement of length and displacement. One method of measuring the displacement at a particular position would be with the use of a linear variable differential transformer (LVDT). An LVDT is a linear displacement electro-mechanical transducer used for providing robust, accurate, and repeatable results. One form of LVDT consists of a primary and two secondary coils, with a central magnetic core, illustrated in Figure 2.4. This operates by generating an electrical output which is proportional to the core's displacement.

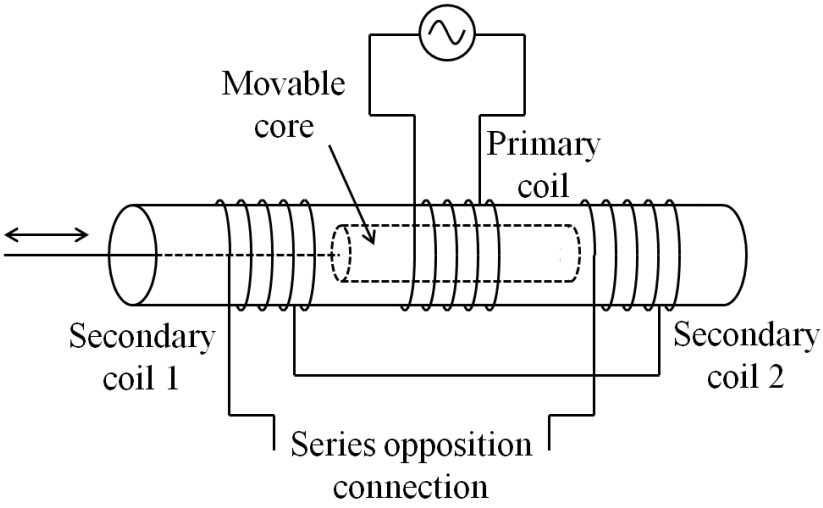

Figure 2.4: Internal structure of a typical LVDT.

The primary coil provides excitation whilst the secondary coils provide the output signal, with the current transfer between the primary and secondary being controlled via the magnetic core position. At the central position the secondary coil voltages are equal and the transducer provides a zero output. When the core moves away from the central position the voltage of one of the secondary coils will increase whilst the voltage of the other will decrease, resulting in a displacement measurement dependant on the direction of travel. The resolution and accuracy of these devices is limited by the accuracy and precision of the coils used.

An alternative approach to LVDT's for linear positioning is the use of optical encoders. Optical encoders use a variety of devices, all of which use light as a means of transforming motion into an electrical signal. The two main components of an optical encoder are the main grating and the detection system, the positions of which, of one with respect to the other, are detected. For performing linear measurements, the main grating, which represents the measurement standard, is one or more sets of parallel lines of constant or specially coded pitch. Optical encoders are used in instrumentation ranging from digital callipers to semiconductor steppers.

Highly developed electrical sensors are commercially available for the measurement of pressure and displacement. These particular sensors do unfortunately have some disadvantages in the application area investigated in this research. The most significant disadvantage of conventional sensors is the dimensions of some sensing areas, which may not permit measurements within close proximity of the measurement position.

This in turn relates to the aforementioned interconnecting pipes used in pressure measurements to carry liquid to a sensor head. These pipes could come under environmental effects such as temperature and air pressure and therefore result in inaccurate measurement results. Fibre optics sensors have demonstrated the potential to overcome these issues and have become commercially available products (6), however such sensors unfortunately do not provide the resolution required to achieve the goals of this research and so alternative approaches must be considered.

2.4. Optical Fibre

Conventional optical fibres are typically a cylindrical waveguide as illustrated in Figure 2.5. The fibre consists of a thin core with a refractive index n_{core} (typically 1.468 for SMF-28), surrounded by a cladding layer with a refractive index, $n_{cladding}$, 0.36% lower than that of the core. Telecommunications has become the major use of optical fibres with development focussing on the transmission of light in the wavelength regions of 1310 nm and 1550 nm. These chosen wavelengths lie in regions of low attenuation and/or dispersion allowing the signal to travel a longer distance without loss/distortion.

2.4.1. Fibre modes and light propagation

The basic types of optical fibres include single mode step index fibre and multi mode step index fibre, the cross section and refractive index profile of such fibres is shown in Figure 2.5. For low loss fibres, the core and cladding layers are generally manufactured from fused silica. To achieve the higher refractive index in the fibre core, in order for the light to propagate through, this is usually doped using germanium. An alternative to doping of the core to achieve a higher refractive index would be to dope the cladding layer as a means to reduce the refractive index. To maintain most of the light energy within the core, the cladding layer must have a minimum thickness of one or two wavelengths of the transmitted light. A protective plastic buffer material is usually used to surround the cladding layer as a method of preventing surface scratches which may degrade the mechanical strength of the fibre and hence reduce reliability.

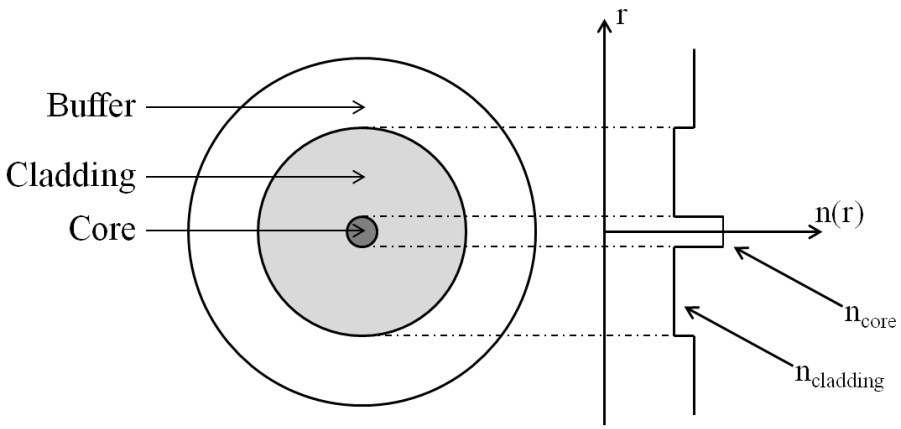

Figure 2.5: Optical fibre showing step index profile.

Optical fibres propagate light through the fibre core via total internal reflection. Snell's Law (7) describes the relationship between the angle of the incident light at the boundary of the core and cladding layers and refraction. Total internal reflection occurs when the light approaches the core-cladding interface at an angle greater than the critical angle, θ_c, given by:

$$\theta_c = \sin^{-1}\left(\frac{n_{cladding}}{n_{core}}\right) \tag{2.1}$$

It is therefore the case that any ray incident on the waveguide boundary at an angle equal to or greater than θ_c will experience total internal reflection, as illustrated in Figure 2.6, however for angles less than θ_c there will be a partial reflection back into the waveguide with a reflectivity predicted by the Fresnel equation (8).

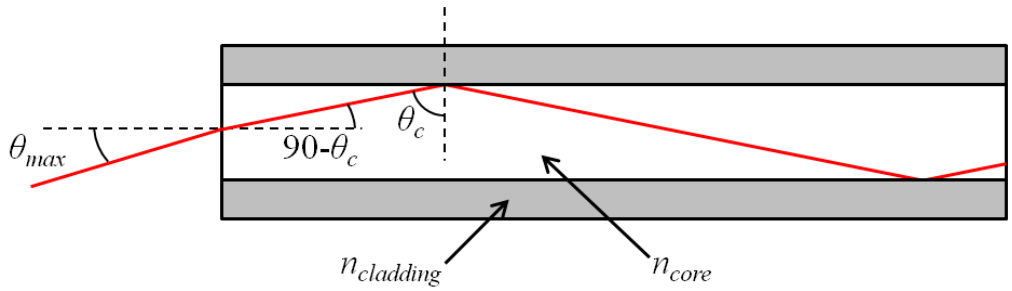

Figure 2.6: Optical fibre showing propagation through total internal reflection due to the incident ray angle being equal to or greater than the critical angle, θ_c. The incident ray is equal to or less than the angle of acceptance, θ_{max}, which gives rise to the numerical aperture of the fibre.

The path that a light ray will propagate through a fibre is dictated by the angle at which it enters the fibre. Figure 2.6 shows the maximum acceptance angle for a ray to propagate, giving rise to the dimensionless parameter of an optical fibre, the numerical aperture (NA), defined as

$$NA = \sqrt{n_{core}^{\ 2} - n_{cladding}^{\ 2}} \tag{2.2}$$

NA is defined as the sine of the angle of acceptance of the fibre and relates to the critical angle of the fibre through Snell's Law

$$NA = n_{air} \sin\theta_{\max} = n_{core} \sin(90 - \theta_c) = n_{core} \cos\theta_c \tag{2.3}$$

The greater the NA of an optical fibre the greater will be the amount of light accepted by the fibre (9).

In multi mode fibres there exists a fibre mode which passes straight through the core of the fibre, known as the m=0 mode. This mode in reality does not pass straight through the fibre, but has the smallest possible allowed angle for a given wavelength, and is the only mode supported by the single mode step index fibre. Single mode fibre is a special case of step index fibre where a small core size is fabricated and the difference in the

core and cladding refractive indexes is minimal such that only a single mode of light energy can propagate through the fibre.

Modal dispersion occurs in multi mode fibres due to rays following different paths through the fibre and consequently arriving at the fibre end at different times (10). Since light reflects at the core-cladding boundary at different angles for different modes, the path lengths of different modes are different, thus different rays take a shorter or longer time to travel the length of the fibre. Although with the use of a single mode fibre modal dispersion is eliminated, chromatic dispersion is still an issue limiting the modulation bandwidth. Chromatic dispersion results due to the effect of the refractive index of the fibre core causing different wavelengths to propagate at different velocities. Since chromatic dispersion is a function of the spectral width of the light source, narrow spectral widths are desirable for high-speed communication systems which transmit data through fibre optics with the use of a monochromatic laser source of a single wavelength. The single mode path reduces scattering and absorption of light throughout the fibre, making single mode fibre the highest speed and lowest loss fibre type, suitable for communications and sensing applications.

The propagation of light through a single mode step index fibre cannot be described via simple total internal reflection. Electromagnetic wave theory, based upon Maxwell's equations (11), provides a detailed description of single mode light propagation, and has been previously covered in texts (12-14).

For a cylindrical fibre, the assumed solution of the wave equation, for the electric field, is given by (15)

$$E = E_0(r,\phi)\exp(i\beta z) \tag{2.4}$$

Where β is the propagation constant, or phase shift per unit length, of a sinusoidal wave measured along the z axis.

An important parameter used in defining the number of modes supported by a fibre is the V-number, given by the following equation.

$$V^2 = U^2 + W^2 = \frac{2\pi a}{\lambda}\sqrt{n_{core}^2 + n_{cladding}^2} \tag{2.5}$$

For large values of *V*, the approximate number of supported modes is equal to $V^2/2$. The conditions for single mode operation are when the value of *V* is < 2.405. Since the V-number is wavelength dependant, there is a specific wavelength above which *V* is < 2.405 and this wavelength is referred to as the cut off wavelength. At wavelengths above the cut off the fibre only supports the fundamental propagation mode.

An optical fibre performance depends on the material quality and the fabrication process, with optical losses occurring due to scattering defects, imperfections in the core-cladding interface, and the spectral transmissivity of fused silica. Bending of optical fibres is also a cause for radiation loss. When a fibre is bent, part of the mode within the fibre core has to travel different distances due to the fibre curvature. As the speed of light is the same however, the mode partly moves into the cladding which has a slightly lower refractive index. Loss in optical power results from such an event occurring.

Additional fibre types along with multimode and single mode fibres include graded index fibres in which the core has a refractive index that decreases with increasing radial distance from the optical axis of the fibre, and also Highly Birefringent fibres which maintain the polarised state of the launched light source along the propagation axis of the fibre.

Single mode fibre has been selected over multi-mode fibre for use in this study. Although multi-mode fibre would still work, the increased number of propagating modes would generate multiple interference fringe patterns. Trying to determine which pattern would be used for analysis would prove an extremely difficult task.

2.4.2. Polarisation and birefringence

In a single mode optical fibre there are two simultaneous modes of propagation allowed through the core which are orthogonally polarised. For an ideal fibre with circular core cross section, the two orthogonal modes, HE_{11}^{x} and HE_{11}^{y}, will be degenerate and will propagate with the same phase velocities. The phase velocities of the two modes, v_{fx} and v_{fy}, are given by (16)

$$v_{fx} = \frac{2\pi f}{\beta_x} \qquad v_{fy} = \frac{2\pi f}{\beta_y} \tag{2.6}$$

Where f is the frequency of the light within the fibre and β is the wave number. An ideal single mode fibre, made from homogenous isotropic material, will exhibit the same refractive index n for both propagation modes, resulting in a conserved polarisation state. A non-ideal fibre, resulting from effects such as bend (17), twist (18), and anisotropic stress, will behave as a birefringent medium with different refractive indices n_x and n_y, and different phase velocities v_{fx} and v_{fy}. The corresponding axes x and y can be referred to as the fast and the slow axes of the fibre, were the difference in refractive indexes of the fast and slow axis determine the fibre birefringence

$$B = n_f - n_s \tag{2.7}$$

The fibre birefringence rate is characterized by beat length l_b, given by

$$l_b = \frac{\lambda}{B} \tag{2.8}$$

The beat length represents the length of fibre necessary for the phase difference between the two orthogonal axes to be 2π. Figure 2.7 shows the change in the state of polarisation over the fibre beat length.

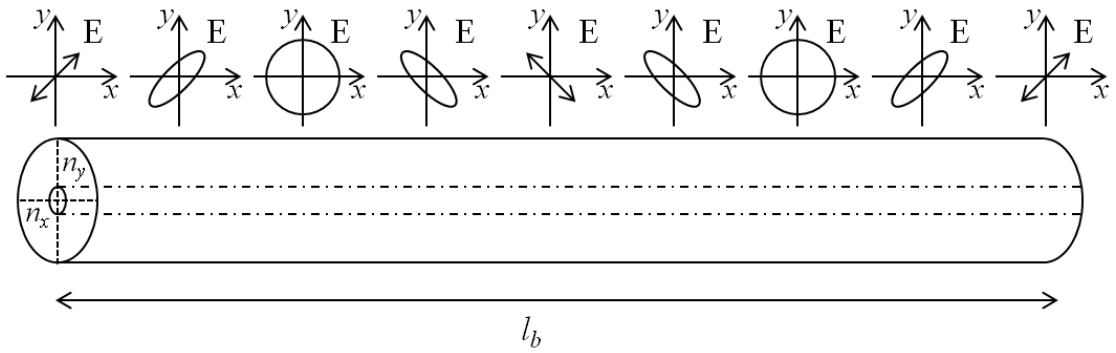

Figure 2.7: State of polarisation transformation through a birefringent fibre with a beat length l_b.

Anisotropic characteristics are observed in crystalline structures, for example, solids with atoms arranged in a regular repetitive array, when the lattice is deformed in one plane relative to the other. Their optical properties are not the same in all directions within the given sample. Birefringence is a form of optical anisotropy within a material, where the different polarisation states of light propagating through the material experience different propagation constants due to changes in refractive index. Birefringence of a fibre can be either intrinsic or induced. Intrinsic birefringence is introduced to the fibre during the manufacturing process and could be caused by the core ellipticity or the cladding eccentricity. Induced birefringence is a result of external forces present of the fibre whilst in use. These include thermal stress, and mechanical bending and twisting. Induced birefringence can be a popular tool to take advantage of for use in fibre optic sensing, however one would like to limit or remove the effects of intrinsic birefringence (19).

A means of controlling the polarisation state of the light propagating through a fibre, by removing or limiting the effects of intrinsic birefringence, would be the use of polarisation maintaining fibre (20). This type of fibre is designed to deliberately introduce some form of birefringence with the inclusion of stress members into the cladding in order to pre-stress the fibre. The formation of a fast and a slow propagation axis in the fibre allows light to be coupled into one particular axis to propagate through the fibre. The propagating light maintains its original polarisation state, even when it is

deployed with variable bends and twists. Polarisation maintaining fibre is more commonly known as Highly birefringent or HiBi fibre.

A further technique used to control the polarisation states within a fibre due to birefringence effects is the use of polarisation controllers (21). These operate by purposely bending and twisting the fibre in a certain orientation and thus inducing a change in the polarisation at that particular point. This is a useful technique if the fibre is stationary and where temperature affects will be uniform across the full fibre length. This is a technique which was utilised for the work carried out in this research, and a further explanation of the working principle will be described later in Chapter 4.

2.5. Optical Fibres for Sensing

It was long realised that the propagation of light through an optical fibre can be affected when exposed to changing environmental factors, such as stress and thermal effects. It was also realised that through analysis of the varying signal that the environmental change itself could be determined and measured. Fibre optic sensors are devices in which the propagation of light is modulated due to a physical quantity. This modulated light is then processed and used in the determination of the change or value of the physical quantity.

Depending on the measurand of the physical quantity, and how this will affect the electric field of the optical signal, fibre optic sensors fall into the following categories, intensity measurement, spectral measurement, polarimetric measurement, and phase measurement. By detecting the change of these parameters resulting from the interaction between the optical fibre and the measurand, fibre optic sensors can be designed to measure a wide variety of physical and chemical parameters such as strain (22), temperature (23), humidity (24), rotation (25), acceleration (26), position (27), and pressure (28). Pressure measurements, as a possible application of the interrogation system to be designed, are of particular relevance for this research however temperature effects on fibres, such as thermal expansion and thermo optic coefficients will also be considered.

As previously stated in section 1.4, optical fibres present a number of attractive features which make them a desirable choice for sensing purposes. The light-weight and small size of a fibre makes them an ideal choice to use in compact industrial areas, along with

the possibility of being embedded into composite materials as a means of creating smart structures. They also offer the advantage of being immune to electromagnetic interference, and, although it has not been utilised within this research, they can be multiplexed allowing for many sensors on one single fibre length. The disadvantages of fibre sensing, along with other sensing techniques, include measurement cross-sensitivity, where a single sensor may have multiple responses to different measurands, for example strain and temperature. The cost of fibre components and the instrumentation required compared to conventional methods will also have an effect on practical use, however in some instances may be the only option available.

As well as being categorised depending on the measurement technique used, fibre optic sensors fall into two separate subcategories, intrinsic and extrinsic. Intrinsic sensors operate in that the measured physical quantity acts upon the fibre which the light, confined within the fibre, is propagating through. The fibre materials are deliberately chosen in order to give sensitivity to the physical parameters. For extrinsic sensors the light exits the fibre, is modulated by the measurand, and is then launched back into the fibre. The performance of an extrinsic sensor is largely independent of the fibre and mainly depends on the sensing element.

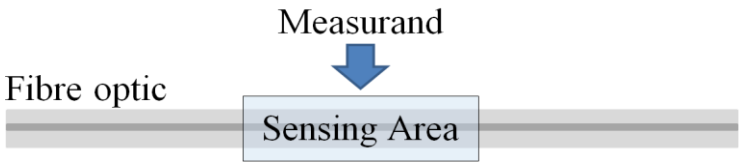

(a) Intrinsic sensor

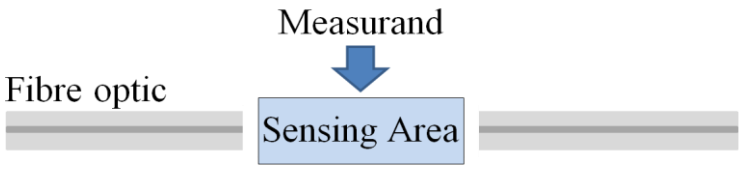

(b) Extrinsic sensor

Figure 2.8: (a) Intrinsic fibre sensor (b) Extrinsic fibre sensor.

Light propagation characteristics through a fibre that may be used to extract measurement information include phase by interferometry, intensity, spectral characteristics and polarisation. There are many texts that describe and review, in greater detail than in this thesis, the field of fibre optic sensors (29-31). The following sections describe some basic principles of fibre sensors based on these measurement techniques described above, to identify the most promising technology to further investigate.

2.5.1. Intensity based sensing

Fibre optic sensors in which the desired measurand has an effect on the light intensity of the propagating light have been demonstrated in both intrinsic and extrinsic form. Such sensor configurations can be used in the measurement of strain (32), temperature (33) and pressure (34).

In the case of pressure measurements, intrinsic intensity based sensors can be clamped between two corrugated plates, as shown in Figure 2.9, causing microbends in the fibre when subjected to an external force. These microbends, as a result of this external force, induce a loss through mode coupling out of the core, reducing the transmitted intensity in proportion with the applied pressure. Through knowledge of the change in intensity for a given force, the pressure exerted on the system could be calculated.

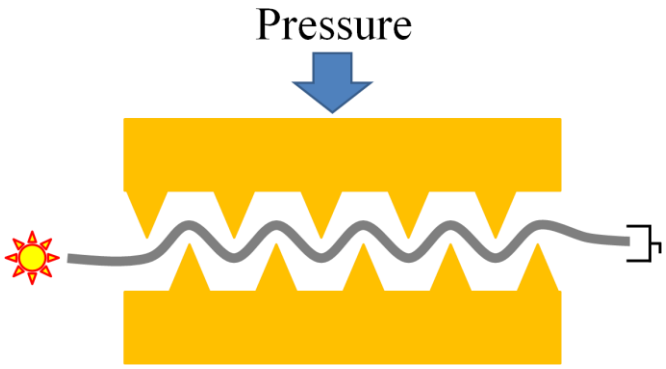

Figure 2.9: Intrinsic intensity based pressure sensor.

In comparison, extrinsic sensors can be used for absorption measurements and position sensing. Light transmitted through one fibre is then coupled into a secondary fibre, after an air gap, where a photo detector records any changes in the signal intensity. Signal attenuation due to absorption or scattering of a material within the air gap will either increase or decrease depending on the material properties, whilst positional measurements due to the alignment of the secondary fibre can be made due to light loss through coupling. This configuration can be used for longitudinal, transverse and angular displacement measurements and can in turn be related to many measurements by configuring the second fibre to move relative to the first based on the measurand of interest.

Due to the configuration simplicity, requiring just a light source, a sensing fibre and a photo-detector, the flexibility, and the fast temporal response, intensity based sensors have many advantages and potential applications in pressure sensing. The disadvantage of these sensor types are that the measurement is made solely on intensity, which, due to fluctuations in the source itself, may not be accurate. Intensity fluctuations as a result of twists and bends in the fibre, and through signal loss in fibre splices or connectors, are indistinguishable from those related to the desired parameter of interest. This may be corrected for with the use of some intensity referencing, however for the purposes of this project where temperature effects on connecting fibre leads may influence the desired pressure measurements, this approach does not look to provide the required measurement accuracy.

2.5.2. Polarisation based sensing

Polarisation based sensor configurations operate on the principle of monitoring changes in the state of polarisation of a birefringent element, whether that be a bulk element such as calcite using connecting fibres to lead light to and from the crystal, or an intrinsic fibre system with the use of highly birefringent fibre.

Highly birefringent fibre, as previously mentioned in section 2.4.2, is a polarisation maintaining fibre manufactured by either introducing a strain element within the cladding of the fibre, or by fabrication of a non-circular core. This introduces linear birefringence along the length of the fibre preventing cross coupling of the two orthogonally polarised modes of a light source as they propagate through the fibre at

different velocities. Measurements using polarisation based techniques are possible as when an additional stress is applied to the fibre through strain (35), temperature (36), or pressure (37), the fibre birefringence will also be altered. Similarly with that of the intensity based sensing technique, a measure of induced pressure can be determined, this time through changes in the state of polarisation of light due to an externally applied force on the birefringent element.

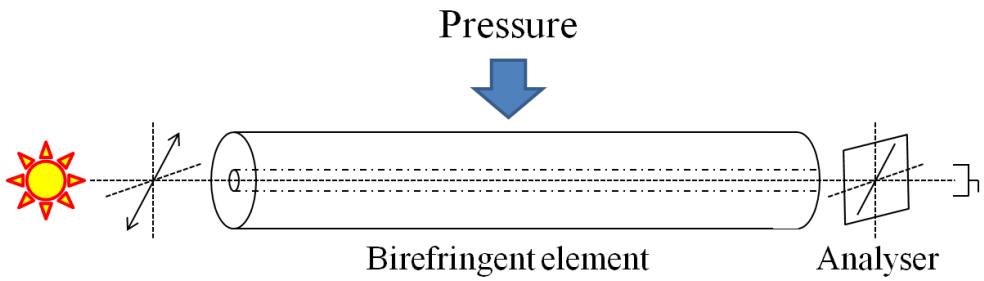

Figure 2.10: Polarisation based pressure sensor.

As shown in Figure 2.10, for polarisation based sensing, typically a narrowband, linearly polarised light source is used with highly birefringent fibre which propagates equally along both polarisation axes. An analyser is also a necessity to observe the polarisation state of the omitted light from the fibre. Any change in the polarisation state from the source will most likely be a result of an applied strain to the fibre causing a phase delay between the two polarisation states. For measurements of pressure, such a fibre could be mounted on a deformable diaphragm. Deformation due to an external force will result in a change in the state of polarisation, through which the applied pressure could be calculated.

Although previous accounts of using a polarisation technique for the measurement of pressure have been demonstrated, the state of polarisation can change within a fibre optic due to bends and twists in the fibre and through exposure to changes in temperature and pressure out with the measurement area of interest. For the purposes of this project, in which large lengths of interconnecting fibre will be used due to the measurement areas being at widely separate locations and the measurement analysis will be carried out at a large distance from the measurement position, a polarisation technique would not be suitable as it would be a difficult task to distinguish whether a

change in polarisation state is the result of the length change of interest or whether addition factors are the cause of such changes.

2.5.3. Fibre Bragg Grating sensors

A Fibre Bragg Grating (FBG) is a section of optical fibre in which a periodic refractive index structure has been inscribed into the core to induce coupling between the forward propagating (LP_{01}) and backward propagating ($-LP_{01}$) core modes.

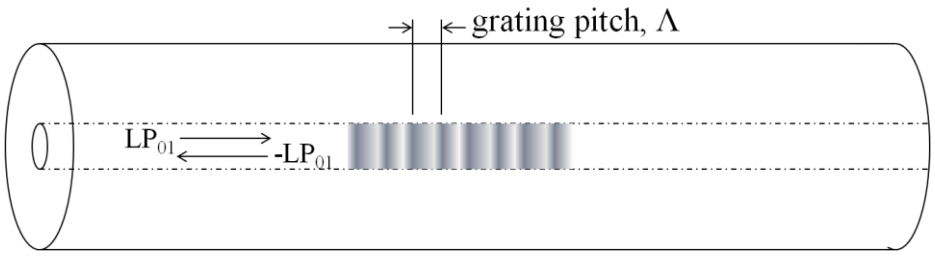

Figure 2.11: Forward and Backward propagating core modes of a FBG.

The discovery of optical Bragg grating was documented in 1985 by Hill (38), when it was found that counter propagating waves from a argon-ion laser produced a standing wave interference pattern inside an optical fibre. This interference pattern resulted in a periodic perturbation of the fibre refractive index. The periodic refractive index structures within the fibre core provide a means of wavelength encoded sensing, as FBG's can be used to form spectral sensing based on the modulation, by some external measurand, of the transmitted or reflected spectrum in the wavelength domain.

There are a variety of proposed configurations for the fabrication for FBG's, however they generally fall into either a bulk optic interferometric configuration (39), or a technique involving the use of a phase mask (40). Each method involves the exposure of an optical fibre to an ultra violet (UV) light source, usually in the 240-250 nm band. This is the optimum wavelength for photosensitivity in standard germanium-doped fibres with the refractive index change generated in fibres at these wavelengths connected with the absorption band of defects in germanosilicate glass (41). The amount of the change depends on the intensity and duration of the exposure as well as

the photosensitivity of the fibre. The photosensitivity of standard optical fibre can be increased by hydrogen loading of the fibre prior to exposure (42).

The interferometric configuration of FGB inscription, as shown in Figure 2.12, involves the splitting and recombining of the UV source. A beam splitter is used to split the source radiation equally between the two mirrors which direct the beams such that interference fringes are produced during recombination. When the fibre is placed in the path of the interference pattern, a periodic refractive index is inscribed in the fibre core. The fringe spacing of the resultant interference pattern and hence the pitch of the grating is dependent on the angle θ between the two beams, allowing different gratings to be produced using the same light source, simply by altering the angle θ.

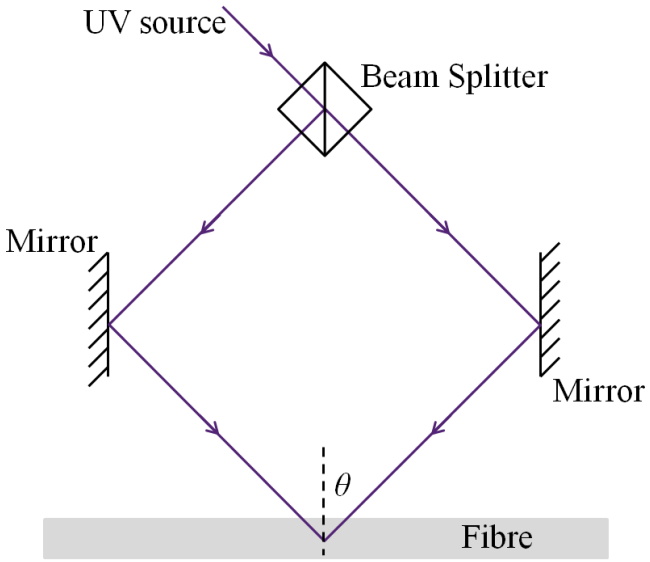

Figure 2.12: Interferometric fabrication of FBG's.

The alternative technique of fabricating FBG's with the use of a phase mask is shown in Figure 2.13. A phase mask is a diffractive element which, when a UV source is passed through it, causes the diffracted beams to interfere to produce the required interference pattern. The use of a phase mask has the advantage that the pitch of the grating is dependent entirely on the pitch of the phase mask and independent of the laser wavelength. This therefore requires a different phase mask for each grating pitch however some tuning of the pitch level is possible through straining of the FBG during fabrication.

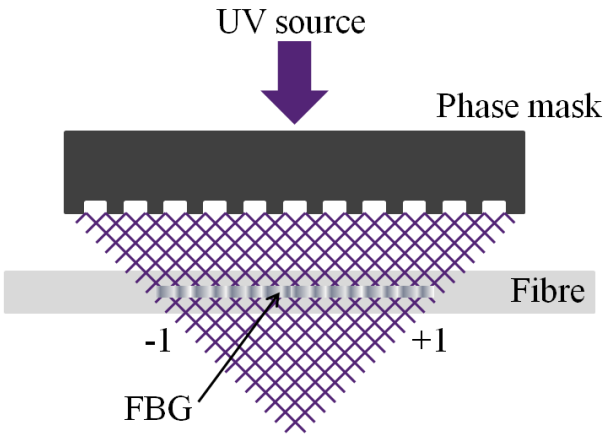

Figure 2.13: Phase mask fabrication of FBG's.

A third technique that is occasionally used for FBG fabrication is a point-by-point technique (43). This process however is slow and changes in fibre temperature and strain can lead to unwanted FBG structure. This approach is normally used when alternative fabrication methods are difficult to carry out.

The refractive index profile acts as a series of stacked Fresnel reflectors with characteristics that are reflective only for a narrow band of wavelengths, centred around the Bragg wavelength λ_B, which is dependent on the effective index of the fibre and the grating spacing. The Bragg wavelength represents the mode coupling condition between the forward and backward propagating modes, as described above, and is given by (44)

$$\lambda_B = 2n\Lambda \tag{2.9}$$

Where n is the effective refractive index of the core and Λ is the grating pitch. The Bragg wavelength may be measured in either reflection, by observing the reflected narrow band peak, or in transmission, by observing the dip in the transmitted spectrum. Figure 2.14 shows the operation of a FBG when illuminated by a broadband light source.

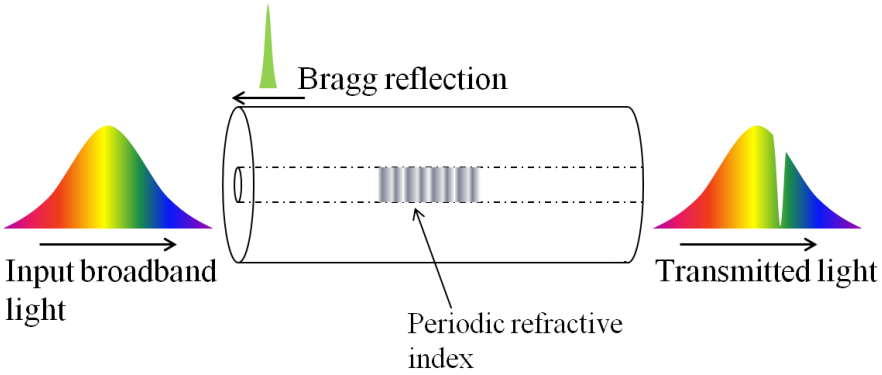

Figure 2.14: FBG illuminated with a broadband light source.

The grating period is a function of strain, temperature, and pressure, and hence when subjected to such parameters causes the Bragg wavelength to shift. For an applied longitudinal strain $\Delta\varepsilon$, the shift in wavelength is due to the photoelestic coefficient ρ_α, of the fibre and is given by (44)

$$\Delta\lambda_B = \lambda_B(1-\rho_\alpha)\Delta\varepsilon \tag{2.10}$$

The response is mainly due to the change in the physical length of the fibre, allowing FBG's to be embedded into structures for internal strain measurements (45).

The temperature response of a FBG is a result of the thermal expansion coefficient, $\alpha_T = \partial L/\partial T$, and the thermo-optic coefficient, $\beta_T = \partial n/\partial T$ of the fibre. For a temperature change ΔT the corresponding wavelength shift is given by

$$\Delta\lambda_B = \lambda_B\left(\alpha_T - \frac{\beta_T}{n}\right)\Delta T \tag{2.11}$$

Finally, pressure measurements can be made, with the response of a pressure change ΔP, given by

$$\Delta\lambda_B = \lambda_B\left(\frac{1}{\Lambda}\frac{\partial\Lambda}{\partial P}+\frac{1}{n}\frac{\partial n}{\partial P}\right)\Delta P \tag{2.12}$$

The shift in the Bragg wavelength as a result of a changing pressure is due to both a change in the effective refractive index of the core and from a change in the physical fibre length. FBG have been shown to reach pressure sensitivities of 48 pm/kPa (46). Although highly sensitive FBG are achievable, it would still prove difficult for determination of the research required differential pressure measurements of 1 Pa. Using the technique employed by the authors of (46), in which an optical spectrum analyser (OSA) is used to monitor the Bragg reflection from a FBG illuminated with a broadband light source, similar to that shown in Figure 2.14, a wavelength resolution of the OSA in the order of 0.048 pm would be required in order to monitor changes in pressure of 1 Pa. As will be discussed in the follow paragraphs, many OSA's will only achieve wavelength resolutions down to 10 pm, making the use of FBG unsuitable for the purposes of this research due to the pressure to be measured.

From equations 2.10-2.12 it is shown that induced strain, temperature and pressure, when applied to a FBG, is measureable. Configurations capable of measuring an applied strain, temperature change, and pressure change have been demonstrated (47-49).

In the case of pressure measurements with the use of FBG's, many sensors are designed to amplify the pressure measurement indirectly by sensing the strain instead. Such measurements can be achieved through via mounting of the FBG to a flexible diaphragm either orthogonally, or in the diaphragm plane where the stress is maximal. Another approach consists of mounting the FBG sensor in cylindrical assemblies so that increased pressure sensitivity is achieved though mechanical amplification schemes. Many designs are proposed in the literature with variations in coatings and assembly (50).

As previously stated, the Bragg wavelength, or change in Bragg wavelength, can be found by measuring the spectral reflection or transmission. As shown in Figure 2.14,

this can be done using a broadband source and a tuneable filter (51). The reflected light is passed through the tuneable filter and the transmitted intensity is recorded as the filter in scanned. The reflection spectra of the FBG can then be determined from the wavelength tuning response of the filter.

An alternative method to using a tuneable filter would be to monitor the reflection or transmission spectra with an OSA. OSA's can be divided into three categories: diffraction grating based, and two interferometer based architectures, the Fabry-Perot and the Michelson.

The Fabry-Perot interferometric method consists of two highly reflective, parallel mirrors that act as a resonant cavity which filters the incoming light. The wavelength is tuned by changing the mirror spacing by a very small amount. This form of OSA has the advantage of having a very narrow spectral resolution, however suffers from the major disadvantage of having a small wavelength range. At any one position multiple wavelengths can be passed by the filter, the spacing between which is termed the free spectral range.

The Michelson interferometer based OSA creates an interference pattern through the separation of the input signal into two separate paths and the subsequent recombination of these. The split beams are reflected back along the same paths via two mirrors, one fixed the other moveable. As a result of the different path lengths the beams create sequentially constructive and destructive interference. The waveform is the autocorrelation function of the input signal enabling direct measurements of the coherence length as well as accurate wavelength measurements. The output electrical signal is mathematically analysed using fast Fourier transform algorithms to reveal the input signal in a wavelength range.

The third type of OSA uses monochromators as the tunable optical filter. A diffraction grating within the monochromator separates the different wavelengths of light, similar to the effect achieved with a prism. In this case, however, it is a diffraction phenomenon as oppose to a dispersion phenomenon. A diffraction grating, constructed of extremely narrowly spaced grooves, provides greater separation of wavelengths allowing for better resolution than would be achieved with the use of a prism. Light incident on the grating will reflect in a number of directions.

The operation of a diffraction grating based OSA is illustrated in Figure 2.15. As the diffraction grating rotates, the instrument sweeps through a range of wavelengths allowing the particular wavelength of diffracted light, dependant on the grating position, to pass through the aperture. This technique covers a wide wavelength range with a typical OSA coverage from 600 to 1700 nm, with resolutions of 0.01 nm.

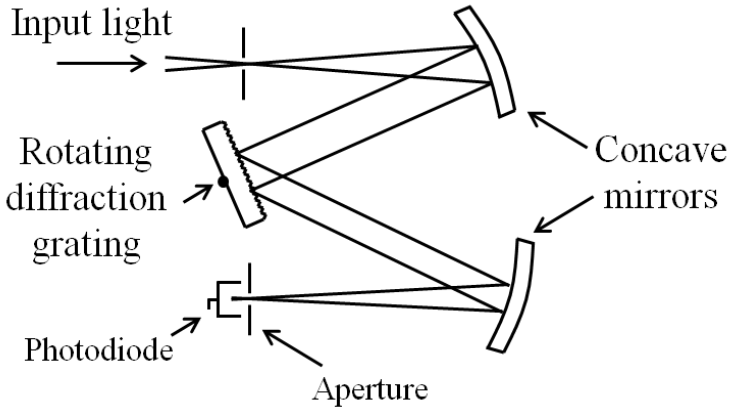

Figure 2.15: Single monochromator, diffraction grating based OSA.

Diffraction grating based OSA's contain either a single monochromator, as shown in Figure 2.15, or a double monochromator, in which two diffraction grating are employed.

FBG sensors have been shown to obtain high bandwidth measurements with high resolution and sensitivity, and have been demonstrated for the measurement of differential pressures (52). In the case of this text, the authors use two cylindrical cavities, separated by a deformable diaphragm, in which a change in pressure entering the cavities through separate inlets acts on the diaphragm creating a measureable strain on the encapsulated FBG. Through monitoring changes in the corresponding Bragg wavelength via an OSA, the differential pressure between the two inlets can be determined, along with verification as to the cavity experiencing the greatest pressure. Although a valuable technique for differential measurements, this approach suffers due to the need of tubes in order to carry the two measurable pressures from the measurement locations, when separated by large distances, to the cylindrical cavities. Twists and bends in such tubes, or changes in the surrounding environment may result in changes to the pressures to be determined.

FBG's suffer from the disadvantage of cross sensitivity between strain, temperature and pressure. To obtain accurate measurements of one of the parameters it is necessary to compensate for the others. This can be achieved to some degree with the use of two FBG's centred at different wavelengths. The response of one parameter at one wavelength will be much greater than the secondary parameter, and vice versa at the other wavelength. This however is still a limited approach and when dealing with large temperature drifts and large separation between measurement points, any thermal gradients between the fibres will reduce the effectiveness. As will be discussed in the following chapters, the design of the differential sensing system for this research will be composed of optical fibre with insensitive downleads between the two measurement locations, and as such, temperature variations in the surrounding fibre environment should not have an effect on the measurand. Although temperature monitoring at the measurement locations is out with the scope of this research it is still important to consider the temperature difference between measurement locations during the design stage of the sensor heads, due to the thermal expansion of materials. Further details of this will be provided in Chapter 6.

2.5.4. Interferometric sensors

Interferometry, a technique used for determining various physical parameters by observing the change in interference of two light beams, has become a common technique for making high precision measurements down to fractions of light wavelengths. A fibre optic interferometer uses the interference between two beams that has propagated through different optical paths or through two different fibres, making the principle component in many fibre optic interferometric configurations a beam splitter and combiner. The transduction mechanism relies upon the change in path length of one of the interferometer arms with respect to the other, and therefore requires that one of the optical paths be arranged to be affected by an external measurand. The change in the optical path length can be as a result of a physical length change of the fibre, or through a change in the refractive index. Since interferometers provide temporal and spectral information, the measurement of interest can be determined through a change in phase, intensity, wavelength, or polarisation.

The four main optical fibre interferometers are the Fabry-Perot, the Michelson, the Mach-Zehnder, and the Sagnac, each with a slightly varying sensing technique. Figure 2.16 shows the fibre optic configurations of these interferometers.

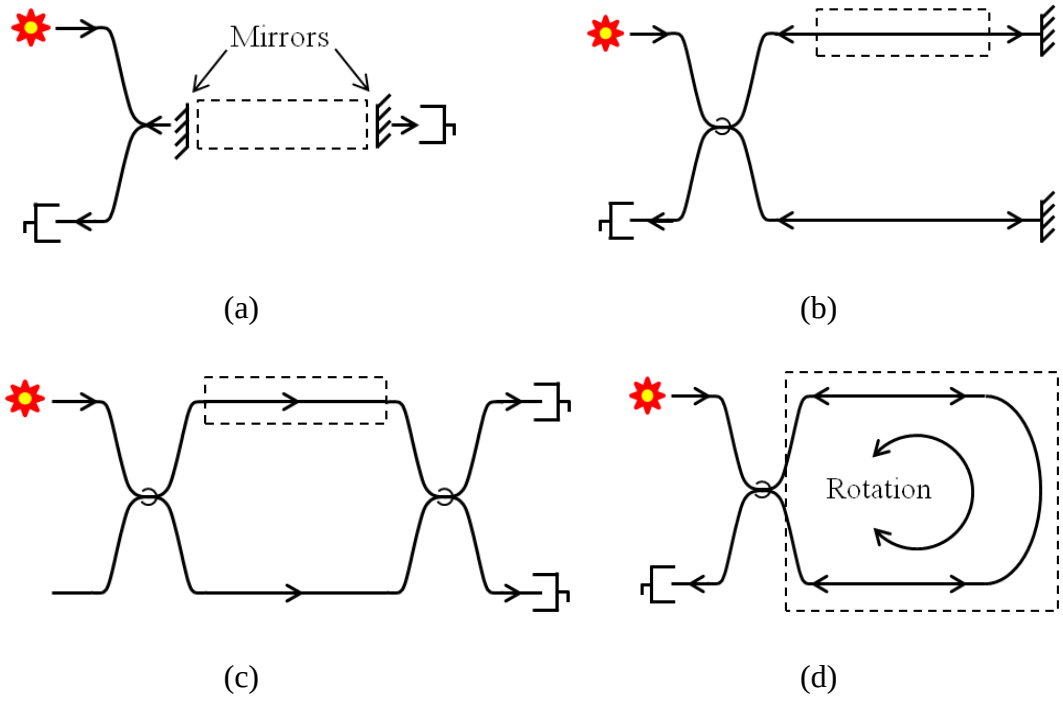

Figure 2.16: (a) Fabry-Perot interferometer (b) Michelson interferometer (c) Mach-Zehnder interferometer (d) Sagnac interferometer

Optical fibre interferometers have been used for the measurement of strain, temperature, pressure, displacement and acceleration. These sensors can operate either intrinsically or extrinsically depending on whether the optical path length change is within or out with the optical fibre, and can be use with both low and high coherent light sources. There have been many reviews on optical interferometric sensors (31, 53, 54), and a more detailed explanation of the chosen interferometer transfer function will be provided in Chapter 3, however a brief description on the different configurations is provided below.

Mach-Zehnder interferometers, as shown in Figure 2.16, consist of two independent arms, a reference and a sensing arm. By using two fibre couplers, the incident light is split between the two arms and then recombined, with any differences in the optical path length of the two arms resulting in the observation of interference fringes. For

sensing applications the reference arm of the interferometer is kept isolated from the sensing arm, and in a controlled environment, to ensure that only external effects, such as strain (55, 56), temperature (57, 58), and pressure (59, 60), contribute to the changing optical path length. This optical path length change and hence the measurand change can be easily detected by analysis of the interference signal.

Michelson interferometers are one of the simplest interferometric arrangements available however are by no means the least important. Michelson interferometers have the advantage over Mach-Zehnder interferometers of double the sensitivity. The arrangement can however be less efficient due to a portion of the reflected signal travelling back towards the source. Precautions can be taken to prevent damage to the source with the use of optical isolators or careful alignment. As shown in Figure 2.16, the basics of a Michelson interferometer are very similar to that of a Mach-Zehnder, in that it comprises again of a reference and a sensing arm. After splitting of the initial signal into the two arms however, the recombination occurs via the same coupler once the beams are reflected via the fibre end, thus propagating through each arm twice. Reflections via the fibre end can be as a result of Fresnel reflections (4% of the incident signal), or by coating the fibre end with a reflective surface to increase the signal intensity. Similarly to the Mach-Zehnder interferometer, the change in optical path length comes from keeping one arm of the interferometer in a stable environment whilst exposing the second arm to an external measurand. Michelson interferometers are capable of generating measurements of strain (61, 62), temperature (63, 64), and displacement (65, 66).

The Sagnac interferometer is slightly different from the Mach-Zehnder and Michelson interferometers, consisting of a fibre loop along which two beams propagate in counter directions. The optical path difference, created by rotating the system, responds to angular velocity, therefore by rotating the system with a given velocity, the path length in one direction will be altered with respect to the other. Sagnac interferometers are commonly used in gyroscopes (67), however they have been demonstrated for use of pressure sensing (68) and strain measurements (69).

Both Mach-Zehnder and Michelson interferometers, due to the sensitivity of environmental effects over the full lengths of the interferometer arms, are ideally suited for the measurement of strain and temperature however these interferometer configurations are not best suited for point measurements. Local measurements can be

made by defining a specific region within one arm of the interferometer which will be subjected to the measurand however sensitivity in the fibre downleads due to temperature and pressure effects creates a disadvantage using such an interferometric arrangement for remote operation where a long downlead is required. Fabry-Perot based sensors offer the possibility of making localised measurements with very low downlead sensitivity. This is achieved by the formation of a cavity on a fibre end resulting in both the reference and sensing beams propagating through a common path in the fibre.

A Fabry-Perot interferometer (or etalon) is generally fabricated by the formation of a cavity composed of two parallel reflective surfaces. The measurement of the optical path length difference comes from the interference obtained due to the multiple superpositions of both the reflected and transmitted beams at the reflective surfaces as shown in Figure 2.17.

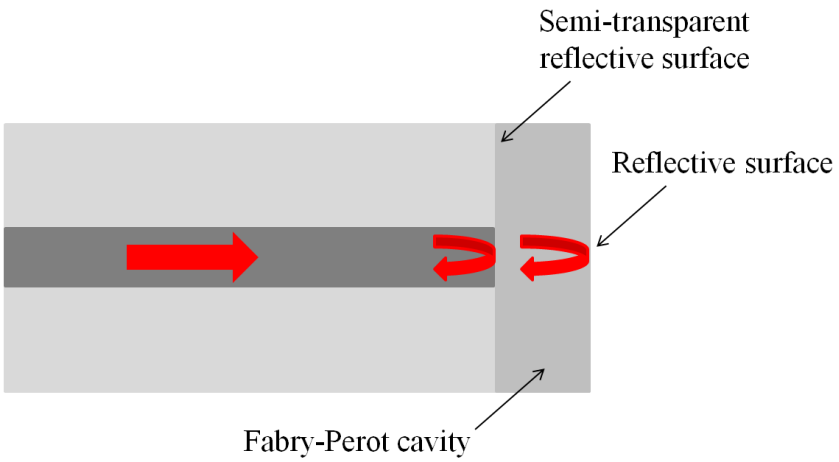

Figure 2.17: Optical fibre Fabry-Perot cavity.

Fabry-Perot interferometers can either be extrinsic (70) or intrinsic (71). Extrinsic cavities are usually formed using the reflections from the end face of the downlead fibre, and a secondary reflecting surface. One method for generating the secondary reflection is the use an additional fibre aligned to the first. The two fibres are held using a hollow tube of usually glass or silica, as shown in Figure 2.18, with a air gap separation forming the Fabry-Perot etalon (72).

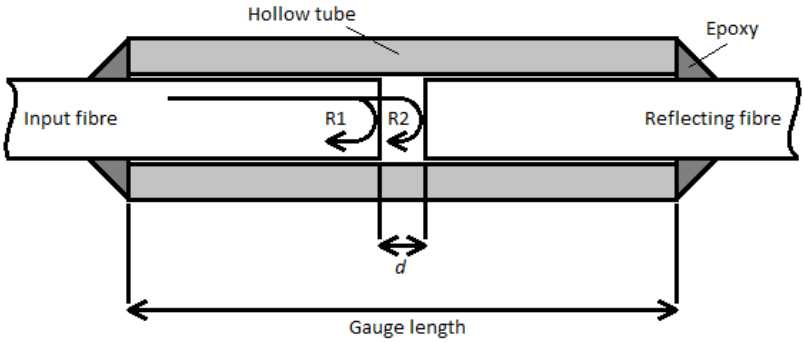

Figure 2.18: Arrangement of a Fabry-Perot cavity formed using two optical fibres.

An alternative configuration for the fabrication of the Fabry-Perot cavity would be with the use of a deformable diaphragm, illustrated in Figure 2.19, with a reflective surface as the secondary reflection (73). Changes in the optical path length (OPL) due to deformation of the diaphragm with applied pressure will result in changes in interference.

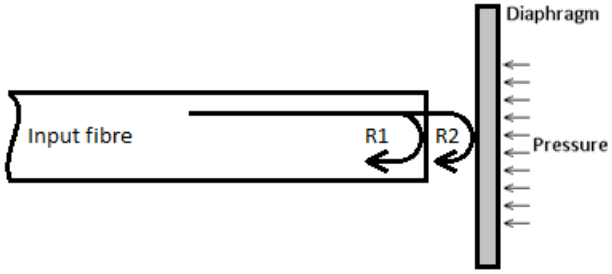

Figure 2.19: Arrangement of a Fabry-Perot cavity formed using an optical fibre and a deformable diaphragm.

The disadvantage of using an extrinsic form of this interferometer is the potential for low coupling efficiency, which therefore requires careful and accurate alignment of the second reflective surface. Intrinsic forms of this interferometer have reflecting components within the fibre, for example in fibre mirrors (74), and as a result, the cavity length can be increased without loss due to the cavity being defined within the fibre core.

Fabry-Perot sensors have been fabricated for the measurement of pressure (75-77) and have been demonstrated in applications such as turbomachinery (78) and down-hole applications (79).

Fabry-Perot interferometric sensors provide high sensitivity, localised measurements, and with the formation of a cavity formed on the end of an optical fibre, allow for small measurement volumes. The insensitivity of the system to environmental effects acting on the downlead fibre make this sensor configuration suitable for carrying out the required measurements for tackling the problem set by this project.

2.5.5. Low coherence interferometry

Basic interferometry with the use of a monochromatic light source has the disadvantage in that the system is only able to monitor continuous changes by summing of the total number of phase changes observed from a nominal start position. For a rapid change of path length in excess of the data capture rate a loss in the reference will occur and therefore invalidate the signal. Such a system also suffers from the inability to determine the direction of motion, unless further monitoring is implemented. To increase the range of unambiguous phase measurements, a source with multiple frequencies can be used. Typically sources with a broad spectral bandwidth and a short coherence length are used, terming the use as low coherence interferometry.

Low coherence interferometry is a technique which was first demonstrated in 1976 as a possible transmission scheme for the use in optical communications. Fibre optic low coherence, or white light, interferometry has become an important technique in the measurement of displacement, offering measurement accuracy which is virtually insensitive to power fluctuations occurring along fibre lengths of an interrogation system. In 1984, Bosselmann and Ulrich, demonstrated a displacement sensor based on fibre optic low coherence interferometry with a resolution of 1 in 10^4 (80). Further reviews into the applications of low coherence interferometry have been carried out in the following texts (81, 82).

Low-coherence interferometry has been successfully developed for optical coherence tomography (OCT), a technique commonly used to provide cross-sectional images of biological tissues, for example, retinal nerve fiber (83).

In the case of a Fabry-Perot interferometer, when the cavity is illuminated with a broadband source having a short coherence length, constructive and destructive interference is observed for those wavelengths which are at half odd and even multiples of the cavity length respectively. In order to observe these interference fringes, an OSA operating using a diffraction grating arrangement is used. As described in section 2.5.3, this device separates the individual wavelengths using a monochromator and allows for the interference fringes to be observed. Figure 2.20 shows a typical interferogram of a Fabry-Perot cavity illuminated with a broadband source.

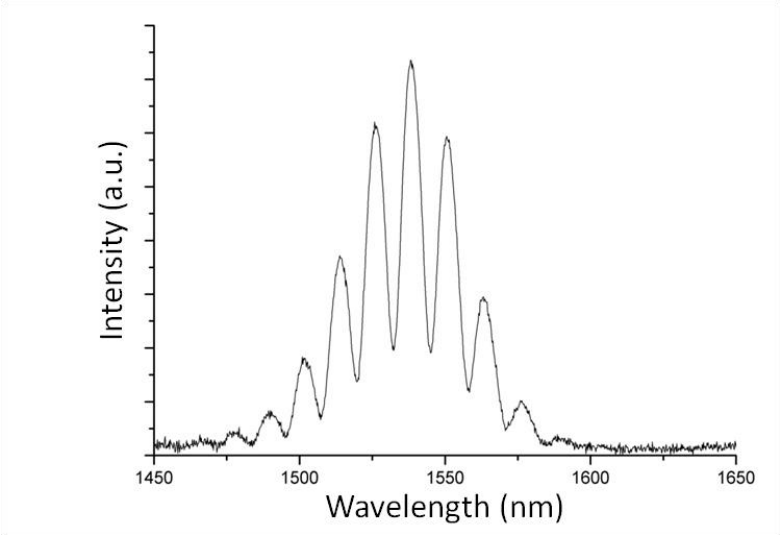

Figure 2.20: Interferogram, recorded using an Advantest OSA model Q8384, from a Fabry-Perot cavity illuminated with a broadband light source.

There are a number of interrogation techniques available as a means of determining the cavity length. Such techniques include FSR analysis whereby the fringe separation is used in determining the cavity length (84). Using the following equation, the cavity length, *d*, is found by taking the wavelength measurement of two adjacent fringe peaks, λ_1 and λ_2.

$$d = \frac{\lambda_1 \lambda_2}{2n(\lambda_2 - \lambda_1)} \tag{2.13}$$

Where *n* is the refractive index of the medium within the cavity.

A further technique would be to calculate the Fast Fourier Transform (FFT) of the interferogram to derive the carrier frequency to determine the cavity length (85). This technique has the advantage over the FSR method of using the full interferogram as oppose to individual points of two adjacent fringes.

Low coherence interferometry has been demonstrated using Fabry-Perot interferometers for the measurements of absolute distance and displacement (27, 86, 87). Making differential length measurements at two separate locations using this technique can be made by simply measuring the absolute lengths of the two independent Fabry-Perot cavities and calculating the difference between them. This however would therefore require two separate interrogation methods running simultaneously in order to accurately measure the two lengths at the same time as not to record the measurement of one cavity length at a different time to the other and calculate an incorrect differential. The overall measurement would also be dependent on the individual measurement accuracy and resolution of each of the interrogation systems for the two arms which poses a challenge if large length changes are introduced.

A method to avoid the need of making two individual measurements of length and determining the difference would be to arrange the two Fabry-Perot cavities in tandem connected via couplers or circulators and simply observe the differential length of the two. This configuration creates a common path for the propagating light to travel such that the offset of the two cavities generates an optical path, which is the measurement of interest. Combining this with a secondary scanning reference interferometer provides a means of obtaining the optical path length and in doing so generates a low coherence tandem interferometer. The optical arrangement for such a system will be discussed in Chapter 4.

2.5.6. Tandem interferometry

Tandem interferometry describes a system in which two interferometers are connected such that a light source will propagate through one interferometer and then through the secondary interferometer as shown in Figure 2.21. The arrangement of the two interferometers is such that interference fringes will only be observed when the interferometers path lengths are matched to within the coherence length of the source, L_0-L_1=L_2-L_3 from Figure 2.21. One of the interferometers is used as the sensing

element, whilst the second interferometer is used as the reference and is normally scanned in some form which controls the optical path length. The two interferometers should be kept separate, with the reference interferometer kept within a controlled environment to avoid path length changes due to temperature and pressure changes.

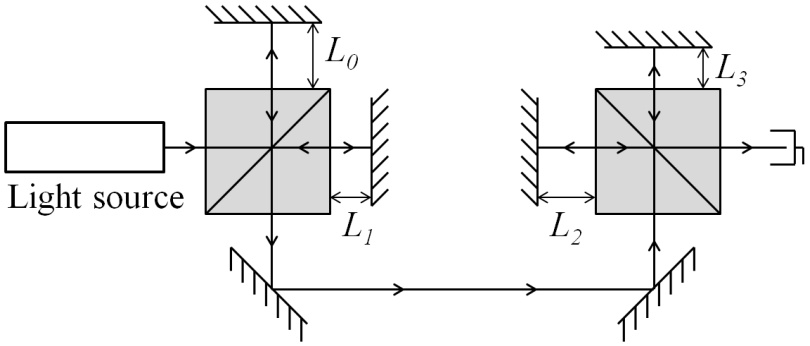

Figure 2.21: Tandem interferometer arrangement using bulk optics.

Typically these systems use a broadband light source with a short coherence length. When the path length difference of the two interferometers is large, there is no variation in the signal intensity at the system output when monitored via a detector. The signal intensity increases as the path length difference becomes smaller, reaching maximum intensity when the path lengths are equal. As the optical path length of the scanning interferometer passes through zero, a further set of interference fringes can be observed. Figure 2.22 shows modelled interference fringes of a tandem interferometer as the reference interferometer is scanned using a broadband light source centred at 1550 nm with a spectral width of 263.93 nm, corresponding to a coherence length of 6.20 μm.

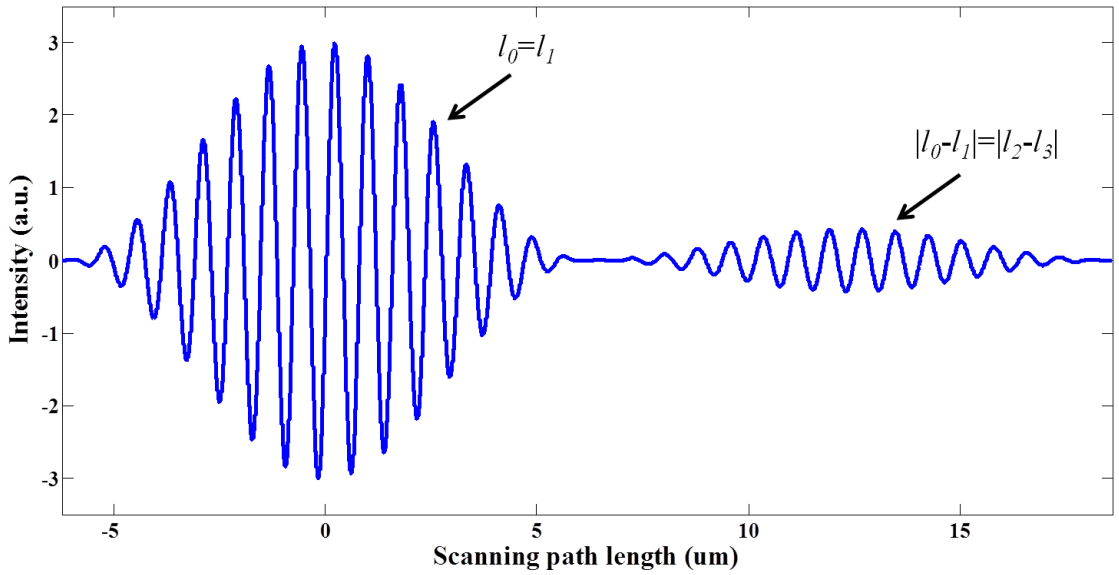

Figure 2.22: Modelled interference fringes from a tandem interferometer arrangement resulting from matched OPL's referring to Figure 2.21. The interference fringes illustrated would be as a result of a broadband light source centred at 1550 nm with a spectral width of 263.93 nm. This corresponds to a coherence length of 6.20 µm.

The typical operation functions of tandem interferometers will be discussed in Chapter 3, however what is to follow is a review of this technique.

Tandem interferometry is a technique that has been demonstrated of used in the measurement of strain (88), temperature (89), and group refractive index and dispersion of optical samples (90, 91). One of the main applications to this form of interferometry however is for displacement measurements, either in the form of gap measurements or thickness measurements.

In 1972 P.A. Flournoy, *et al*, demonstrated a technique for the measurement of film thicknesses over a range of 2.5-500 µm using white light interferometry in a bulk optical arrangement (92). Using a Michelson interferometer composed of a beam splitter and two mirrors, interference fringes are observed when the optical path length of the two Michelson arms are equal to zero. When using the reflected light from the two surfaces of a thin film sample to feed into this interferometer, white light fringes are seen in addition to the zero-order fringes whenever the path difference of the Michelson, introduced by scanning one of the mirrors, is nearly equal to the retardation introduced between the reflected rays from the sample. If the scanning mirror is moved at a

constant linear velocity, the path difference becomes a linear function of time and therefore the time interval between the zero order fringes and the side interference fringes, if the refractive index is known, can indicate the film thickness. This is a technique which could be utilised for the length measurement of a Fabry-Perot cavity, or in the case of this research, the differential length between two Fabry-Perot cavities.

This method of determining material thickness has since been demonstrated for measurements of liquid crystal display cell gaps (93), SiO_2/Si film thicknesses (94), and biological sample thicknesses (95) in the micro meter range. Developing this technique and introducing convolution and correlation signal processing algorithms, has led to measurements in the nanometer scale with resolutions in the region of 10 nm (96).

Low coherence tandem interferometry has become a useful technique for the remote length measurements when combined with fibre optics. A. Hirai and H. Matsumoto demonstrated that the length of a 50 mm gauge block could be made with a standard deviation of 0.12 µm, with a separation of 3 km between the reference and the sensing interferometers (97). By coupling low coherent light into a single mode optical fibre once it has propagated through a bulk optic scanning Michelson, the fibre can then be used to emit this light on to a measurement bulk optic Michelson interferometer 3 km away. This was further expanded using a fibre length between the two interferometers of 20 km (98). In this instance, remote length measurements of a gauge block were achieved with losses in the 20 km fibre kept low at 7.60 dB. This demonstrates that with the use of optical fibre, length measurements are capable even at large separations with low signal loss. This is of particular interest for this thesis as the distance between differential measurement points could possibly be up to tens of meters apart. Further reports have been made in which optical fibres have played a role in the delivery or collection of light between interferometers in a tandem configuration.

Demonstrations have been made for the measurement of single gap thicknesses and although it is possible to measure the individual length at two positions using separate arrangements and from them determine the differential, it may not be possible to do this using only one tandem arrangement. The gap lengths may therefore not be measured simultaneously resulting in an inaccurate differential measurement. For the case of this project, a multiple measurement from a single tandem arrangement would be required. S. H. Lu, *et al*, report a technique based on the previously mentioned demonstrations using a scanning Michelson interferometer and bulk optic arrangement, that is capable

of measuring multiple sample thicknesses without the need to change the sample position each time (99). The technique, which involves the use of multiple beam splitters to separate the light into several beams directed onto individual samples constructed using microscope slides, has the potential of measuring the individual lengths of two gap thicknesses simultaneously, or separately with the use of shutters along the beam path.

This proposed technique could have a potential use in the design requirements for the research carried out in this thesis. With the substitution of a deformable diaphragm as one of the reflective surfaces of the gap to be measured, a change in the calculated thickness from the initial could be used to determine the external pressure exerted on the diaphragm having knowledge of the deformation characteristics. The bulk optical arrangement could also be replaced with a fibre optic version to allow for a more flexible system, through which, measurements at largely separated locations could be made. The authors of (99) demonstrate single gap thickness measurements from 132 μm to 152 μm, measuring at intervals of 5 μm with the use of a motorised stage, recording a best-fit line of 0.9984. Although there are no recorded experimental data provided for the measurements of dual gap thicknesses, it does demonstrate that such a technique of a tandem arrangement and separate scanning interferometer can be utilised in such a way that could prove useful for the goals of this research.

Whilst the above method allows for measurement of gap thicknesses at two individual points, it does however suffer from the set back that if the two gap lengths are within the coherence length of the light source to each other, the interference fringes that would result from these individual path lengths matching that of the scanning interferometer would overlap and be indistinguishable. In order to accurately determine the gap length from the associated fringe packet, the lengths would have to differ by greater than the light source coherence length. This, in the case of measuring the length of a fibre optic Fabry-Perot cavity, could result in significant coupling losses for larger cavity lengths. The reference interferometer scanning range must also be large in order to cover the full cavity length range.

By utilising the techniques of tandem interferometry used for measurements of gap thicknesses, it is possible to construct an all fibre optic arrangement which uses a scanning Michelson interferometer connected to two Fabry-Perot cavities arranged in tandem, to measure the differential length of the two. Such a method, in which the

propagating light within the fibres follows a common path, does not depend on the individual cavity lengths, however simply observes the difference between the two.

2.6. Discussion

As has been reviewed throughout this chapter, there are many different techniques which can be deployed for the measurements of pressure, or length with the view of being converted into a pressure measurement. Each of these methods has its advantages and disadvantages, thus paving the way for the development of a differential pressure measurement approach which differs from the previously demonstrated techniques as a means of achieving the goals and guide specifications of this research.

There are many readily available commercial pressure sensors on the market capable of measuring both absolute and differential pressures. Operating through the use of piezoresistive effects, some commercial sensors have been fabricated to operate up to high pressures (ranging from 3.4 kPa to 68.9 MPa), with a measurement accuracy of 0.1% to 0.2% of the full scale (5). Due to the presence of high background pressures up to 100 kPa, and a requirement to measure differential pressures at 1 Pa, these sensors become insufficient. These sensors also suffer in the measurement location being away from the point of interest. Long tubing is required to carry the pressure from the point of interest to the sensor head, during which time external factors acting on the tubing from environmental changes may result in inaccurate measurements.

Commercially available fibre optic sensors (6) can be used in order to obtain pressure measurements at the point of interest, however as with the piezoresistive sensors, they suffer from below par measurement resolutions for the design goals of this research. It is apparent however that due to the capability of localised measurements, optical fibre sensors are the best approach. Fibre optics also provide flexibility and insignificant signal loss over large distances which may not be achievable through a bulk optic approach.

Many optical fibre sensors have been demonstrated for the measurement of pressure or length, some of which have been reviewed within this chapter. There consists many variations and techniques which can be used as a means of determining a measurand. One of the most common fibre based sensor is the FBG, shown to measure such parameters as strain and temperature, along with pressure measurements. Such a

technique monitors the shift in Bragg reflection when the grating experiences an external force. FBG's with pressure sensitivities of 48 pm/kPa have been demonstrated (46). This sensitivity range however is unfortunately insufficient for pressure measurements down to 1 Pa as in most cases the wavelength shift is monitored via an OSA which typically has a wavelength resolution down to 0.01 nm, greater than the wavelength change for such small pressures. FBG's have also been used in differential pressure measurements demonstrating pressure sensitivities of 821.87 nm/MPa (52), however the same problem of monitoring the wavelength shift of the Bragg reflection at low pressures persists.

Other fibre optical sensors have been demonstrated using interferometric techniques whereby changes in the interference pattern of a light source can be analysed to calculate changes in optical length. Through the characterisation of a deformable diaphragm such length changes could be converted into a pressure measurement.

One of the most common techniques for the determination of a length measurement is low coherence interferometry. This particular method involves the use of a broadband light source. In some of these instances a tandem arrangement of two or more interferometers are used whereby the measurement, by one interferometer, is made through an induced change in a secondary interferometer. Demonstrations have been shown that through a combination of a Fabry-Perot cavity and a scanning Michelson interferometer, length measurements are possible with resolutions in the region of 10 nm (96). This particular approach was found using a bulk optical arrangement for the measurement of a single gap length. Further demonstrations have gone on to show how multiple length measurements can be made using a similar arrangement, again utilising bulk optical components (99). As would be the case of these two methods, in order to obtain a differential measurement, the difference would have to be taken between two separate measurements individually taken.

As a means of achieving the goals of this research, an optical arrangement is to be developed incorporating similar techniques previously used in which a differential measurement is to be found through the measurement of one single parameter. Such a system would also be insensitive to environmental changes of the surrounding optical fibres used to carry light to and from the measurement locations of interest.

2.7. Conclusion

In this chapter a brief introduction to pressure was introduced, along with current conventional techniques for the measurements of pressure and length being reviewed and the limitations of such components discussed. These limitations have lead on to the possibility of using optical fibre sensors as a means of determining such measurements.

Different measurement methods which involve the use of optical fibre sensors, such as intensity based sensing, FBG's, and interferometric sensing, have been reviewed, discussing the benefits of each and the areas in which these have the greatest success, and the limitations or setbacks involved for the measurement of pressure and length.

From this review it was decided that for the purposes and goals of this thesis, that an interferometric sensing configuration based on low coherence interferometry, should provide a solution for the differential measurement of two Fabry-Perot cavities, arranged in tandem, whilst being separated by up to tens of meters.

2.8. References

1. The Engineering ToolBox, U-Tube Manometer [Available from: http://www.engineeringtoolbox.com/u-tube-manometer-d_611.html.
2. IT Instrumentation Today, Bourdon Tube 2015 [Available from: http://www.instrumentationtoday.com/bourdon-tube/2011/09/.
3. Engineers Edge LLC, Bellows Pressure Detector 2000-2015 [Available from: https://www.engineersedge.com/instrumentation/bellows_pressure_detector.htm
4. Aznial R, Bashir M. Diaphragm Mechanical Analysis of Fiber Optic Pressure Sensor. ICCBT2008. p. 295-302.
5. Honeywell International Inc. Sensing and Control [Available from: http://www.honeywellscportal.com/sensinghome.
6. FISO Technologies Inc. www.fiso.com2009 [Available from: http://www.fiso.com/section.php?p=20.
7. Hecht E. Optics. Fourth ed. San Francisco: Addison Wesley; 2002.
8. Born M, Wolf E. Principles of optics : electromagnetic theory of propagation, interference and diffraction of light. 7th (expanded) ed. ed. Cambridge: Cambridge University Press; 1999.
9. Hoss RJ, Lacy EA. Fiber optics. 2nd ed. ed. Englewood Cliffs, N.J.: P T R Prentice-Hall; 1993.
10. Teja NR, Babu MA, Prasad TRS, Ravi T. Different Types of Dispersions in an Optical Fiber. International Journal of Scientific and Research Publications (IJSRP). 2012;2(12).
11. Ungar S. Fibre optics : theory and applications: John Wiley & Sons; 1990.
12. Yariv A. Optical Electronics in Modern Communications. 5th ed. New York: Oxford University Press; 1997.

13. Senior JM. Optical Fiber Communications: Principles and Practice. United Kingdom: Prentice Hall International, Incorporated; 1985.
14. Ghatak A, Thyagarajan K. An Introduction to Fiber Optics. United Kingdom: Cambridge University Press; 1998.
15. Snyder AW, Love J. Optical Waveguide Theory: Chapman & Hall; 1983.
16. Drexler P, Fiala P. Recent Progress in Optical Fiber Research: InTech; 2012.
17. Wang Q, Rajan G, Wang P, Farrell G. Polarization dependence of bend loss for a standard singlemode fiber. Optics Express. 2007;15(8):4909-20.
18. Smith AM. Birefringence induced by bends and twists in single-mode optical fiber. Applied Optics. 1980;19(15):2606-11.
19. Yeh C. Handbook of fiber optics : theory and applications. San Diego: Academic Press; 1990. xv, 382 p. p.
20. Noda J, Okamoto K, Sasaki Y. Polarization-maintaining fibers and their applications. Lightwave Technology, Journal of. 1986;4(8):1071-89.
21. Lefevre HC. Single-mode fibre fractional wave devices and polarisation controllers. Electronics Letters. 1980;16(20):778-80.
22. Jiang Y, Tang C. High-finesse micro-lens fiber-optic extrinsic Fabry–Perot interferometric sensors. Smart Materials and Structures. 2008;17(5).
23. Lee CE, Taylor HF. Fiber-optic Fabry-Perot temperature sensor using a low-coherence light source. Lightwave Technology, Journal of. 1991;9(1):129-34.
24. Noor MYM, Khalili N, Gang-Ding P. All-Fiber Optic Humidity Sensor Based on Photonic Bandgap Fiber and Digital WMS Detection. Sensors Journal, IEEE. 2013;13(5):1817-23.
25. Ulrich R. Fiber-optic rotation sensing with low drift. Optics Letters. 1980;5(5):173-5.
26. Wenjun Z, Xinyong D, Yongxing J, Chun-Liu Z, editors. Cantilever-based FBG sensor for temperature-independent acceleration measurement. Communications and Photonics Conference and Exhibition (ACP), 2009 Asia; 2009 2-6 Nov. 2009.
27. Liu T, Fernando GF. A frequency division multiplexed low-finesse fiber optic Fabry-Perot sensor system for strain and displacement measurements. Review of Scientific Instruments. 2000;71(3):1275-8.
28. Gander MJ, MacPherson WN, Barton JS, Reuben RL, Jones JDC, Stevens R, et al. Embedded micromachined fiber-optic Fabry-Perot pressure sensors in aerodynamics applications. IEEE Sensors Journal. 2003:102-7.
29. Grattan KTV, Sun T. Fiber optic sensor technology: an overview. Sensors and Actuators A-Physical. 2000:40-61.
30. Lee B. Review of the present status of optical fiber sensors. Optical Fiber Technology. 2003;9(2):57-79.
31. Kersey AD. A Review of Recent Developments in Fiber Optic Sensor Technology. Optical Fiber Technology. 1996;2(3):291-317.
32. Chun-Liu Z, Dong X, editors. Temperature- independent strain sensor based on intensity measurement using a highly birefringent photonic crystal fiber loop mirror. Communications and Photonics Conference and Exhibition (ACP), 2009 Asia; 2009 2-6 Nov. 2009.
33. Wang A, Xiao H, Wang J, Wang Z, Zhao W, May R. Self-calibrated interferometric-intensity-based optical fiber sensors. Journal of Lightwave Technology. 2001:1495-501.
34. Kinugasa S. Differential pressure sensor using common optical fiber path. 2006 IEEE Sensors, Vols 1-3. 2006:1039-42.

35. Ye C-C, Staines SE, James SW, Tatam RP. A polarization-maintaining fibre Bragg grating interrogation system for multi-axis strain sensing. Measurement Science and Technology. 2002;13(9):1446.
36. Jun Long L, Hu DJJ, Shum PP, Yixin W, editors. Temperature response of polarization-maintaining photonic crystal fiber based interferometer. Microwave Photonics, 2011 International Topical Meeting on & Microwave Photonics Conference, 2011 Asia-Pacific, MWP/APMP; 2011 18-21 Oct. 2011.
37. Passy R, Gama AL, Gisin N, Von der Weid JP. Pressure dependence of polarization mode dispersion in HiBi fibers. Lightwave Technology, Journal of. 1992;10(11):1527-31.
38. Hill KO, Fujii Y, Johnson DC, Kawasaki BS. Photosensitivity in optical fiber waveguides: Application to reflection filter fabrication. Applied Physics Letters. 1978;32(10):647-9.
39. Meltz G, Morey WW, Glenn WH. Formation of Bragg gratings in optical fibers by a transverse holographic method. Optics Letters. 1989;14(15):823-5.
40. Thomas J, Wikszak E, Clausnitzer T, Fuchs U, Zeitner U, Nolte S, et al. Inscription of fiber Bragg gratings with femtosecond pulses using a phase mask scanning technique. Applied Physics A. 2007;86(2):153-7.
41. Slattery SA, Nikogosyan DN, Brambilla G. Fiber Bragg grating inscription by high-intensity femtosecond UV laser light: comparison with other existing methods of fabrication. Journal of the Optical Society of America B. 2005;22(2):354-61.
42. Wei CY, Ye CC, James SW, Tatam RP, Irving PE. The influence of hydrogen loading and the fabrication process on the mechanical strength of optical fibre Bragg gratings. Optical Materials. 2002;20(4):241-51.
43. Malo B, Hill KO, Bilodeau F, Johnson DC, Albert J. Point-by-point fabrication of micro-Bragg gratings in photosensitive fibre using single excimer pulse refractive index modification techniques. Electronics Letters. 1993;29(18):1668-9.
44. Rao Y. In-fibre Bragg grating sensors. Measurement Science & Technology. 1997:355-75.
45. Kerrouche A, Boyle WJO, Tong S, Grattan KTV, Schmidt JW, Taljsten B. Strain Measurement Using Embedded Fiber Bragg Grating Sensors Inside an Anchored Carbon Fiber Polymer Reinforcement Prestressing Rod for Structural Monitoring. Sensors Journal, IEEE. 2009;9(11):1456-61.
46. Song D, Zou J, Wei Z, Yang S, Cui H-L, editors. High-sensitivity pressure sensor based on fiber Bragg grating and metal bellows2009.
47. James SW, Tatam RP, Twin A, Morgan M, Noonan P, editors. Strain response of fibre Bragg grating sensors at cryogenic temperatures. Optical Fiber Sensors Conference Technical Digest, 2002 OFS 2002, 15th; 2002 10-10 May 2002.
48. Seongmin J, Watekar PR, Won-Taek H, editors. Highly sensitive temperature sensor using fiber Bragg grating on Pb/Ge-codoped fiber. Optical Fiber Communication - incudes post deadline papers, OFC 2009; 22-26 March 2009.
49. Yanling X, Jing H, Wenlong Y, Linwen S, Wei G, Yang C, editors. Research on FBG pressure sensor of flat diaphragm structure. Measurement, Information and Control (MIC), 2012; 18-20 May 2012.
50. Pinet É, editor Pressure measurement with fiber-optic sensors: commercial technologies and applications2011.
51. Allan WR, Graham ZW, Zayas JR, Roach DP, Horsley DA. Multiplexed Fiber Bragg Grating Interrogation System Using a Microelectromechanical Fabry–Perot Tunable Filter. Sensors Journal, IEEE. 2009;9(8):936-43.

52. Sheng H, Liu W, Lin K, Bor S, Fu M. High-sensitivity temperature-independent differential pressure sensor using fiber Bragg gratings. Optics Express. 2008;16(20):16013-8.
53. Jackson DA. Recent progress in monomode fibre-optic sensors. Measurement Science and Technology. 1994;5(6):621.
54. Lee BH, Kim YH, Park KS, Eom JB, Kim MJ, Rho BS, et al. Interferometric fiber optic sensors. Sensors. 2012;12:2467-86.
55. Jahed NMS, Nurmohammadi T, Ounie S, Bonabi RS, editors. Enhanced resolution fiber optic strain sensor based on mach-zehnder interferometer and displacement sensing principles. Electrical and Electronics Engineering, 2009 ELECO 2009; 2009 5-8 Nov. 2009.
56. Chen X, Yu Y, Xu X, Huang Q, Ou Z, Wang J, et al. Temperature insensitive bending sensor based on in-line Mach-Zehnder interferometer. Photonic Sensors. 2014;4(3):193-7.
57. Yuan L, Yang J. Multiplexed Mach-Zehnder and Fizeau tandem white light interferometric fiber optic strain/temperature sensing system. Sensors and Actuators A-Physical. 2003;105(1):40-6.
58. Yu Y, Jiang L, Wang S, Yang J, Li B, editors. Strain-insensitive optical fiber Mach-Zehnder interferometric temperature sensor. International Conference on Optical Instruments and Technology: Optical Sensors and Applications; 2011.
59. Porte H, Gorel V, Kiryenko S, Goedgebuer JP, Daniau W, Blind P. Imbalanced Mach-Zehnder interferometer integrated in micromachined silicon substrate for pressure sensor. Journal of Lightwave Technology, 1999;17(2):229-33.
60. Wagner D, Frankenberger J, Deimel PP. Optical pressure sensor using two Mach-Zehnder interferometers for the TE and TM polarization. Journal of Micromechanics and Microengineering. 1994;4(1):35.
61. Valis T, Tapanes E, Liu K, Measures RM. Passive-quadrature demodulated localized-Michelson fiber-optic strain sensor embedded in composite materials. Journal of Lightwave Technology, 1991;9(4):535-44.
62. Yuan L, Yang J, Zhou L, Jin W, Ding X. Low-coherence Michelson interferometric fiber-optic multiplexed strain sensor array: a minimum configuration. Applied Optics. 2004;43(16):3211-6.
63. Elsarnagawy TD, editor A High Resolution Interferometric Fiber-Optic Temperature Sensor "FOTS". Biomedical Engineering Conference, 2008 CIBEC 2008 Cairo International; 2008 18-20 Dec. 2008.
64. Jing Z, Hao S, Ruohui W, Dan S, Tuan G, Zhongyao F, et al. Simultaneous Measurement of Refractive Index and Temperature Using a Michelson Fiber Interferometer With a Hi-Bi Fiber Probe. Sensors Journal, IEEE. 2013;13(6):2061-5.
65. Smith LM, Dobson CC. Absolute displacement measurements using modulation of the spectrum of white light in a Michelson interferometer. Applied Optics. 1989;28(16):3339-42.
66. Alzahrani K, Burton D, Lilley F, Gdeisat M, Bezombes F. Automatic Absolute Distance Measurement with One Micrometer Uncertainty Using a Michelson Interferometer. Proceedings of the World Congress on Engineering2011.
67. Lefevre HC, editor Fundamentals of the interferometric fiber optic gyroscope1996.
68. Fu HY, Tam HY, Shao L-Y, Dong X, Wai PKA, Lu C, et al. Pressure sensor realized with polarization-maintaining photonic crystal fiber-based Sagnac interferometer. Applied Optics. 2008;47(15):2835-9.

69. Dong X, Tam HY, Shum P. Temperature-insensitive strain sensor with polarization-maintaining photonic crystal fiber based Sagnac interferometer. Applied Physics Letters. 2007; 90(15).
70. Chen J, Zhao J, Huang X, Huang Z. Extrinsic fiber-optic Fabry-Perot interferometer sensor for refractive index measurement of optical glass. Applied Optics. 2010:5592-6.
71. Chen X, Shen F, Wang Z, Huang Z, Wang A. Micro-air-gap based intrinsic Fabry-Perot interferometric fiber-optic sensor. Applied Optics. 2006;45(30):7760-6.
72. Rao Y-J. Recent progress in fiber-optic extrinsic Fabry–Perot interferometric sensors. Optical Fiber Technology. 2006;12(3):227-37.
73. Yu B, Kim DW, Deng J, Xiao H, Wang A. Fiber Fabry-Perot Sensors for Detection of Partial Discharges in Power Transformers. Applied Optics. 2003;42(16):3241-50.
74. Lee CE, Taylor HF. Interferometric optical fibre sensors using internal mirrors. Electronics Letters. 1988;24(4):193-4.
75. Wang W, Wu N, Tian Y, Niezrecki C, Wang X. Miniature all-silica optical fiber pressure sensor with an ultrathin uniform diaphragm. Optics Express. 2010;18(9):9006-14.
76. Cibula E, Pevec S, Lenardic B, Pinet E, Donlagic D. Miniature all-glass robust pressure sensor. Optics Express. 2009:5098-106.
77. Rao YJ, Jackson DA, Jones R, Shannon C. Development of prototype fiber-optic-based Fizeau pressure sensors with temperature compensation and signal recovery by coherence reading. Journal of Lightwave Technology, 1994;12(9):1685-95.
78. MacPherson WN, Kilpatrick JM, Barton JS, Jones JDC. Miniature fiber optic pressure sensor for turbomachinery applications. Review of Scientific Instruments. 1999;70(3):1868-74.
79. Aref SH, Latifi H, Zibaii MI, Afshari M. Fiber optic Fabry–Perot pressure sensor with low sensitivity to temperature changes for downhole application. Optics Communications. 2007;269(2):322-30.
80. Bosselmann T, Ulrich R, editors. High-Accuracy Position-Sensing With Fiber-Coupled White-Light Interferometers, OFS'84, 1984.
81. Dufour M, Lamouche G, Detalle V, Gauthier B, Sammut P. Low-coherence interferometry - an advanced technique for optical metrology in industry. Insight. 2005;47(4):216-9.
82. Rao Y, Jackson D. Recent progress in fibre optic low-coherence interferometry. Measurement Science & Technology. 1996:981-99.
83. Ojima T, Tanabe T, Hangai M, Yu S, Morishita S, Yoshimura N. Measurement of retinal nerve fiber layer thickness and macular volume for glaucoma detection using optical coherence tomography. Japanese Journal of Ophthalmology. 2007;51(3):197-203.
84. Du Y, Yan H, Nie Y, Zhang X, Zheng M. New data-processing technique for measurement of metallic foil thickness with differential white-light interferometry. Optics and Lasers in Engineering. 2007;45(1):240-4.
85. Jiang Y. Fourier transform white-light interferometry for the measurement of fiber-optic extrinsic Fabry-Perot interferometric sensors. IEEE Photonics Technology Letters. 2008;20(2):75-7.
86. Majumdar A, Huang H. Development of an in-fiber white-light interferometric distance sensor for absolute measurement of arbitary small distances. Applied Optics. 2008;47(15):2821-8.

87. Bosbach C, Pfeifer T, Depiereux F, editors. Absolute distance measurement with miniaturized fiber-optic white light interferometer. XVII IMEKO World Congress; 2003; Dubrovnik, Croatia.
88. Bohnert K, de Wit G, Nehring J. Interrogation of a remote elliptical-core dual-mode fiber strain sensor by using a tandem interferometer configuration. Optics Letters. 1992;17(9):694-6.
89. Kim JH. An All Fiber White Light Interferometric Absolute Temperature Measurement System. Sensors. 2008;8(11):6825–45.
90. Matsumoto H, Sasaki K, Hirai A. In situ measurement of group refractive index using tandem low-coherence interferometer. Optics Communications. 2006;266(1):214-7.
91. Chlebus R, Hlubina P, Ciprian D. Spectral-domain tandem interferometry to measure the group dispersion of optical samples. Optics and Lasers in Engineering. 2009;47(1):173-9.
92. Flournoy PA, Wyntjes G, McClure RW. White-Light Interferometric Thickness Gauge. Applied Optics. 1972;11(9).
93. Kao C, Tsai S, Lu S. Measuring Cell Gap of Liquid Crystal Displays by Scanning White-Light Tandem Interferometry. Japanese Journal of Applied Physics. 2009;48(10).
94. Ohta T, Koshimizu C, Kawasaki K, Takeda K, Ito M. Simultaneous measurement of substrate temperature and thin-film thickness on SiO_2/Si wafer using optical-fiber-type low-coherence interferometry. Journal of Applied Physics. 2009;105(1):013110--7.
95. Kim D, Song C, Ilev I, Kang J. Axial-scanning low-coherence interferometer method for noncontact thickness measurement of biological samples. Applied Optics. 2011;50(6):970-4.
96. Xu Z, Shilpiekandula V, Youcef-toumi K, Yoon S. White-light scanning interferometer for absolute nano-scale gap thickness measurement. Optics Express. 2009;17(17):15104-17.
97. Hirai A, Matsumoto H, editors. Low-coherence tandem interferometer for remote calibration of gauge blocks. Recent Developments in Traceable Dimensional Measurements II; 2003.
98. Matsumoto H, Sasaki K. Remote Measurements of Practical Length Standards Using Optical Fiber Networks and Low-Coherence Interferometers. Japanese Journal of Applied Physics. 2008:8590-4.
99. Lu S, Chang C, Kao C, Furlong C, Gorecki C, Novak E. Multi-point gap measurement by low coherence tandem interferometry. Interferometry XV: Applications. 2010;7791.

Chapter 3: Theory

3.1. Introduction

The review in Chapter 2 suggests low coherence tandem interferometry as a potential solution to the problem detailed in Chapter 1 for the measurement of a differential pressure through the determination of a differential length. Such an arrangement incorporates two Fabry-Perot cavities, from which the differential length will be determined. These are arranged in tandem and connected to a scanning reference Michelson interferometer.

Low coherence interferometry will be used as a means of determining the differential length of the two sensor cavities. Along with this, a DFB laser source will also be used as a reference measurement of the optical path length within the Michelson interferometer.

This chapter provides a review of the theory of the optical properties of interferometry beginning by taking into consideration the individual optical properties of the Michelson interferometer and the Fabry-Perot cavities, and then discussing the properties of a tandem configuration of these. This understanding is important in order to develop a suitable interrogation and analysis technique. The characteristics of both high and low coherent light sources will be discussed, and how the resultant interference patterns from the interactions with such an arrangement are achieved and can be used in determining the desired length measurement.

A suitable interrogation technique that can be implemented on the interference patterns in order to provide analysis of the fringes is described, along with the theory behind this technique and the reasons why it was selected as a suitable method will also be discussed.

The final sections of this chapter will tie together the important theoretical aspects of optical interferometry that have been reviewed and the described analysis techniques, leading on to investigations of the characteristics of piezoelectric materials as a process of inducing an optical length change within an optical fibre due to piezo material expansion properties with applied voltage.

3.2. Michelson Interferometer

Interferometry is a technique used to investigate optical phenomena through the creation of interference patterns with transverse waves of light. When two waves of same wavelength and amplitude travel through the same medium, their amplitudes combine, resulting in the formation of a wave of greater or less amplitude than the original. Traditionally, interferometry is used for the measurement of length, whether that is a physical length or an optical length due to the change in refractive index of a medium.

There are many different interferometers available depending upon the circumstances in which it is to be used. All interferometers, in one shape or form, involve the separation, and recombination of a light source between two or more paths. The separate paths, depending on the form of splitter and reflective component, give rise to the formation of interference fringes when the paths differ in optical length. From these resultant interference fringes, occurring when the OPL changes, measurements in terms of the wavelength of the light used can be directly determined.

The Michelson interferometer, invented in 1881 by Albert Michelson as a means to measure a standard meter in units of the wavelength of the red line of the cadmium spectrum (1), is perhaps the simplest example of an amplitude splitting interferometer. Figure 3.1 shows the simplified diagram of a Michelson interferometer using bulk optical components. This interferometer, used in 1887 in the famous Michelson-Morley experiment (2), demonstrated the non-existence of an electromagnetic wave carrying ether, thus paving the way for the Special theory of Relativity.

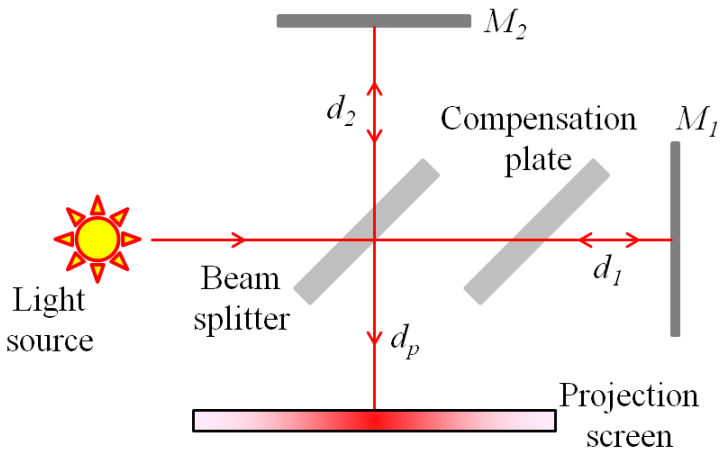

Figure 3.1: Bulk optic Michelson interferometer.

Consider light leaving from the source and falling on the beam splitter, orientated at a 45° angle to the direction of travel. The beam splitter comprises of a partially reflective surface causing the light to be separated, usually half transmitted, half reflected, between the two different light paths through which it then propagates. The partially transmitted beam travels length d_1 before being redirected back to the beam splitter, along the same path, by reflective mirror M_1. The partially reflected light beam via the beam splitter propagates along path d_2 to mirror M_2, from where it is reflected, again along the direction of incidence, back to the beam splitter.

From Figure 3.1, where bulk optics are used to construct the Michelson interferometer, it can be seen that the partially reflective surface of the rectangular shaped beam splitter is on the rear side, and as such, light undergoing the reflection via mirror M_2 will pass through the beam splitter three times, compared to the light undergoing the reflection via mirror M_1, which will only pass through the splitter once. The OPL through the beam splitter, dependent on the glass refractive index, will therefore alter the OPL difference of the two propagating beams. It is due to this geometry that a compensation plate of the same material, or material with the same refractive index, and thickness as that of the beam splitter is inserted into the path between the beam splitter and reflective mirror M_1.

This is not always the case, and in most circumstances a compensation plate in not necessary for a bulk optical Michelson interferometer arrangement. This is due to the use of a beam splitter cube, as oppose to a plate. The geometrical arrangement of a beam splitter cube permits for equal travel within the cube material of both propagating beams from the beam splitter to the corresponding mirror and therefore renders the compensation plate unnecessary.

Having travelled along their respective path lengths within the system, the two propagating light beams recombine at the beam splitter resulting in an interference pattern which can be observed via the projection screen. It is because of the coherent waves, derived from the same point source that the interference pattern produced is of a circular fashion, as shown in Figure 3.2, similar to those of Newton's rings.

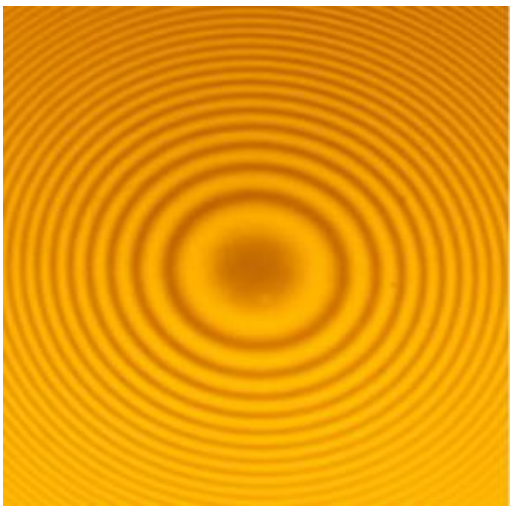

Figure 3.2: Circular interference fringes generated from the Michelson interferometer configuration illustrated in Figure 3.1 (3).

The interference occurs due to the difference in path lengths travelled between the beam splitter and the corresponding mirrors. Each path is travelled twice by the light beams within the medium of refractive index *n*, resulting in a path length difference given by

$$2n\left(d_2 - d_1\right) \tag{3.1}$$

This path length difference can be altered by changing the position of mirror, M_2, usually mounted on a translation stage. As the mirror position is adjusted, dependant on the direction of travel, the observable interference rings appear to either grow, with new rings appearing at the central point, or shrink, with existing rings disappearing at the central point. An alternative method of altering the path length differential, and in turn the positions of the interference fringes, is by changing the medium of one of the interferometer arms, through which the light travels. This can be achieved by placing one of the paths in a vacuum chamber and evacuating in order to change the refractive index. The light will travel faster in the evacuated chamber, and as this is brought back up to atmospheric pressure the interference rings will either grow or shrink in size.

In order to derive the path length change from the interference fringes we must consider the light in general. The amplitude, *A*, and intensity, *I*, of a wave propagating from the source are generally described in the following terms,

$$A(x,t) = E\cos(\omega t - kx)$$
$$I \propto \langle A \rangle^2 \tag{3.2}$$

As previously stated, on interaction with the beam splitter the light amplitude is split, travelling the distance between the beam splitter and the reflective mirrors twice, *2d*, and then on to the projection screen along distance d_p. This gives the following representation of the separate propagation paths,

$$A_1(x,t) = \frac{E}{\sqrt{2}}\cos(\omega t - 2kd_1 - kd_P)$$
$$A_2(x,t) = \frac{E}{\sqrt{2}}\cos(\omega t - 2kd_2 - kd_P) \tag{3.3}$$

Where the energy is halved along each propagation path and the phase is described in terms of the lengths travelled to the corresponding mirror and projection screen.

The output of the interferometer, through superposition of the above wave equations, can be described in terms of intensity as

$$I_p = I_0\cos^2(k(d_1 - d_2)) \tag{3.4}$$

Where I_0 is the intensity of the source light, and the cos^2 function arises from the conversion from amplitude to intensity.

Substituting the definition of the standard wave number k given by, $k = 2\pi/\lambda$, into the above equation for the Michelson interferometer output intensity, the conditions for achieving a maxima and minima are given as

$$Maxima = \Delta d = \frac{m\lambda}{2}$$
$$Minima = \Delta d = \frac{\left(m + \frac{1}{2}\right)\lambda}{2} \tag{3.5}$$

Where m is equal to an integer order number ($m=0, 1, 2, ...$).

Changing the path length by altering the position of one of the mirrors changes the relative phase of the two beams, resulting in circular fringes either appearing or disappearing at the central position when using a monochromatic light source. It is through this variation of interference fringes that the change in length can be monitored and calculated, as will be discussed in section 3.5.3.

The same principles apply when using a fibre optic Michelson interferometer as oppose to a bulk optical arrangement. Changes in the OPL due to variations in the physical length of the fibre or through variations in temperature and pressure can be monitored, and is the reason why the Michelson interferometer is a common choice as a measurement technique.

It is due to its simplistic measurement method and arrangement that the Michelson interferometer was chosen as the reference interferometer for determining the differential length for this project. Using a monochromatic light source, changes in the OPL of the interferometer can be monitored without this compromising the differential length measurement of the Fabry-Perot cavities of interest.

3.3. Fabry-Perot Cavity

In the previous section, 3.2, the Michelson interferometer and the characteristics of such an arrangement, as a means of determining a measured length change, were described

using the method of interferometry. As with the Michelson interferometer, the Fabry-Perot cavity utilises the technique of interferometry as a method of determining a length, defined between the reflective walls of the cavity. This arrangement can be used in both the transmitted and reflected methods using multiple-beam interference principles.

For the experimental configuration carried out in this project, the Fabry-Perot cavity will not be used in the standard arrangement as a means of determining the individual cavity length, or change due to an external measurand. It is, however, still important to understand the principles behind the Fabry-Perot interferometer in order to optimise the configuration in which it will be deployed.

The Fabry-Perot interferometer is a very simple device, consisting of two parallel mirrors precisely aligned to form a reflective optical cavity, or resonator, as illustrated in Figure 3.3.

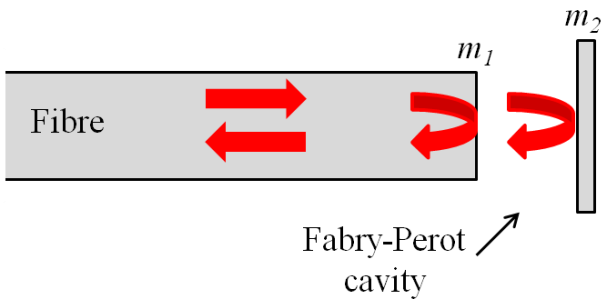

Figure 3.3: Basic fibre optic Fabry-Perot cavity construction.

The interferometric cavity is formed between mirror m_1, through which the initial light enters the cavity, and mirror m_2, which defines the end of the cavity. In the case illustrated above, and as will be the case for this thesis, mirror m_1 is formed from a cleaved optical fibre, resulting in a 3.6% reflective surface, at 1550 nm, due to Fresnel's equations (4). The cavity will have both transmission and reflection, characterised by the properties of the two cavity mirrors. In an ideal situation, mirror m_2 will have little or zero absorption properties, allowing maximum light propagation due to the lossless properties of Fresnel's reflections. This is never the case and so optical loss through absorption will have to be taken into consideration.

Taking the simplest case of the Fabry-Perot cavity, where it can be assumed that the mirrors are ideally lossless and their reflections are sufficiently small, such that the surfaces will have zero thickness and zero phase change, and only one reflection will occur at the interfaces, the reflected intensity, I_r, will be defined as,

$$I_r = E_r \cdot E_r^* \tag{3.6}$$

Where

$$E_r = E_0\left(r_1 + r_2 e^{i\phi}\right) \tag{3.7}$$

E_0 and E_r are the incident and reflected electric fields respectively, E_r^* is the complex conjugate of the reflected electric field, r_1 and r_2 are the respective amplitude reflection coefficients, and ϕ is the optical phase given by

$$\phi = \frac{4\pi n l}{\lambda} \tag{3.8}$$

Where l is the optical path length of the cavity and n is the refractive index of the substrate within the cavity.

The phase change within a Fabry-Perot cavity is twice that of the standard relationship between phase and optical path length, due to the complete round trip the light travels within the cavity.

For the above case it is assumed that the coherence length is large compared to the cavity length and that the source within the cavity is spatially coherent. It is also assumed that the polarisation within the cavity remains unchanged throughout. It can therefore be determined from the above equation that the reflected intensity is given by

$$\frac{I_r}{I_0} = R_1 + R_2 + \sqrt{R_1 R_2}\cos\phi \tag{3.9}$$

Where $R_1 = r_1^2$, $R_2 = r_2^2$, and I_0 is the initial input intensity of the source. If losses, η, due to coupling efficiency are taken into consideration, the output intensity can be expressed as (5)

$$I_r = I_0\left[R_1 + \eta^2 R_2(1-R_1)^2 + 2\eta\sqrt{R_1 R_2(1-R_1)\cos\phi}\right] \tag{3.10}$$

Where

$$\eta = \frac{2w_0 w(2l)}{{w_0}^2 + w^2(2l)} \tag{3.11}$$

As the beam propagates into the cavity, divergence along the cavity length must be taken into consideration. The return beam from the reflection at the secondary mirror will therefore be broadened, and will inject into the fibre partially with the coupling coefficient determined by interchange interrogation as expressed above. Generally, due to the light divergence at the input to the cavity through mirror m_1, the percentage of radiation reflected from the secondary cavity mirror, m_2, depends on the distance between the cavity mirrors, l, the beam spot size, w, and the beam waist, w_0, at the fibre tip. Figure 3.4 shows the effect of light divergence from the optical fibre end.

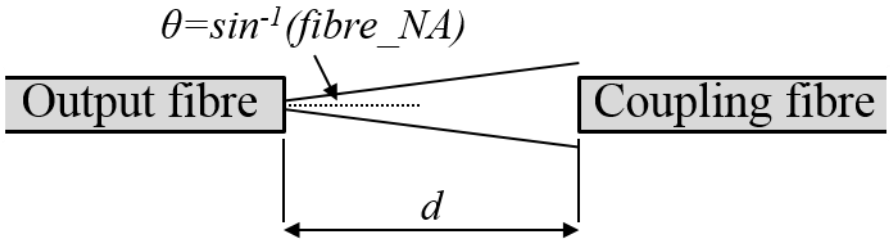

Figure 3.4: Effect of light spread from the fibre. The half angle at which the light exits the fibre, θ, is dependent on the numerical aperture, NA, of the fibre core.

The cavity, or fringe, visibility, *V*, can also be taken into consideration. This parameter defines the quality of the optical interference and is determined by the expression

$$V = \frac{I_{\max} - I_{\min}}{I_{\max} + I_{\min}} = \frac{2\eta\sqrt{R_1 R_2}\left(1 - R_1\right)}{R_1 + \eta^2 R_2\left(1 - R_1\right)^2} \tag{3.12}$$

Where I_{max} and I_{min} are the respective maximum and minimum intensities of the optical interference. As is shown above, the cavity visibility is dependent on the surface reflectivity's R_1 and R_2, and cavity length, the three parameters that can be altered to obtain maximum visibility.

Through rearrangement of equation 3.12, a cavity visibility of 100% is possible if the following relationship is obtained

$$\eta^2 = \frac{R_1}{R_2\left(1 - R_1\right)^2} \tag{3.13}$$

When the cavity transfer function is generated via the first reflections from the cavity mirrors, m_1 and m_2, the above analysis, commonly known as the two-beam approximation, provides an analytical expression for low reflectivity cavities.

The visibility of a Fabry-Perot cavity describes the limits of the interference intensities, however, it is customary to define a numerical value to which the width, or sharpness, of the maxima can be characterised. This value is referred to as the finesse, *F*, of an interferometer, and is defined as the ratio of peak distance to peak half width. The expression of the finesse is given as

$$F = \frac{4R}{\left(1 - R\right)^2} \tag{3.14}$$

Where R is the cavity facet reflectivity. As only the influence of the reflectivity on the line width is considered here, it is often termed as the reflectivity finesse as a means of distinguishing it from other properties influencing the transfer function.

A 'high finesse', typically implying a facet reflectivity greater than 90%, can be useful for optical spectrum analysis, because it allows the combination of a large free spectral range with a small resonator bandwidth. Therefore, a high spectral resolution in a wide spectral range is possible.

There is, however, a drawback to improving the cavity resolution by increasing the optical path difference between the two reflecting surfaces, in that as the spectral range increases, so do the interference orders, leading to problems of overlapping orders. Typically, the working range of a Fabry-Perot cavity, whereby there exists no overlapping orders, is defined as the free spectral range (FSR), given by the following equation

$$FSR = \Delta\lambda_{FSR} = \frac{\lambda_0^2}{2nl} \tag{3.15}$$

Where λ_0 is the central wavelength, and l is the optical cavity length. $\Delta\lambda$ is the optical wavelength between two successive reflected or transmitted optical intensity maxima of the interferometer, as illustrated in Figure 3.5.

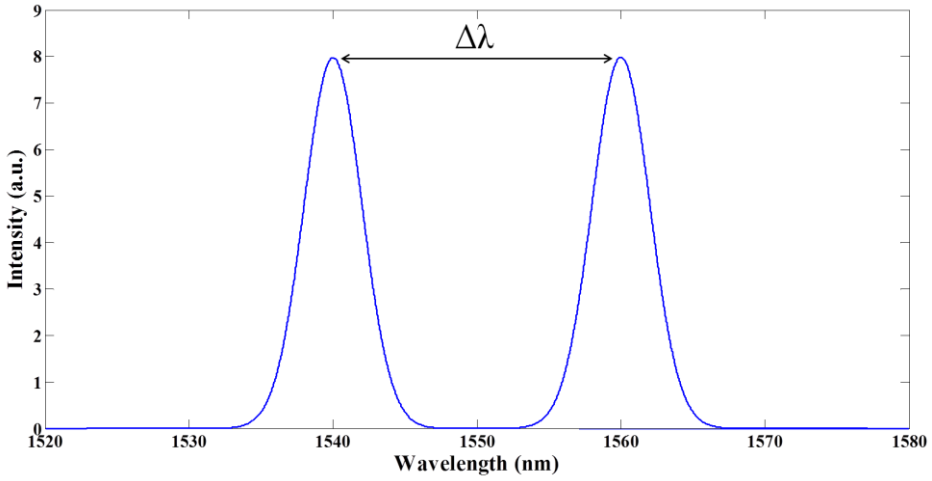

Figure 3.5: Free spectral range definition.

When using a broadband light source to illuminate a Fabry-Perot cavity for the generation of interference fringes, the FSR can be used for analysis in determining the absolute optical cavity length be measuring the wavelength spacing between two adjacent peaks.

3.4. Tandem Interferometry

So far, details of the Michelson interferometer and the Fabry-Perot interferometer have been described, and individual analysis given as to how interference effects occur within each of the interferometers. Further details as to how, with the use of different light sources, these interferometers can be used as a means of providing length measurements will be given in the sub-sections to follow. The measurements obtained from these interferometers are, however, when using a broadband light source, limited to the FSR of the arrangement. One method to overcome this problem and provide measurements over an extended range is based on tandem interferometry.

A tandem interferometer configuration, usually employing a broadband light source to utilise the properties of low coherence interferometry, consists of two interferometric arrangements, where the output from one interferometer, known as the sensing interferometer, couples into a secondary interferometer, known as the receiving interferometer. The use of low coherence light reduces the sensitivity of environmental effects on the connecting optical paths between the two interferometers, making this an ideal solution when measurements are at widely separate locations. A simple tandem interferometric arrangement is shown in Figure 3.6.

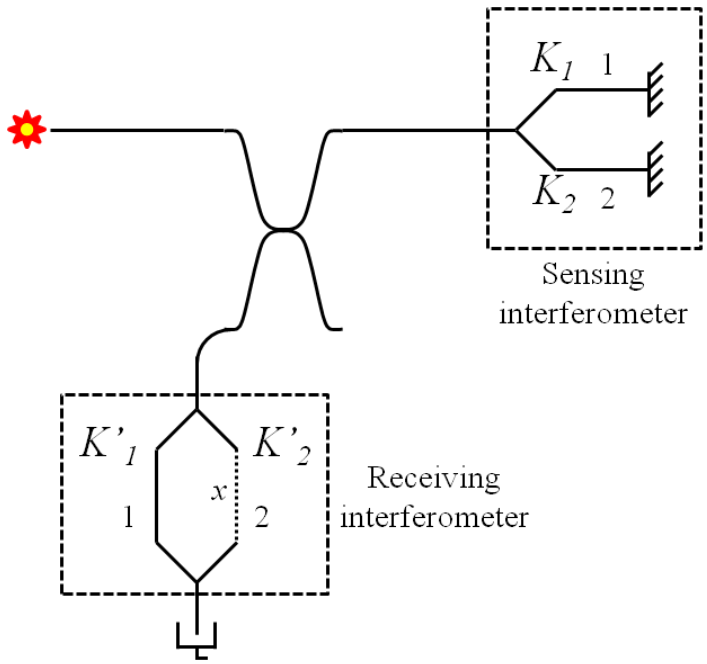

Figure 3.6: Simple fibre optic tandem interferometer arrangement.

The sensing interferometer is usually positioned within the measurand field of interest, whilst the receiving interferometer is commonly isolated from this and kept within a controlled environment. The OPL difference of each interferometer is arranged to be larger than the coherence length of the light source, such that when individually illuminated, interference fringes will not be observed due to the delayed imbalance present in both.

When a variable optical path is introduced into the receiving interferometer, illustrated by length *x* in Figure 3.6, interference effects are observed when the OPL difference of this interferometer and the OPL difference of the sensing interferometer are matched to within the coherence length of the light source. The phase and visibility of the resulting interferometric signal will be a function of the two interferometer OPL differences.

Considering the arrangement as illustrated in Figure 3.6, showing the different optical paths through which the light can propagate, the electric field output of this tandem configuration can be expressed in the following way (7)

$$E = E_{11} + E_{12} + E_{21} + E_{22} \tag{3.16}$$

E_{ij} is the component of the electric field generated from light propagation through the i^{th} arm of the receiving interferometer and the j^{th} arm of the sensing interferometer, given by (7)

$$\begin{aligned} E_{11} &= A_{11}e^{i\phi} \\ E_{12} &= A_{12}e^{i(\phi+kX_1)} \\ E_{21} &= A_{21}e^{i(\phi+kX_2)} \\ E_{22} &= A_{22}e^{i(\phi+k(X_1+X_2))} \end{aligned} \tag{3.17}$$

Where A_{ij} is the wave amplitude, k and ϕ are the wave number and the phase respectively of E_{ij}, and X_1 and X_2 are the OPL differences between the sensing and receiving interferometers.

In order to obtain the intensity at the output, the time averaged square of equation 3.17 is taken. This is the product of the overall output electric field and its complex conjugate. If the terms that, due the coherence length of the source, are equal to zero are removed and if I_4 is the intensity of the path in which the OPL difference of the two interferometers is less than the source coherence length, the output intensity will be given as follows (8)

$$I = I_0\left\{1 + I_4\left|\gamma(X_1 - X_2)\right|\cos\left[k(X_1 - X_2)\right]\right\} \tag{3.18}$$

Where $\left|\gamma(X)\right|$ is the absolute value of the normalised autocorrelation function.

If it is assumed that the autocorrelation function of the low coherence light source has a Gaussian profile, and the power splitting ratios (K_1, K_2, K'_1, K'_2) of the two interferometers are taken into consideration, the output intensity can be rewritten as (8)

$$I = I_0\left\{1 + 2\sqrt{K_1K_2K'_1K'_2}\,e^{-\left(2(X_1-X_2)/l_c\right)^2}\cos\left[k(X_1 - X_2)\right]\right\} \tag{3.19}$$

When the power splitting ratios of the interferometers are all equal, the fringe visibility is maximised when X_1-X_2 is equal to zero. Any change of OPL in the sensing interferometer with respect to the receiving interferometer will result in a change to the fringe visibility and the phase of the signal.

Changes to the OPL can be monitored via scanning the receiving interferometer with changes in the central fringe position used to determine the absolute OPL change of the sensing interferometer. It is also possible to incorporate a secondary light source, usually a highly coherent laser source, as a means of monitoring changes in OPL. This is an approach which has been utilised in this research, with details of how the different light sources will interact with such an arrangement to follow.

3.5. Light Sources

There exist many different types of light source which can be used in interferometric systems in order to produce a range of interference effects which can, in their own particular way, give information regarding the effects which are observed. The common used light sources include, laser (or monochromatic) sources, for example Helium-Neon (HeNe), light emitting diodes (LED's), super-luminescent diodes (SLED's), super-continuum light sources, and Xenon lamp sources. The three latter light sources are also commonly referred to as broadband or white light sources. Each light source has a different emission profile, as shown in Figure 3.7, and so the interaction of each with an interferometric system will provide different results.

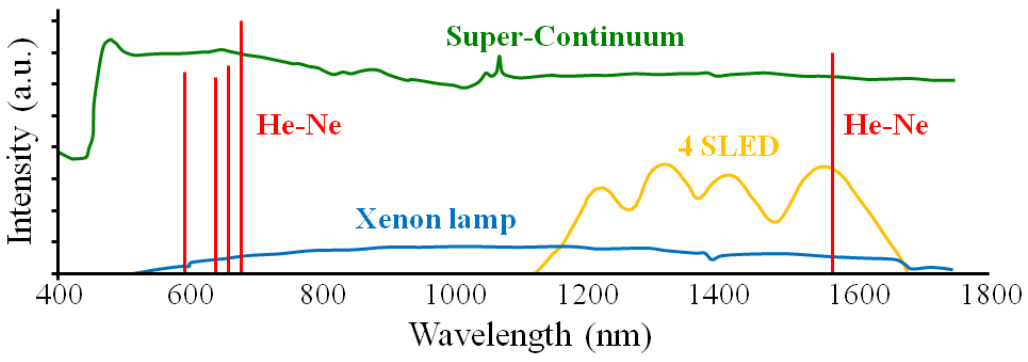

Figure 3.7: Emission profile for different light sources (9)

For the purposes of this research, focus will be paid on the properties of laser light and SLED's. Before reviewing the interference effects these light sources will exhibit when exposed to the Michelson interferometer and the Fabry-Perot interferometer, the properties which will effect these interactions, in particular, the spectral width, and coherence length will firstly be discussed. Additionally the previously mentioned, FSR is also an important property with respect to evaluating interference fringes generated from an interferometer.

Although super-continuum and Xenon lamp light sources have a greater spectral width than SLED sources they were not considered for this research. Although they theoretically are beneficial to achieve an accurate determination of the central location of an interference fringe burst, the use of such light sources requires the use of optical components which support a very wide spectral bandwidth. However commercially available fibre optic components rarely exhibit a usable spectral bandwidth in excess of 40-60 nm. Outwith this operating bandwidth the properties are unknown and at specific wavelengths of a super-continuum or Xenon lamp source the component may not be operating in its characterised fashion. It may also be the case, although it may not be clear due to the arbitrary unit intensity scale used in Figure 3.7, that the optical output powers from super-continuum and Xenon lamp sources over a small bandwidth region may not be as sufficient as that generated from an SLED source.

3.5.1. Spectral width

Every light pulse has a spectral width, or bandwidth, over which light is transmitted. The spectral width is defined as the width of the optical spectrum of the output of a light source, usually specified in terms of frequency or wavelength. The spectral width is measured across the region where the power of the light is equal to half the maximum power, or where the magnitude is equal to -3dB, as illustrated in Figure 3.8. This position, and also the value of the spectral width, is commonly referred to as the full width half maximum (FWHM).

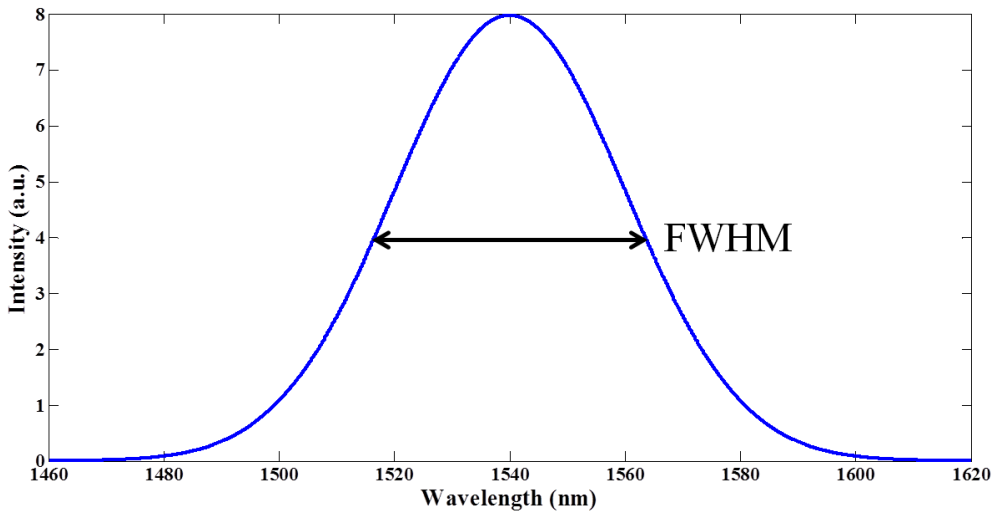

Figure 3.8: Measurement of a light source spectral width.

FWHM is an expression of the extent of a function, given by the difference between the two extreme values of the independent variable at which the dependent variable is equal to half of its maximum value. Not only is the FWHM applied to the duration of a pulse waveform and the spectral width of a light source, but it is also used in describing spectrometer resolution.

The FWHM method may be difficult to apply when the spectrum has a complex shape. Another method of specifying spectral width is a special case of root-mean-square deviation where the independent variable is wavelength, λ.

Due to the inverse relationship of frequency and wavelength, the conversion factor between gigahertz and nanometers depends on the centre wavelength or frequency. The following equation is used when converting a small wavelength interval into a frequency interval

$$\Delta\nu = \frac{c}{\lambda^2}\Delta\lambda \tag{3.20}$$

As will be discussed in the following section for determining the coherence length of a light source, the spectral width, or bandwidth, can be measured in terms of either wavelength or frequency.

3.5.2. Coherence length

Coherence is one of the most important concepts in interferometry and describes the ability of light to exhibit interference effects. Coherence, dependant on the characteristics of the light source, is a measure of the correlation that exists between the phases of a wave measured at different points. A light field is called coherent when there is a fixed phase relationship between the electric field values at different locations or at different times. Partial coherence means that there is some correlation between phase values.

There exist two different aspects of coherence which need to be considered, spatial and temporal. When a source is said to be spatially coherent, there exists a fixed phase relationship between the electric fields at different locations across the beam profile. This is the essential requirement for strong directionality of laser beams. A strong temporal coherence means there is a fixed phase relationship between the electric fields at one location but different times.

The coherence length of a light source is the propagation distance from the source to a point where an electromagnetic wave maintains a specified degree of coherence. The significance is that interference will be strong within the coherence length of the source, but not beyond it, where phase relations between two different rays become random. In long-distance transmission systems, the coherence length may be reduced by propagation factors such as dispersion, scattering, and diffraction.

The coherence length, l_c, is given by the coherence time, t_c, the degree of first order temporal coherence via the time over which the coherence is lost, multiplied by the speed of light in a vacuum, c,

$$l_c = ct_c \tag{3.21}$$

This also characterises the temporal coherence via the propagation length, and propagation time, over which coherence is lost.

The coherence length of light can also be defined in terms of the spectral width of the source, given by

$$l_c = \frac{c}{n\Delta\nu} = \frac{\lambda^2}{n\Delta\lambda} \tag{3.22}$$

Where λ is the central wavelength of the source, n is the refractive index of the medium, and $\Delta\nu$ and $\Delta\lambda$ is the spectral width of the source in terms of frequency and wavelength respectively.

In the case of laser light sources, where the spectral width is small, the coherence length can reach up to hundreds of meters, making this a suitable source for use in determining length changes over a large distance. Broadband sources on the other hand, which can have relatively large spectral widths, may only have a coherence length in the order of micrometers. This makes for a difficult task in matching OPL's in order to observe interference effects as the lengths may have to be matched to within a few micrometers of each other. They can however be useful in situations where precise measurements of small lengths are required.

3.5.3. Laser light source

A device that emits light through a process of optical amplification based on the stimulated emission of electromagnetic radiation is referred to as a 'laser' source, an acronym of "light amplification by stimulated emission of radiation". A laser differs from other light sources as it emits light coherently. Spatial coherence allows a laser to be focused to a tight spot, enabling applications like laser cutting and lithography. Spatial coherence also allows a laser beam to stay collimated over long distances, making such devices as laser pointers possible.

It is the high temporal coherence of a laser that allows them to have a very narrow spectral width, and in turn a very large coherence length. Typically a HeNe laser, which emits light at a wavelength of 632.8 nm, has a spectral width down to 1 MHz (10). This equates to having a coherence length, in free space, of 300 m. Due to the high coherence length of using a laser source, it allows interference fringes to be observed

without the need to have the OPL's of the two arms of a Michelson interferometer closely matched.

As commented on in section 3.2, when illuminated with a light source, which could be a laser, the output of the Michelson interferometer, shown in Figure 3.1, when viewed on a projection screen, will exhibit interference rings, previously illustrated in Figure 3.2. If as oppose to monitoring the full interference rings and instead, using an indium gallium arsenide (InGaAs) photodiode to monitor the centre of the rings, the intensity of the light, when the Michelson is in a stationary position, will either by at a maximum if the optical path difference is equal to half the wavelength of the source, a minimum if the optical path difference is equal to the wavelength of the source, or at a intermediate power dependant on the difference.

A change to the OPL of one of the Michelson interferometer arms, as a result of a change in mirror position if using a bulk optical arrangement, or a change in the physical length or through a pressure or temperature change if using a fibre optic arrangement, will therefore result in a sinusoidal varying intensity, through maxima and minima, measured at the photodiode. The interference fringes resulting from the laser light intensity change as the OPL difference is being altered is illustrated in Figure 3.9. The fringes shown are a modelled representation of a Michelson interferometer with a changing OPL in one arm illuminated with a 1310 nm DFB laser source.

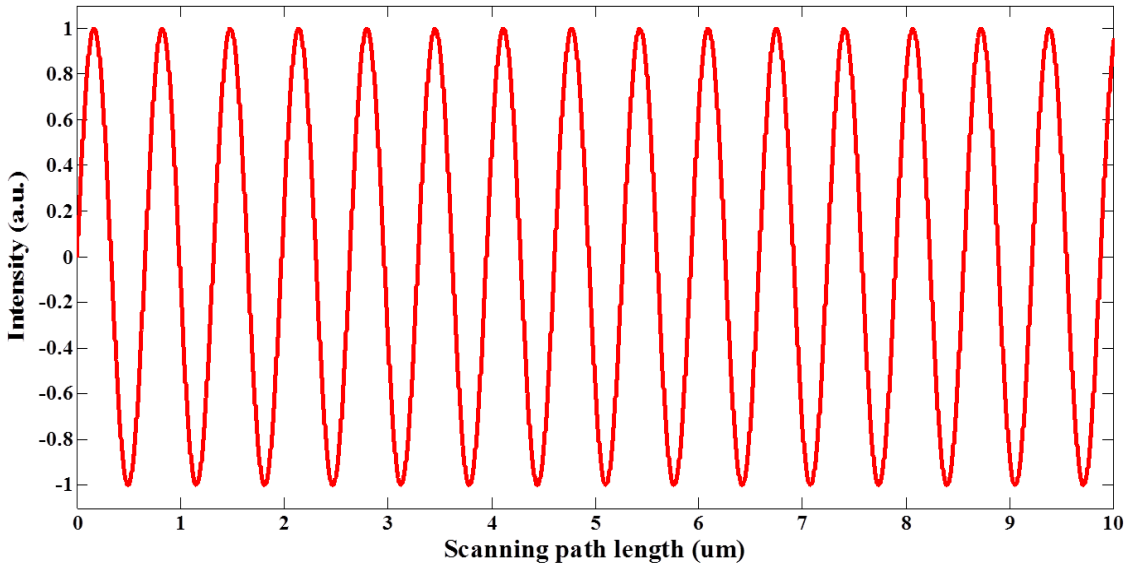

Figure 3.9: Modelled interference fringes, generated through implementation of Equation 3.4, of a 1310 nm DFB laser source from a Michelson interferometer due to a changing OPL of one arm.

Maxima correspond to changes in length of half the wavelength of the light source, and minima are observed when the change corresponds to the beams being 180° out of phase, therefore, it can be deduced that for one full fringe to appear, the optical path displacement must be equal to half the wavelength of the light source. Knowing this, the optical path length change can be determined from,

$$d = \frac{N\lambda}{2} \tag{3.23}$$

Where N is the number of interference fringes generated during the process of optical displacement.

It is as a consequence of the short spectral width and corresponding large coherence length of a laser light source, that it is possible to observe sinusoidal interference fringes from a Michelson interferometer due to a change in OPL of one of the interferometer arms over a wide range. As will be discussed in the following section, this would not be a possibility when using a broadband light source with a large spectral width. It is for this reason, that for use in this project whereby the Michelson interferometer is acting as

a reference interferometer as a means of measuring a optical path length change, that a laser light source is used alongside a fringe counting technique to accurately determine optical displacements.

3.5.4. Super-luminescent light source

An SLED, similarly to a laser diode, is based on an electrically driven pn-junction. When this junction is in the forward biased direction it becomes optically active, generating amplified spontaneous emission (ASE) over a wide wavelength range. The active material and the current injection level are responsible for the peak wavelength and intensity at which the diode emits. Unlike a laser diode, an SLED has insufficient feedback to achieve lasing, as they are typically designed to have single pass amplification for the spontaneous emission generated along the wavelength (11).

In comparison to a laser light source, which has a very narrow spectral width, SLED's can have a very broad spectral width, in some cases up to hundreds of nanometers, as shown in Figure 3.10.

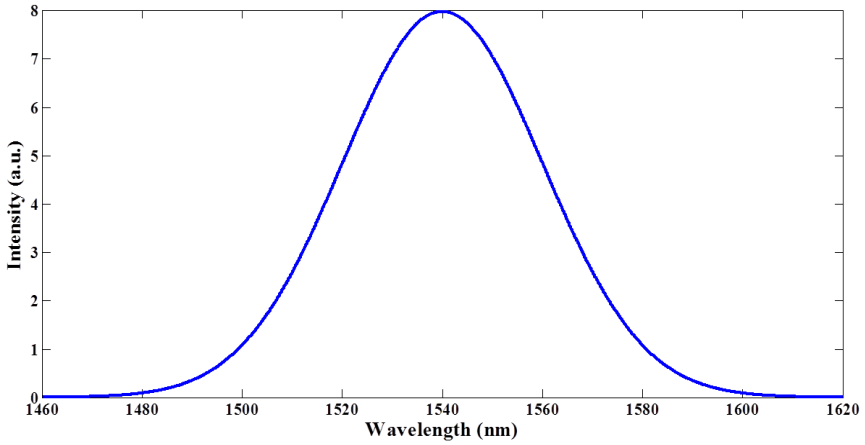

(a)

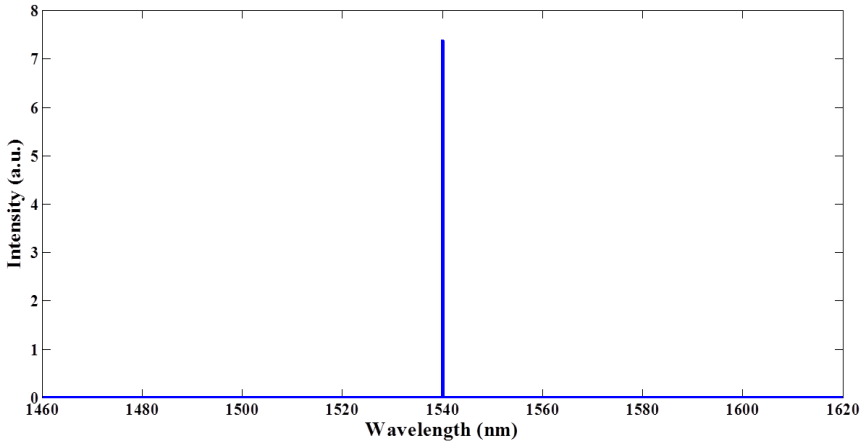

(b)

Figure 3.10: FWHM comparison between (a) a broadband light source and (b) a laser light source.

As a result of this large spectral width, the coherence length of most SLED's is very short, and can be as little as micrometers in length. As interference effects are not permissible out with the coherence length of a source, using broadband light for length measurements with a Michelson interferometer can be a difficult task as only OPL differences within the coherence length can be monitored.

If, as before, when the output intensity from a Michelson interferometer is being monitored via an InGaAs photodiode, interference fringes will be observed when the OPL of one of the interferometer arms is changing with respect to the other, however, in

contrast to using a laser light source, this interference pattern will only be observable when the OPL difference of the two arms comes within the coherence length of the source. The envelope of the interference pattern follows that of the source profile, with the maximum intensity occurring when the OPL's are equal, as illustrated in Figure 3.11. The fringes shown are a modelled representation of an interferometer with a matched OPL between two arms illuminated with a broadband light source centred at 1550 nm with a spectral width of 263.93 nm. This particular light source will have a coherence length of 6.20 μm within an optical fibre arrangement.

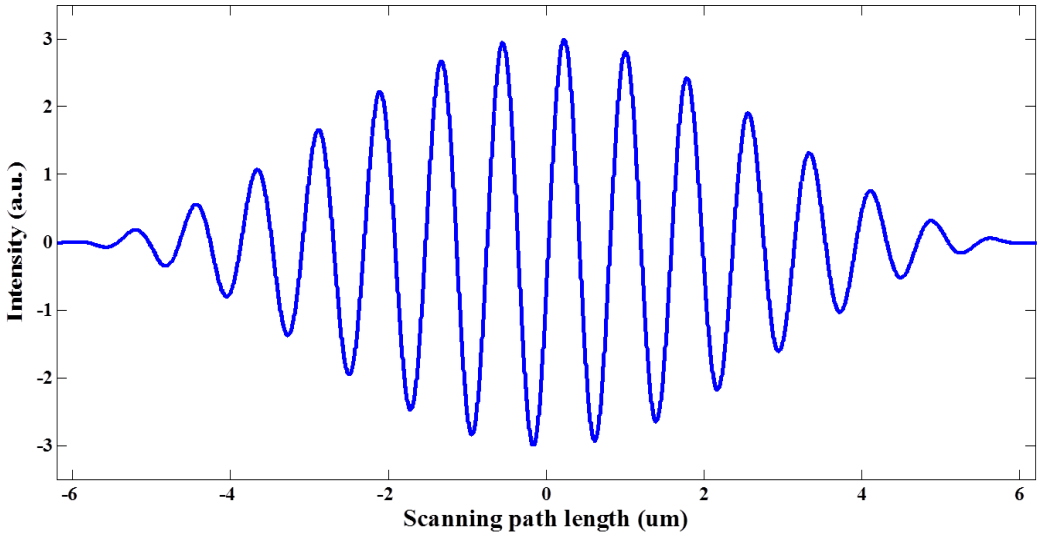

Figure 3.11: Modelled interference fringes, generated through implementation of Equation 3.19, from an equal OPL of a Michelson interferometer using a broadband light source centred at 1550 nm with a spectral width of 263.93 nm, corresponding to a coherence length of 6.20 μm.

As the resultant interference fringes only span over the coherence length of the source and are therefore not permissible over a large range, broadband light sources are not suitable for measuring the optical path displacement of a Michelson interferometer through fringe counting analysis, as would be possible with use of a laser source. It can however provide a reference measurement when arranged in tandem with a secondary interferometer, as will be described in the paragraphs to follow.

The interference fringes generated when using a light source with a wide spectral width, and small coherence length, occur when the OPL's are matched to within the coherence

length of the source. As is the case with interferometers arranged in a tandem configuration, as illustrated in Figure 3.12, when the OPL difference of the first interferometer is matched to the OPL of the secondary interferometer, interference fringes as in Figure 3.11 are again observable.

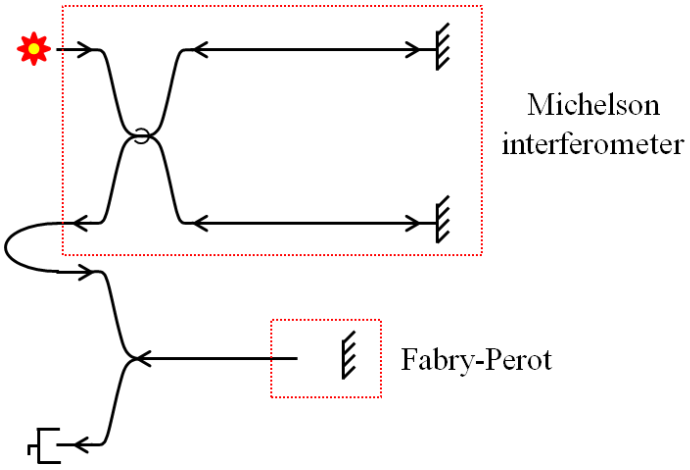

Figure 3.12: Fibre optic tandem arrangement of a Michelson interferometer and a Fabry-Perot interferometer.

Figure 3.12 shows a Michelson interferometer connected in tandem with a Fabry-Perot cavity, however it is possible to have any interferometer arrangement, for example a two Michelson configuration. The above arrangement however, forms the basis of the configuration used for determining length measurements in this study. Resulting interference fringes are observable via the photodiode detector when the Michelson interferometer OPL's are equal, and also when the difference in the OPL's is equal to the Fabry-Perot cavity length. The secondary fringe packet from the matched optical lengths with the Fabry-Perot cavity follows the same shape and covers the same span as that of the first fringe packet, however due to the loss of light through coupling in the Fabry-Perot cavity, the intensity of the resulting fringes is less, as shown in Figure 3.13. The fringes shown are a modelled representation of a tandem interferometer arrangement illuminated with a broadband light source centred at 1550 nm with a spectral width of 263.93 nm. This particular light source will have a coherence length of 6.20 μm within an optical fibre arrangement.

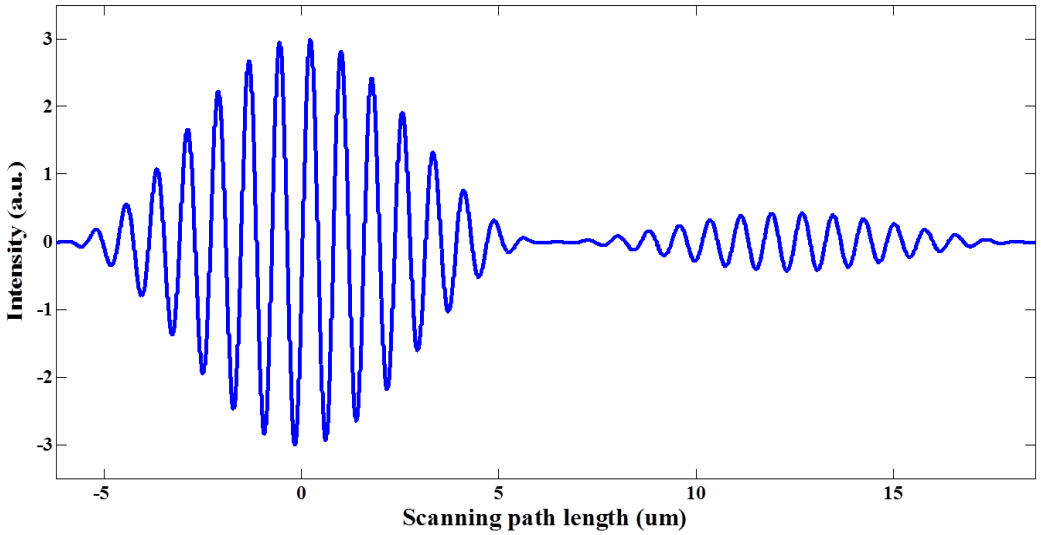

Figure 3.13: Modelled interference fringes, generated through implementation of Equation 3.19, from a tandem interferometer arrangement illuminated with a broadband light source centred at 1550 nm with a spectral width of 263.93 nm, corresponding to a coherence length of 6.20 μm.

It was mentioned previously that when using an SLED, it would not be possible to measure optical length displacement through a fringe counting technique due to the limited range over which interference fringes are observable due to the coherence length of the light. It is however possible to use this as a reference in order to obtain length measurements of a secondary interferometer when arranged in a tandem configuration. This is the principle applied to the arrangement and resulting interference fringes from Figures 3.12 and 3.13 respectively.

Knowing that, when the Fabry-Perot interferometer cavity remains constant, the two sets of generated fringe packets correspond to different OPL's of the Michelson interferometer, it is possible to determine the Fabry-Perot length through displacement analysis of the adjustable Michelson mirror between consecutive fringe patterns. The important aspect for accurate measurements is the determination of the central position of the fringe packet, possible through obtaining the interference fringe packet envelope. One means of acquiring the desired envelope is with the use of the Hilbert transform.

3.6. Hilbert Transform

When using a broadband light source to illuminate an optical interferometer, interference fringes are visible when the path imbalance of the two interferometer arms is equal to zero, or when equal to the path imbalance of an adjacent interferometer connected in tandem. The width of this interference pattern is determined by the spectral width, and in turn the coherence length of the light source.

When using a tandem arrangement, where one interferometer is acting as a reference point, determination of the central position of the interference fringe packet is an essential aspect. It is at this position where the OPL's of the reference interferometer are equal and from where the measurement must be taken in order to obtain accurate readings. The interference fringe pattern, and spacing between adjacent fringes, is determined by the coherence length of the source. It could be said that in order to obtain the central fringe pattern position, one could simply find the peak amplitude of the interference pattern, as shown in Figure 3.14.

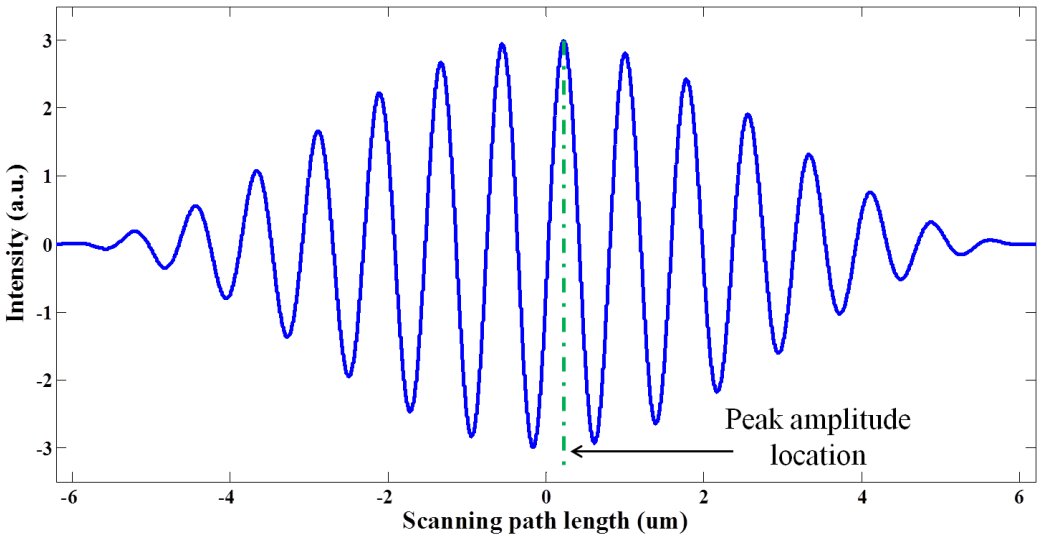

Figure 3.14: Modelled low coherence interference fringes, generated through implementation of Equation 3.19, from a broadband light source centred at 1550 nm with a spectral width of 263.93 nm, corresponding to a coherence length of 6.20 μm, showing the peak amplitude position.

This may seem like the easiest method for determining the central position, especially when the spectral width of the source results in a limited number of fringes being generated within the coherence length, however it is inaccurate to assume that the maximum peak amplitude corresponds to the central fringe within the packet. This is also not an accurate definition for the central position as with the introduction of noise uncertainty along the signal, the maximum peak intensity could correspond to a neighbouring fringe or position of a large noise burst.

An alternative, and more accurate, approach for the determination of the central interference fringe packet position would be to obtain the envelope shape of the overall fringe packet, and from this, obtain the central position, as illustrated in Figure 3.15.

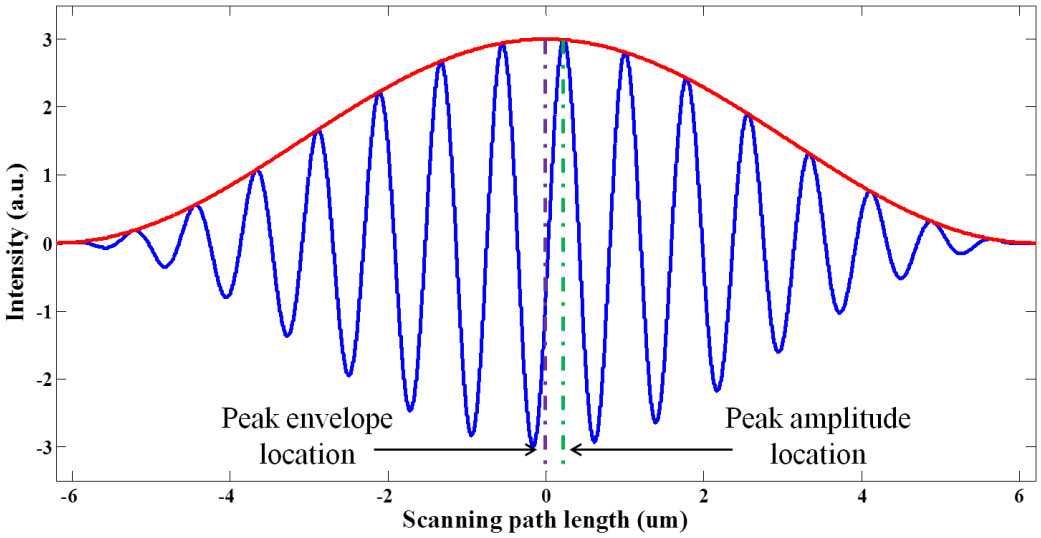

Figure 3.15: Modelled low coherence interference fringes, generated through implementation of Equation 3.19, from a broadband light source centred at 1550 nm with a spectral width of 263.93 nm, corresponding to a coherence length of 6.20 μm, showing the peak envelope location and the differing location of the peak amplitude.

There are a number of techniques for obtaining a signal envelope. One method in particular which was deployed in this project is the Hilbert transform.

The Hilbert transform, named after David Hilbert who first introduced the operator in order to solve a special case of the Riemann–Hilbert problem for holomorphic functions (12), is a common tool used in mathematics and in signal processing. It was originally

defined as the transformation of *sin ωt* as *cos ωt* and was then introduced to signal processing as a generalisation of Euler's formula, $e^{jz} = \cos(z) + j\sin(z)$, as the complex analytical signal $\psi(t) = u(t) + jv(t)$, where *v(t)* is the Hilbert transform of *u(t)* (13).

When using a white light source, the mathematical expression of an optical interferogram at an individual location can be expressed as (14),

$$g(z) = a + bc(z-h)\cos\left(\frac{4\pi(z-h)}{\lambda_0} + \varphi\right) \tag{3.24}$$

Where *a* and *b* are the offset of the interferogram and modulation intensity respectively, *z* and *h* are the longitudinal co-ordinate and the height profile of the measured object respectively, and *c* is the interferogram envelop function. Typically the envelope of a broadband light source will have a Gaussian form.

The interferogram envelope is calculated from the interferogram given by equation 3.24 using the Hilbert transform, denoted as

$$H(\omega) = -i\,\mathrm{sgn}(\omega) \tag{3.25}$$

Where sgn(ω) equals

1 for $\omega > 0$

0 for $\omega = 0$

-1 for $\omega < 0$

The Hilbert transform of the product of two functions with non-overlapping spectra equals the product of the low frequency function by the Hilbert transform of the high frequency function. For the interferogram described above, the low frequency function is the interferogram envelope, and the high frequency function is the cosine function.

Applying the Hilbert transform to the interferogram alters the phase and also removes the offset (15), calculating the envelope as

$$e_j = bc\left(j\Delta z - h\right) \tag{3.26}$$

Where Δz is the sampling step, and j is the sample order number (j = 0, 1, 2, ...). The subscript j expresses that both the interferogram and the envelope are sets of discrete values defined for $z_j = j\Delta z$ (14).

By extracting the envelope profile of the interference fringe packet generated from the tandem interferometric arrangement when illuminated with a broadband light source, analysis can be made in order to determine desired cavity lengths, and changes in them.

3.7. Piezoelectric Theory

The theory detailed in this chapter so far shows that interference effects are observable when an optical fibre system, illuminated with either a broadband or laser light source, undergoes a change in OPL of one of the interferometer arms. Such a change can achieved through modifying the index or physical length of the fibre. In the case of this research whereby it will be required to periodically scan through a length change in an optical fibre, one method of achieving this would be via stretching of the fibre length with the use of a piezoelectric ceramic.

For many flow experiments quasi-static pressure measurements are often sufficient and, in the case of the requirements of this research, a bandwidth equivalent to one measurement every ten to twenty seconds would be suitable for such a system. This is plausible with the use of a piezoelectric ceramic as the applied voltage across the material can be periodically scanned resulting in expansion and contraction of the optical fibre coiled around the ceramic length.

Piezoelectricity, discovered in the 1880's by brothers Pierre and Jacques Curie, is a property exhibited by certain crystalline materials, in which the crystalline structure produces a voltage, proportional to a mechanically applied pressure (16). Alternatively, when an electric field is applied to such a material, the structure changes shape

producing dimensional changes in the material. Certain compounds can be made piezoelectric by the application of a high electric field and are termed ferroelectric materials. Examples of piezoelectric materials are quartz and ferroelectric crystals.

Another important group of piezoelectric materials are the piezoelectric ceramics, such as PZT. These polycrystalline ferroelectric materials, made with a perovskite crystal structure, are solid solutions of lead Titanate ($PbTiO_3$), and lead Zirconate ($PbZrO_3$), modified by additives. Each cell of the crystal lattice in a ferroelectric crystal spontaneously polarises along one of a series of allowed directions. This spontaneous polarisation is no longer observable at a critical temperature, known as the Curie point. A PZT ceramic can be regarded as a series of randomly oriented crystallites before polarisation, due to which the material will be isotropic and will exhibit no piezoelectric effect. The ceramic will be made piezoelectric in a chosen direction by a poling treatment. During this treatment the ceramic will be exposed to a high electric field across the poling direction, usually at an elevated temperature, causing switching or realignment of the dipoles in the ferroelectric material as shown in Figure 3.16.

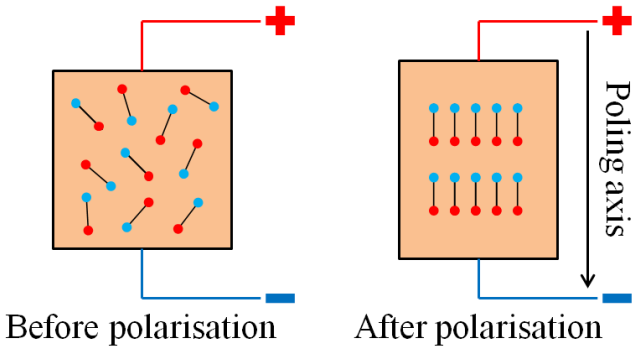

Figure 3.16: Schematic showing the alignment of the dipoles in a PZT material.

After removal of the electric field there is a remanent polarisation in the ceramic which is responsible for its piezoelectric properties. The resulting ceramic is also anisotropic. PZT components usually have metal electrodes positioned perpendicular to the poling axis in order to allow the application of a voltage across them resulting in a distortion along the poling axis.

Figure 3.17 shows the piezoelectric effects due to applied voltage along the poling axis for a PZT ceramic rod. When the applied voltage is of the same polarity as the poling

voltage, the rod will lengthen. Alternatively if the applied voltage is the opposite to that of the poling voltage, the rod will shorten. Figure 3.17 also shows the effect of applying an alternating voltage across the electrodes. In this case the PZT rod will expand and contract at the same frequency as that of the applied voltage.

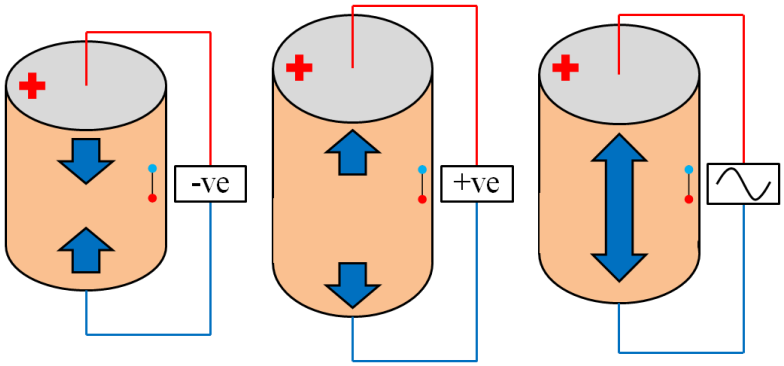

Figure 3.17: Schematic showing the expansion and contraction effects of a PZT rod with applied voltage across the polling axis.

In the case of this research, as will be discussed in further detail in Chapter 4, where expansion of an optical fibre to induce an optical length change will be the result of a fibre length coiled around a PZT tube, the poling axis and applied voltage directions are shown in Figure 3.18

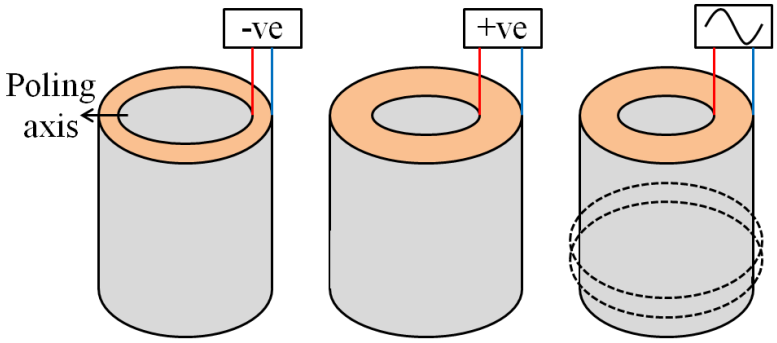

Figure 3.18: Schematic showing the poling directions of a PZT tube and the expansion and contraction with applied voltage.

By applying a positive voltage to the piezoelectric tube, the outer diameter of the tube will expand. The following equations detail the length and diameter expansion of the ceramic tube with the applied voltage.

$$\Delta l = \frac{2d_{31}Vl}{(d_o - d_i)} \qquad \Delta d_m = \frac{d_{33}d_m V}{t} \tag{3.27}$$

Where l is the tube length, V is the applied voltage, d_{31} and d_{33} are strain constants of the material, d_o and d_i are the tube's outer and inner diameters respectively, t is the tube thickness, and $d_m=(d_o+d_i)/2$.

Greater expansion of the piezoelectric tube can be achieved with a greater applied voltage. There is however a limitation to this. A piezoelectric ceramic can be depolarised by a strong electric field with polarity opposite to that of the poling voltage, as would be the case during the voltage drop if applying an alternating voltage cycle. This limit is dependent on the material properties, the duration of the application, and the operating temperature. In the case of the piezoelectric tubes used in this work, the limit of applied electric field is 500 V/mm, of the tube thickness.

3.8. Diaphragm Theory

So far within this chapter a theoretical review has been carried out, investigating the techniques which could be incorporated in order to develop a suitable arrangement for the measurement of a differential length. By utilising the characteristics of a deformable diaphragm, it is possible to convert such a length measurement into a pressure measurement.

A diaphragm is assumed to be a plate consisting of an elastic, homogeneous, isotropic material with a uniform thickness for which the deflection is small in comparison with the diaphragm thickness. Theoretical analysis of diaphragm characteristics has been covered in texts (17, 18), however it is important for the purposes of optimising pressure sensing to understand the key parameters that influence the diaphragm performance. Material type, thickness, and diameter can all be varied to optimise the

sensor performance in order to maximise, for a given sensing range, the diaphragm deflection, pressure sensitivity, and frequency response.

The general types of diaphragm shape that can be used in pressure sensing (19), are circular (20) and square (21). A circular diaphragm, due to the negligence of the residual stress at the circumference of the diaphragm surface, compared with a square diaphragm, has been considered for the construction of the sensor head used for differential measurements. The relationships of the diaphragm deflection, sensitivity, and frequency response with the material thickness and diameter are all considered in the following sections.

3.8.1. Diaphragm deflection

When an external pressure is applied, a circular diaphragm clamped around its circumference, will be uniformly loaded causing deformation, as illustrated in Figure 3.19.

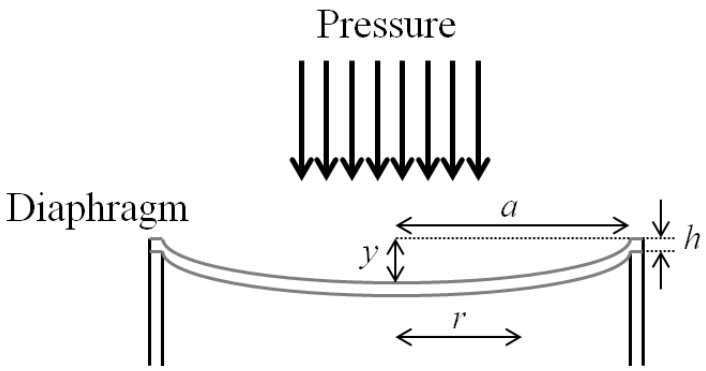

Figure 3.19: Deformation of a circular diaphragm due to pressure.

The differential pressure will result in the diaphragm bending into a quasispherical shape in the centre, but will reverse its curvature at a finite distance from the centre as a result of reactive moments at the periphery (22).

The surface deflection, *y*, of a diaphragm under differential pressure, *P*, in the linear regime, as a function of the pressure difference at any radius position, *r*, given as (23)

$$y(r) = \frac{3(1-\mu^2)P}{16Eh^3}\left(a^2 - r^2\right)^2 \tag{3.28}$$

Where *a* and *h* are the radius and the thickness of the diaphragm respectively, and *E* and μ are Young's modulus and Poisson's ratio of the diaphragm material respectively.

If the considered sensor design consists of the optical fibre used to carry light to and from the cavity, positioned at the centre of the diaphragm as shown in Figure 3.19, it is assumed that the cavity length is defined as the distance from the centre of the diaphragm and the optical fibre. The sensor sensitivity, described as the ratio of diaphragm deflection to applied pressure, can be estimated from the deflection of the centre of the diaphragm given as

$$y(0) = \frac{3(1-\mu^2)Pa^4}{16Eh^3} \tag{3.29}$$

For the diaphragm pressure sensor, the maximum tolerable pressure P_m corresponds to the maximum tolerable tensile stress, occurring at the central position of the diaphragm, at which the diaphragm is expected to break. This is given by

$$P_m = \sigma_m \frac{8}{3(1+\mu)}\frac{h^2}{a^2} \tag{3.30}$$

Where σ_m is the maximum tensile stress of the diaphragm material.

Ideally the diaphragm deflection should have a linear response to the exerted pressure, however, it is known that the diaphragm response will never be truly linear. The maximum linear response pressure P_0, which is defined as the maximum pressure

within which the diaphragm strain/pressure relation remains approximately linear, to within 2%, is given by

$$P_0 = \frac{8E}{3\left(1-\mu^2\right)}\left(\frac{h}{a}\right)^4 \tag{3.31}$$

If it is possible to operate within the linear regime then signal processing is simplified, however it is important to note that it is the burst pressure that defines the maximum operating pressure limit.

3.8.2. Diaphragm sensitivity

The diaphragm will be deflected when there is a differential pressure, *P*, between the inside and the outside of a sealed cavity. When monitoring the deflection at the centre of the diaphragm equation 3.29 can be used for determination of the diaphragm sensitivity, δ_{diap}.

Through rearrangement of equation 3.29 the diaphragm sensitivity, defined as the ratio between the deflection and the pressure, is given as

$$\delta_{diap} = \frac{y(0)}{P} = \frac{3\left(1-\mu^2\right)a^4}{16Eh^3} \tag{3.32}$$

For the monitoring of pressure, a diaphragm with high deflection sensitivity is desirable.

3.8.3. Frequency response

An important aspect to consider when designing the sensing diaphragm is the frequency response, as generally, in order to obtain a flat response within a specific frequency range, the function point should be set far lower than the natural frequency. In order to measure dynamic pressure at high frequency, a high natural frequency is desired. The diaphragm can be described as a free vibrating circular disc clamped at its sides, and so the frequency response is analysed in terms of its resonant frequency. A resonance

occurs when the oscillation frequency matches the natural frequency of the diaphragm. The natural frequency, f_{mn}, is expressed as (23)

$$f_{mn} = \frac{\alpha_{mn}}{4\pi}\sqrt{\frac{E}{3\rho(1-\mu^2)}}\left(\frac{h}{a^2}\right) \tag{3.33}$$

Where α_{mn} is a constant relating to the vibrating modes of the diaphragm, and ρ is the mass density of the diaphragm material.

The lowest natural frequency, f_{00}, corresponds to a mode in which the maximum oscillation amplitude is at the centre of the diaphragm and only the clamped edges are stationary, therefore there are no additional nodes or anti-nodes associated with higher order vibration modes.

At this frequency, α_{mn} is equal to 10.21, giving the equation for the natural frequency (23),

$$f_{00} = \frac{10.21}{2\pi a^2}\sqrt{\frac{D}{h\rho}} \tag{3.34}$$

Where

$$D = \frac{Eh^3}{12(1-\mu^2)} \tag{3.35}$$

D is termed as the flexural rigidity of the diaphragm. To ensure that the diaphragm operates within the linear range, the resonance frequency of the diaphragm should be three to five times the size of the applied frequency (22).

3.8.4. Flexural rigidity

The radius and the thickness of a sensing diaphragm are major contributors to the deflection and sensitivity when pressure is applied, however the material characteristics and thus the stiffness of the diaphragm must be also taken into consideration. The

flexural rigidity, expressed in equation 3.35, is defined as the force couple required to bend a rigid structure, and can be used to examine the stiffness of the diaphragm.

The expression for the flexural rigidity demonstrates that as the thickness of the diaphragm is increased the structure becomes more rigid and less flexible, which in turn causes the deflection of the diaphragm to decrease. Combining equations 3.29 and 3.35, the following expression shows the relationship between the flexural rigidity of a diaphragm and the maximum deflection at the centre where the radial distance is zero,

$$y = \frac{Pa^4}{64D} \tag{3.36}$$

It can be concluded that a thin diaphragm with a low flexural rigidity will provide the highest deflection and sensitivity due to the applied external pressure.

3.8.5. Diaphragm thickness

The relationship between an applied pressure and a diaphragm deflection is linear only when the deflections are small. When the deflection of an edge clamped diaphragm is even 10% of the thickness, tensile stresses will appear, and as the deflection is increased, the relationship between pressure and deflection will become non-linear. Diaphragms will however perform well even when the deflection is 30% of the thickness. At this deflection the terminal-based linearity is 2%, provided that the stress level is well within the proportional limit of the material.

The previous equations are therefore valid within the linear range when the diaphragm deflection is no more than 30% of the thickness, hence $y_{max}=0.3h$.

3.9. Theoretical Implementation for Experimental Work

In this chapter a theoretical review has been carried out. The theory within this chapter will be used throughout the following chapters as a means of developing a suitable technique for the measurement of a differential pressure through the determination of a

differential length. In order to develop such a sensing system the key theoretical knowledge has to be extracted and the methods of implementation considered.

Interference effects due to the differing coherence length characteristics of both broadband and laser light sources were discussed. Details of the different interference patterns generated from said light sources when interacting with interferometers in the forms of a Michelson and a Fabry-Perot were given, along with the conditions of how such fringes are produced for the individual interferometer arrangements. A theoretical analysis of a tandem arrangement of interferometers was also considered.

Interference of broadband light, generating a pattern with an envelope matching that of the source, occurs when the lengths of two optical paths are matched to within the coherence length of the light source. Due to the typically small coherence length of many broadband light sources this phenomenon could be utilised for the design goals of this research. With two Fabry-Perot sensing cavities arranged in a tandem configuration such that the differential length between them creates a measurable OPL, a Michelson interferometer with a changing OPL in one arm can be connected to this tandem arrangement in order to produce interference fringes, when illuminated with a broadband light source, when the mismatch in OPL of the two Michelson interferometer arms is equal to the OPL formed from the differential length of the sensing cavities. From a measure in the Michelson interferometer arm length mismatch, the corresponding differential length of the Fabry-Perot cavities can be found.

With a procedure in place for the determination of the differential length of interest, the Hilbert transform is implemented as a method of calculating the central position of the interference fringes, where the lengths of the two optical paths in question are equal to zero. From finding the central position of the zero order interference fringes of the Michelson interferometer, the location where the two interferometer arm lengths are equal, to the central position of the first order interference fringes, the location where the OPL difference of the two interferometer arms is equal to the OPL differential of the two Fabry-Perot cavities, an accurate determination of the change in length can be calculated.

Accurate determination of the differential length of interest is performed with the use of a secondary reference light source in the form of a DFB laser. Due to the different optical properties between a laser light source and a broadband light source, the corresponding interference patterns and the conditions under with they are formed are

different. Where a broadband source only forms fringes over a short range equal to the coherence length of the source, a laser light source, due to the large coherence length it possesses, can generate interference fringes over a wide range. When illuminating the Michelson interferometer with a laser source, interference fringes in a sinusoidal pattern are generated during the change in OPL of one of the interferometer arms. This is a physical change in the optical fibre length, generated via the expansion and contraction of a piezoelectric ceramic, around which the fibre is wound. Using a fringe counting analysis of the laser interference pattern generated between the zero order and first order broadband interference locations, the DFB laser becomes particularly useful for the determination of the length change in the Michelson interferometer, and subsequently the differential length of the two Fabry-Perot sensing cavities.

Through utilisation of the theory reviewed within this chapter, a sensing configuration for the measurement of a differential length can be developed, the full arrangement of which is described in Chapter 4. Diaphragm characteristics can then be deployed in such a system as to provide an accurate technique for differential pressure measurements.

3.10. Conclusion

In this chapter a review of the theory behind the optical arrangement which will be deployed within this project has been discussed and why these particular configurations have been selected due to their working principles.

The operational characteristics of a Michelson interferometer and of a Fabry-Perot interferometer have been described, in particular, light propagation throughout such a system configuration and the means in which interference effects become present. A similar approach was investigated with a tandem interferometric arrangement in which the output light from one interferometer will couple through a second interferometer before being detected via a photodiode. Such an arrangement is commonly used with low coherence light sources as a means of increasing the range over which measurements can be recorded.

Laser light and broadband light sources were investigated with focus on how each individual source, when illuminating the previously mention interferometers, generates differing interference patterns, due to the differences in the lights spectral profile.

Spectral width and coherence length were discussed and how, due to the differences in these for the two light sources used, the resulting interference fringes can be used for determining length changes in the optical paths of the corresponding interferometer.

The theory behind the Hilbert transform and how this transform can be used to obtain the envelope of an interference fringe packet, generated with the use of a broadband light source was discussed.

The expansion properties of piezo ceramics was considered as this will provide a means of inducing an OPL change within an optical fibre removing the need of light re-coupling if this change were to be achieved using a separate translation stage mounted mirror. As is the case with piezo ceramics, nonlinear expansion with applied voltage, and expansion hysteresis must be taken into consideration when dealing with high resolution measurements. These effects are considered in Chapter 4 along with a proposed technique which removes the need to consider the consequences of these characteristics.

Finally, how the reviewed theory can be implemented into a practical system is discussed and the key factors that are to be taken into consideration, along with deformable diaphragm theory for incorporation of such a system as a differential pressure sensor. The full sensing arrangement for the measurement of differential length will be described in Chapter 4.

3.11. References

1. Michelson AA. Détermination expérimentale de la valeur du mètre en longueurs d'ondes lumineuses: Gauthier-Villars et fils; 1894.
2. Michelson AA, Morley EW. On the Relative Motion of the Earth and the Luminiferous Ether. American Journal of Science. 1887;34:333–45.
3. University of New South Wales, Physclips www.animations.physics.unsw.edu.au/jw/light/Newton's-rings.html: School of Physics; [Available from: http://www.animations.physics.unsw.edu.au/jw/light/Newton's-rings.html.
4. Born M, Wolf E. Principles of optics : electromagnetic theory of propagation, interference and diffraction of light. 7th (expanded) ed. ed. Cambridge: Cambridge University Press; 1999.
5. Chen J, Chen D, Geng J, li J, Cai H, Fang Z. Stabilization of optical Fabry–Perot sensor by active feedback control of diode laser. Sensors and Actuators A: Physical. 2008;148(2):376-80.
6. Marcuse D. Loss Analysis of Single-Mode Fiber Splices. Bell System Technical Journal. 1977;56:703–18.

7. Jackson DA, Jones JDC. Fibre Optic Sensors. Journal of Modern Optics. 1986;33(12):1469-503.
8. Rao Y, Jackson D. Recent progress in fibre optic low-coherence interferometry. Meas Sci Technol. 1996;7(7):981-99.
9. Supercontinuum Generation in Photonic Crystal Fibres http://www.nktphotonics.com/supercontinuum: NKT Photonics; 2014 [
10. Melles Griot, Helium Neon Lasers 2015 [Available from: http://mellesgriot.com/products/Lasers/Helium-Neon-Lasers.
11. Velez C, Occhi L, Roschle M. Superluminescent LEDs Enter the Mainstream. Photonics Spectra. 2005;39(10):90-5.
12. Oppenheim AV. Study Guide for Discrete-Time Signal Processing: Cram101; 2010.
13. Hahn SL. Hilbert Transforms in Signal Processing: Artech House; 1996.
14. Pavliček P, Michálek V. White-light interferometry—Envelope detection by Hilbert transform and influence of noise. Optics and Lasers in Engineering. 2012;50(8):1063-8.
15. Onodera R, Hiroto W, Yukihiro I. Interferometric phase-measurement using a one-dimensional discrete Hilbert transform. Optical review. 2005;12:29-36.
16. Curie J, Curie P. Développement par compression de l'électricité polaire dans les cristaux hémièdres à faces inclinées. Bulletin de la Société minérologique de France. 1880;3:90-3.
17. Voorthuyzen JA, Bergveld P. The influence of tensile forces on the deflection of circular diaphragms in pressure sensors. Sensors and Actuators. 1984;6(3):201-13.
18. Schellin R, Hess G, Kühnel W, Thielemann C, Trost D, Wacker J, et al. Measurements of the mechanical behaviour of micromachined silicon and silicon-nitride membranes for microphones, pressure sensors and gas flow meters. Sensors and Actuators A: Physical. 1994;41(1–3):287-92.
19. Wang W, Wu N, Tian Y, Niezrecki C, Wang X. Miniature all-silica optical fiber pressure sensor with an ultrathin uniform diaphragm. Optics Express. 2010;18(9):9006-14.
20. Cibula E, Đonlagi D. Miniature fiber-optic pressure sensor with a polymer diaphragm. Applied Optics. 2005;44(14):2736-44.
21. Wang X, Li B, Lee S, Sun Y, Roman HT, Chin K, et al. A New Method to Design Pressure Sensor Diaphragm. NSTI-Nanotech2004. p. 324 - 7.
22. Di Giovanni M. Flat and Corrugated Diaphragm Design Handbook. New York: Marcel Dekker; 1982.
23. Xu J, Pickrell G, Wang X, Yu B, Cooper K, Wang A. Vacuum-sealed high temperature high bandwidth fiber optic pressure and acoustic sensors. Proc of SPIE. 2005;5998.

Chapter 4: Interrogation System Design

4.1. Introduction

In Chapter 1 a problem was set for the development of a sensing configuration that would be capable of measuring the differential length of two sensing cavities at widely separated locations for the potential use in the measurement of pressure. As a means of achieving this task the differential length would be made between two independent extrinsic fibre optic Fabry-Perot cavities.

As was reviewed in Chapter 2 there are a number of methods, both conventional and optical, in which the measurement of pressure and length can be achieved. It is apparent for this research however that such available devices are unable to meet the guide specifications, detailed in Table 4.1, due to the below resolution requirement over the high measurement range of interest. Having reviewed the current techniques it was decided that an all fibre optic interferometric approach could provide the desired solution.

Operating pressure range	1kPa – 100 kPa
Differential pressure resolution	1 Pa
Operating temperature range	15 – 200 °C

Table 4.1: Typical sensor specifications. These specifications are a guide towards a potential sensing application in pressure studies.

As was detailed in Chapter 3 for many flow experiments quasi-static pressure measurements are often sufficient and a bandwidth equivalent to one measurement every ten to twenty seconds would be suitable for such a system.

Table 4.1 details the operating temperature range, an important parameter which has to be taken into consideration at the sensing locations. Due to the potentially large separation of the sensing cavities, variations in temperature will have an effect on the cavity lengths and therefore the differential length to be measured. One approach to compensate for this effect would be through the material design of the sensor head arrangement and with the use of additional temperature monitoring at the sensing locations for determining material thermal expansion. Techniques for temperature monitoring are out with the scope of this research however further details regarding the sensor head arrangement will be provided in Chapter 6.

It is not only the temperature variation at the sensing locations which needs to be taken into consideration but the effects of temperature and air pressure, due to the surrounding vicinity, on the optical fibre downleads of the system between the sensing cavities. This effect was taken into account during the design phase of the interrogation system and was investigated with the findings detailed in Chapter 5, section 5.5.

The aim of this chapter is to describe an all fibre optic sensing system capable of measuring the differential length of two Fabry-Perot cavities separated by up to tens of meters where the cavities are arranged in tandem.

A differential length measurement has many applications and can be particularly utilised for the measurement of differential pressure. In certain circumstances the ratio between the required differential pressure resolution and the absolute pressure is in the order of $1{:}1\times10^{5}$. Hence as a means of achieving a differential pressure measurement through the process of measuring the absolute pressure at the two individual measurement positions and subtracting, would require a measurement ratio better than that of $1{:}1\times10^{5}$ to account for uncertainty in the separate measurements, which is an extremely difficult task. The proposed system outlined in this chapter circumvents the problem of requiring this extremely high resolution by eliminating any common mode background pressure from the metrological chain. The sensing configuration also demonstrates the insensitivity on the optical fibre interconnecting leads as a result of environmental effects such as temperature and air pressure, due to the tandem arrangement of the cavities.

For the development of a sensing system in which a differential pressure is to be determined through the measurement of a differential length, the relationship between these two has to be considered in terms of measurement range and resolution. As will

be described later in the chapter and again in Chapter 5, the measurement range of the system will be determined via the induced change in OPL of the scanning Michelson interferometer. This will be dependent on the fibre length of the interferometer arm and the applied voltage, to induce material expansion, across a piezoelectric ceramic, around which the fibre length will be coiled. The limiting factors in maximising the scanning range of the Michelson interferometer include the maximum voltage which can be applied to a piezo ceramic without depolarisation of the material, and the optical fibre length wound along the length of a piezoelectric tube.

With the guide specifications of this research requiring a differential pressure resolution of 1 Pa with a range up to 100 kPa, the differential length to be measured and the scanning range of the Michelson interferometer have to cope with such requirements, which in turn relates to the diaphragm characteristics of the final sensing arrangement as will be discussed in Chapter 6.

This chapter commences by showing the full arrangement of the sensor configuration, highlighting each component used in the design. Continuing from this, each individual section of the full configuration is discussed in further detail, illustrating how it contributes to the system, the fabrication that was involved, and why this particular style was chosen. Having described the full configuration and the operating components, Chapter 5 will discuss the system characterisation, analysis, and refinement.

4.2. Sensor Design

In Chapter 2 it was discussed that a possible solution to solving the problem of measuring the differential length between two widely separated locations would be to use an all fibre optic sensor configuration consisting of two extrinsic Fabry-Perot cavities arranged in tandem with each other, and connected to a scanning reference Michelson interferometer. Figure 4.1 shows the configuration of such a differential sensor arrangement.

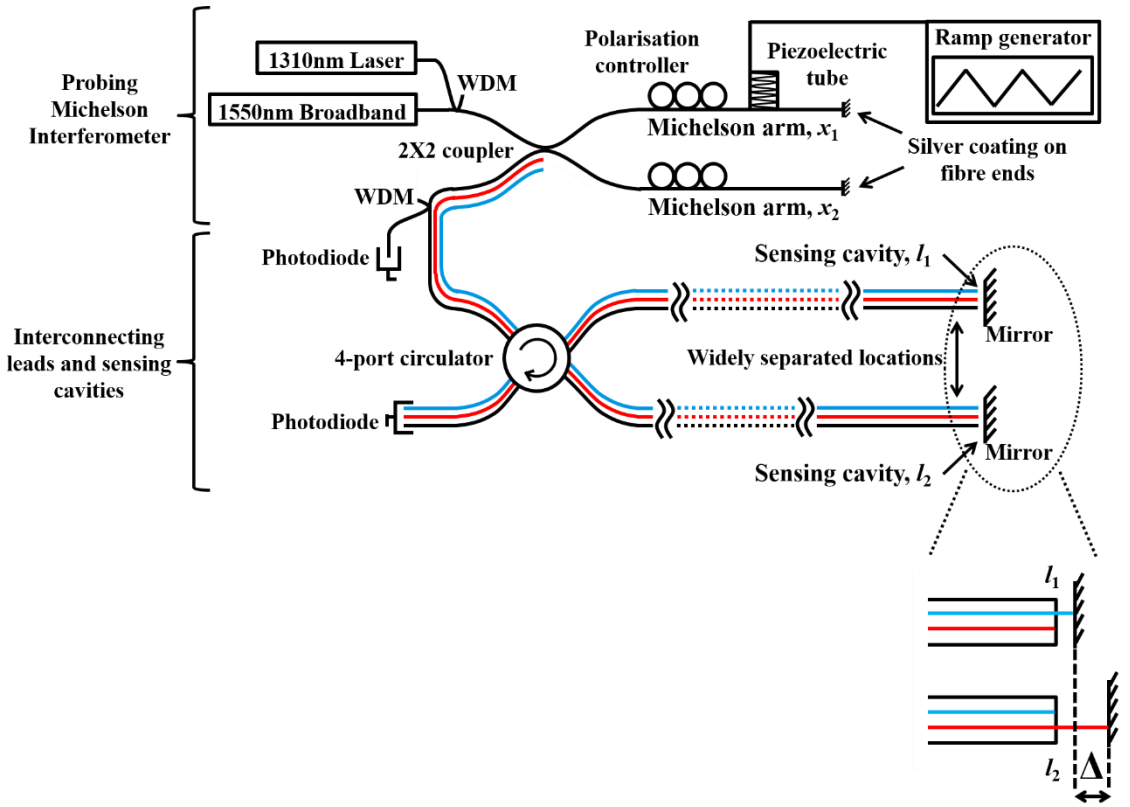

Figure 4.1: Schematic of the sensor configuration for the measurement of differential length. The black line shows the optical fibre leads with the blue and red lines tracing the two possible paths through which the 1550 nm broadband light can propagate after the Michelson interferometer. The insert shows the interactions of the two light paths with the individual Fabry-Perot sensing cavities and the differential length, Δ, to be measured. The 1310 nm laser source is used as a reference for determining the change in the OPL of the scanning Michelson interferometer.

After exiting the Michelson interferometer the 1550 nm broadband light source used for generating the low coherence interference fringes from which the differential length measurement of the two Fabry-Perot cavities can be determined, follows a common path throughout the system, except when interacting with the individual sensing cavities, l_1 and l_2. As can be seen from Figure 4.1, from exiting the Michelson interferometer, the blue line traces one possible path which the light follows, whilst the red line traces a secondary path which the light follows resulting in the formation of a differential length between the two Fabry-Perot cavities. The purpose of the 1310 nm laser source, as will be discussed in the following sections of this chapter and in more

detail in Chapter 5, is to provide a reference measurement of the change in OPL induced in the scanning Michelson interferometer.

Due to the tandem configuration of the Fabry-Perot cavities, the common path followed by the broadband light source leads to the generation of an OPL Δ. This OPL is the differential length of the two Fabry-Perot cavities and is the measurement of interest for this project.

Chapter 5 describes the measurement principle of the light sources used for this thesis project however the remainder of this chapter examines the individual components and sections of the system configuration, discussing the purposes behind their choice and the fabrication involved.

4.2.1. Michelson interferometer

In Chapter 2 the Michelson interferometer was introduced and described as a sensing interferometer that has been demonstrated for use in the measurements of strain (1), temperature (2), and displacement (3). It is however due to the sensitivity of the fibre downleads, between the fibre coupler and the fibre end face where measurements are to take place, to such parameters as strain and temperature that makes this interferometer a disadvantage for making point measurements at a single position, without some form of compensation analysis.

Although the Michelson interferometer does suffer from environmental changes altering the optical path length in each of the interferometer arms, it can be deployed, as described in section 2.5.6, in a tandem interferometric configuration as a scanning reference interferometer.

Interrogation technique

In a tandem interferometric arrangement, two interferometers, a reference and a sensing interferometer, are connected such that light will propagate through one, followed by the next. In section 2.5.6, tandem interferometry was described as a sensing configuration with examples given for the measurement of length. In most cases the

reference, or scanning, interferometer is a Michelson interferometer, keeping one arm length fixed whilst altering the OPL of the secondary arm.

In the case of this research the tandem arrangement of Fabry-Perot cavities is connected to a scanning Michelson interferometer which is used in the determination of the differential mismatch of the cavity lengths, Δ. The Michelson interferometer, as shown in Figure 4.2, is an all optical fibre arrangement using a 50/50, 2×2 coupler as a means of splitting the input light equally down the two arms.

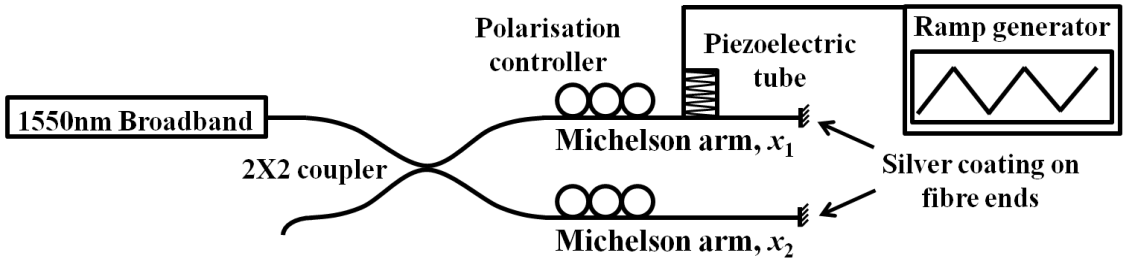

Figure 4.2: Schematic of the scanning Michelson interferometer used in providing an optical path length change.

As described in section 3.5.4, when the OPL mismatch between the two arms of the Michelson interferometer is zero, interference fringes are generated, the characteristics of which are as a consequence of the broadband light source. This interference packet can be referred to as the zero order fringes. In the case of this research, as the OPL is increased due to the change in path length of one of the interferometer arms, further interference fringes, known as the first order fringes, occur when the mismatch in length is equal to that of the mismatch in length between the Fabry-Perot micro cavities. This is the differential length of interest and can be calculated by monitoring the OPL change in the arm of the Michelson interferometer between the zero order and first order interference fringes.

As the differential length is determined through the change in the optical path of the Michelson interferometer, it is important to accurately determine such a change. For the case of a bulk optic Michelson, the path length can be altered by mounting one of the optical mirrors on a linear translation stage which can propagate back and forth. The stage can be made to move a fixed distance from which the length change can be

calculated. One method of altering the OPL, without the use for an external mirror and translation stage, would be to stretch the fibre with the use of a piezo stretcher as discussed in section 3.7. In order to monitor the change in length caused by using a piezo stretcher, one could measure the change in length caused when the maximum voltage is applied and determine a unit length change per applied voltage, and simply monitor the voltage. As will be discussed later in the chapter however, the piezo expansion is in many cases not linear with the applied voltage, and so as an alternative method for obtaining the optical length change of the fibre, a laser source can be coupled into the Michelson interferometer with the output interference fringes, resulting from the changing length, being monitored. Again, further details of this approach will be discussed.

Interferometer fabrication

As described in the previous section, the Michelson interrogation interferometer was constructed using an all optical fibre arrangement, utilising a 50/50, 2×2 coupler to separate the light equally into the two arms. The input light source, once separated, propagates through each arm of the interferometer before being reflected via the end face of the fibre. The light then propagates back into the coupler and throughout the remainder of the system. To prevent light from transmitted back into the source, an optical isolator is used between the source and the coupler, thus eliminating any possibility of the reflected light affecting the optical performance of the source due to optical feedback.

In section 3.5 the properties of a low coherent light source were introduced, in particular the coherence length of such a source. As was explained, in order for the interference fringes of a low coherent light source to be observed, the optical path lengths of the interferometer arms must be matched to within the coherence length of the source. When dealing with laser light sources this does not present a problem as the coherence length of such sources can be in the range of kilometres, however when using broadband light sources, the optical path lengths may have to be matched to within 10's of micrometers. In the case of the research poised here, the optical path lengths would have to be matched to within 27.02 µm.

The individual arm lengths of the Michelson interferometer are relatively long, in the region of 15 meters each, due to the coiling around the piezo stretcher, the process of which will be discussed in the following sections. This presents a difficult task in not only accurately measuring but also cleaving these to within micrometers of one another.

The first stage would be to measure the fibre length to within roughly 1-2 mm of each other. This can be achieved by simultaneously measuring out the lengths by hand applying an equal, or near equal, strain to each fibre. Equal strain is applied to both fibres preventing additional expansion in one compared with the other when measured over 15 meters. For example, from equation 4.1, if a 10 g tensile load is applied to an initial fibre length, l, of 15 meters, the resultant length change, Δl, of the fibre would be ~1.6 mm.

$$\Delta l = \frac{(F/A).l}{E} \tag{4.1}$$

Where F/A is the applied force per unit area and E is the Young's modulus of the fibre, 72 GPa.

Having cleaved the fibre ends of the interferometer to provide a Fresnel reflection, there are two methods available to determine the mismatch between them. The first, and probably simplest method, would be to couple a broadband source into the interferometer and, using an OSA operating with a monochromator and diffraction grating arrangement, observe any interference pattern as a result. The interferogram generated would be in the form of that illustrated in Figure 2.20. The differential length of the two interferometer arms can be found using equation 2.13, the free spectral range (FSR) technique.

Using the refractive index of the core of an optical fibre, 1.4682 @ 1550 nm (4), the length difference between the Michelson interferometer arms can be found. The disadvantage of obtaining the length mismatch using this approach is that it is not known as to which interferometer arm is longer than the other. In order to overcome this problem it is possible to stretch one fibre length and observe whether the interference fringe spacing increases or decreases. An increase in fringe spacing

indicates the differential length is moving closer to zero, thus the fibre being stretched must be the shorter of the two.

An alternative method would be that shown in Figure 4.3 whereby again a broadband source is coupled into the interferometer however in this case, as opposed to using an OSA to monitor the output a simple InGaAs detector is used. Positioning a mirror on a movable translation stage perpendicular to the end face of one optical fibre arm, and increasing the gap length between the mirror and the fibre end to effectively increase the path length of that particular interferometer arm, interference fringes will be detected when the mirror passes through the point of equal optical path length between the two interferometer arms. Measuring this gap length and using the fibre refractive index, the fibre differential length can be determined. It is important to take into consideration the generation of fringes that will occur when the mirror is first moved away from the fibre end face due to the formation of a Fabry-Perot cavity within the coherence length of the source.

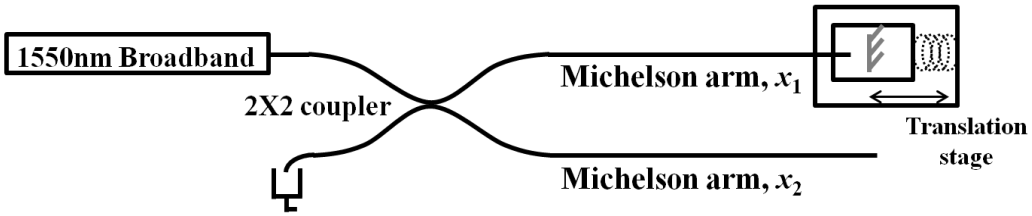

Figure 4.3: Arrangement for measuring path length imbalance between the arms of a Michelson interferometer. A mirror mounted on a linear translation stage is moved away from the end face of the optical fibre to a position where interference fringes are detectable on the photodiode. At this position the optical path lengths are equal.

There is again a disadvantage with applying this method in that as it is initially unknown as to which fibre length is longer, it could be possible that the mirror is initially positioned at the incorrect fibre. Such would be known if no interference fringes are observed as the mirror gap length increases. A further disadvantage is the loss of light coupled back into the fibre as the mirror gap increases. For a large mismatch in arm length to begin with, the signal may become too weak as the mirror gap increases and the interference signal may be lost within the background noise.

In order to selectively remove the correct amount of fibre having obtained the length mismatch information and which interferometer arm is greater in length, a setup as shown in Figure 4.4, involving a fibre cleaver, microscope, translation stage and LVDT, was constructed.

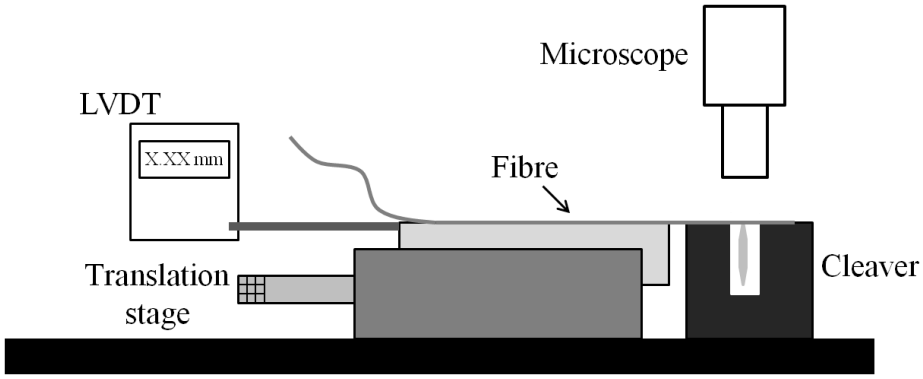

Figure 4.4: Arrangement for removal of specific fibre length. The microscope is used to view the fibre location above the cleaver blade whilst monitoring via the LVDT, the fibre length inserted to be removed.

Arranging the microscope over the fibre cleaver such that the cross-hairs are focussed on the cleaving blade, the edge of the optical fibre to be cleaved is aligned with that of the cleaver blade. Having mounted the optical fibre on the movable translation stage, the LVDT is used to observe the fibre length fed through the cleaver in order to accurately measure the length of fibre being removed. The LVDT, the operation of which was described in section 2.3, has a digital resolution of 1 μm making it suitable for the required measurement in order to achieve the matched interferometer arm lengths to within the coherence length of the light source. Figure 4.5 shows the experimental arrangement used within the lab for the removal of specific fibre lengths.

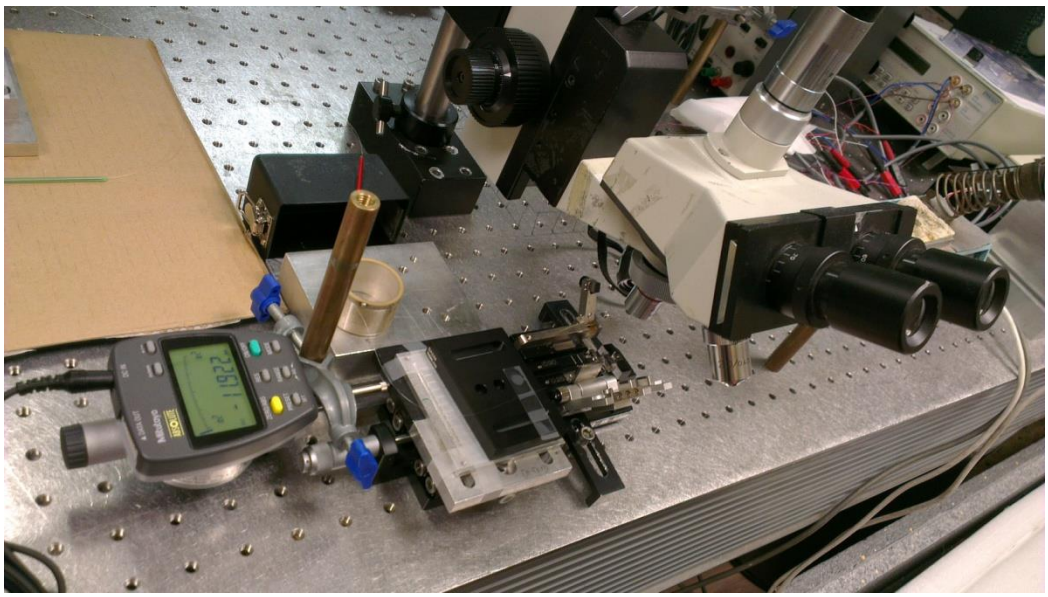

Figure 4.5: Lab arrangement used for accurate optical fibre length removal.

When coupled light into the Michelson interferometer interacts with the end face of the optical fibre at the fibre-air interface, the resultant reflection is due to the 3.6% Fresnel reflection, hence a significant amount of light is being lost through transmission at the fibre end. This has implications on the signal-to-noise throughout the remainder of the system and so it is therefore beneficial to maximise the return signal at this interface. As the end face of the fibre interferometer does not have an effect on the differential measurement being made, these fibre ends can be coated with a reflective layer in order to increase the reflectivity from 3.6% to a value nearing 100%, and thus increase the signal strength in the system. Silver was chosen as the reflective layer to be coated having an average reflectivity > 97.5% at 1550 nm (5).

There are a number of different methods that can be used for applying a silver coating to a fibre end. One approach involves the use of thermal evaporation carried out in a vacuum chamber (6). This method has the advantage that a silver coating can be evenly applied to the fibre ends and depending on the particular vacuum chamber the applied thickness can be monitored whilst coating. Figure 4.6 shows a fibre end coated with a 200 nm layer of silver, providing a potential reflectivity > 97.5%. This image was taken using a Leica microscope model DM6000M, illuminating the fibre end surface using front illumination for imaging purposes.

The disadvantage of using such a coating technique is the size of the vacuum chamber, which in some cases can be relatively small. As the fibre ends need to be coated once the lengths have been matched in length, the full Michelson interferometer arrangement needs to be inserted into the vacuum chamber or alternatively a feed through could be used. In both cases this may be tricky in order to avoid any damage to the fibre lengths.

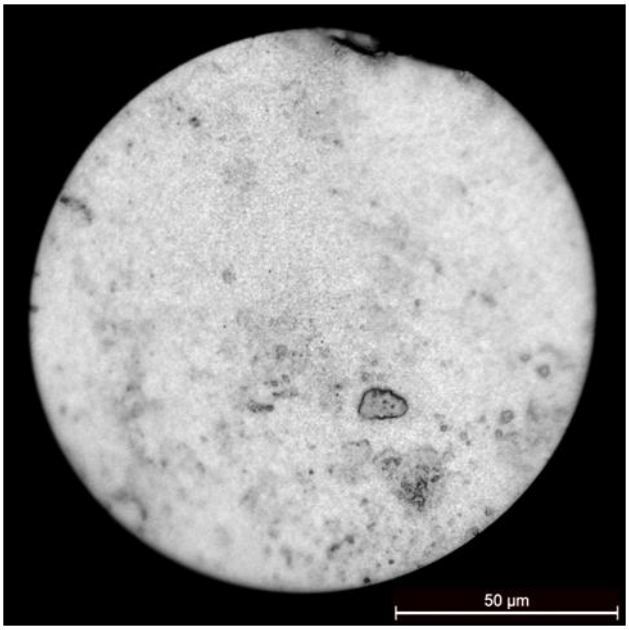

Figure 4.6: Silver coated fibre end via thermal evaporation method. This image was taken using a Leica microscope model DM6000M using front illumination.

An alternative method for silver coating an optical fibre end is a chemical approach, which is often used in the fabrication of silver mirrors (7). This method involves the combination of silver nitrate, potassium hydroxide, glucose, and ammonia in order to create a silver solution in which the fibre ends can be submerged in producing a mirrored finish on the fibre surface.

As with thermal evaporation, the chemical approach creates an even silver layer over the face of the cleaved optical fibre providing a high reflectivity at the interface. This method also prevents the need to condense the Michelson interferometer into a small space and it is simply the fibre ends which need to be submerged within the silver solution. The slight disadvantage with using this technique is the uncertainty in the thickness of the silver layer as without any protection, a thin silver layer may oxidise

over time, reducing the film reflectivity. Figure 4.7, again taken using a Leica microscope model DM6000M illuminating the fibre end surface using front illumination for imaging purposes, shows a silver coated optical fibre which, over time, has been affected by oxidisation.

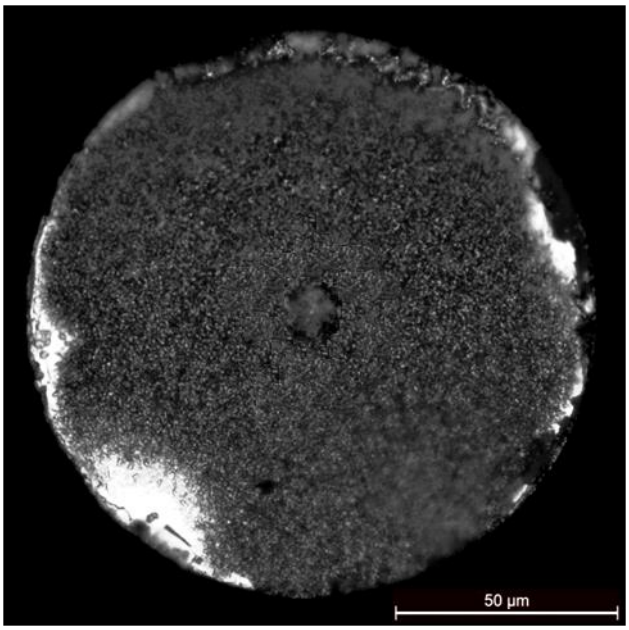

Figure 4.7: Silver coated optical fibre affected by oxidisation due to no protection and prolonged exposure to air. This image was taken using a Leica microscope model DM6000M using front illumination.

Oxidation of the silver layer will occur over time causing the silver to tarnish. For silver thicknesses of 200 nm the oxidation may occur on the outer surface and may not penetrate through to the fibre/silver interface, thus not having an effect on the reflectivity. It would still, however, be prudent to limit this effect. A technique to prevent oxidisation of the silver layer would be to immediately coat the fibre end in a protective layer, for example, some form of lacquer or adhesive, once the silver process is complete.

Table 4.2 shows the input power to the Michelson interferometer and the power output with bare fibre ends (~3.6% reflectivity) and with silver coated fibre ends (> 97.5% reflectivity assuming maximum return at 1550 nm (5)).

	Power (mW)
Input into the Michelson interferometer	9.671
Output from the Michelson interferometer with bare fibre ends (~3.6% reflectivity)	0.110
Output from the Michelson interferometer with silver coated fibre ends (> 97.5% reflectivity)	3.229

Table 4.2: Power measurements from a Michelson interferometer for different fibre end reflectivities.

From the values obtained in Table 4.2, of the output intensity for the two Michelson interferometer end reflectivities, if the output with an end reflectivity of 3.6% is 0.110 mW it can be calculated that with a 100% reflectivity the output should measure 3.056 mW. As the output of the Michelson with the silver coated fibre ends measures 3.229 mW this would suggest that the reflectivity of the silver layer is >100%, which is not possible. The increase in power could possibly be as a result of reduced bend losses within the system, a consequence of necessary loops of fibre being removed from the piezo stretcher between the two measurements in order to provide suitable lengths during the silver coating procedure. The removal of fibre from the piezo stretcher would subsequently remove bend losses associated with it, which would have been present during the measurement with the bare fibre ends.

It can be stated that a very high reflectivity is achieved due to the silver coating and as such the resultant increase in output power therefore increases the signal strength throughout the interrogation system.

Piezo fibre stretcher

For the purpose of this research, the interrogating Michelson interferometer is used as a scanning reference interferometer, and is used as a means of determining the OPL of a

secondary interferometer. In order to achieve a measureable OPL change of the Michelson interferometer the length of one of the interferometer fibre arms is altered with respect to the other through a means of stretching. This stretching of the fibre length is achievable via the use of a fibre stretcher in the form of a piezoelectric tube (8), around which the fibre length is coiled.

Construction of the piezo fibre stretcher was implemented 'in-house' and had to be carried out prior to the measurement and cleaving of the two fibre lengths to achieve a matched length within the coherence length of the broadband light source. This is as a means of avoiding damage to the fibre lengths or the reflective coating on the fibre ends during the coiling process. The task of constructing such a device was not a simple one as an equal continuous strain had to be applied to the fibre length during the winding of the fibre such that there would be an even distribution around the piezo ceramic tube, and to prevent any loose fibre loops. With the full 15 m fibre length suspended from a height of ~ three storeys, and with a small mass attached to the fibre end as a means of applying a continuous strain, the piezo ceramic tube was manually rotated slowly in order to wrap the fibre with a compact and even distribution along its length of 25 mm. The fibre was held in place using adhesive as to limit the expansion effects of the piezo ceramic material with applied voltage.

In order to achieve a large range over which the Michelson fibre arm length could be stretched, a significantly high voltage, however not exceeding the maximum applicable voltage of 1500 volts for the piezoelectric tube used, must be applied. Considering that the outer diameter of the piezoelectric tube will only increase by a small amount, even with a large number of fibre turns around it, it would still require a great voltage level in order to achieve a range in the order of hundreds of microns. The use of a high voltage amplifier can help in achieving the desired voltage level by which the tube can be suitably expanded. The high voltage amplifier used in this work was supplied by Applied Kilovolts Ltd (9), having an input up to 10 V with an output up to 2.5 kV at 4 mA.

In order to drive the voltage amplifier and in turn the piezoelectric fibre stretcher, a signal generator was used to create a triangular waveform allowing the voltage to ramp up and down periodically. Although, for the purposes of this research, it is only the rising voltage that is of interest in order to increase the OPL of the fibre, to avoid ringing of the piezoelectric tube and to allow full discharge before applying a forward

bias voltage again, the reverse voltage is decreased gradually. It is for this reason that the signal generator is used in producing a symmetric triangular waveform as oppose to a saw tooth waveform with a rapid decline from the maximum to the minimum voltage level.

One drawback to using a piezoelectric tube as a method of increasing the OPL of the Michelson interferometer arm through stretching of the fibre length is the non-linearity of the piezo ceramic. In an ideal situation, the change in the tube thickness would scale linearly with the applied voltage. This is unfortunately not the case, and so although it is a fair assumption to say that when the maximum voltage is applied, the fibre length will have increased by a known factor, it is not correct to assume that by simply applying half the voltage the fibre will increase in length by half this factor. It is for this reason that alternative methods of monitoring the change in fibre length whilst the piezoelectric tube is expanding need to be implemented. It is also important to monitor the changing OPL of the fibre as during the expansion process, as a result of the varying voltage through it, thermal effects as a result of a temperature increase may cause the piezoelectric tube to expand. One such monitoring method which was utilised and will be discussed in Chapter 5 involved the analysis of an interference pattern produced via a DFB laser source at a different wavelength to that of the broadband light source whilst the Michelson interferometer path length is altering.

Temperature stabilisation

When using a tandem interferometric arrangement in which the measurement is dependent on a reference interferometer, it is important to keep the arms of this interferometer stable and isolated from environmental factors such as temperature and pressure which could cause the optical path length of the interferometer arms to change. Temperature affects in particular could have a significant effect on the optical path length with fused silica having a thermal expansion coefficient of $0.55\times10^{-6}/°C$ (10). Each of the two Michelson interferometer arms must be temperature stabilised such that any temperature alterations in the surrounding vicinity will be equally distributed across both interferometer arms. In this case the only change in optical path length between the two would be as a result of the changing dimensions of the piezoelectric fibre stretcher with applied voltage.

Temperature stabilisation can be achieved through packaging of the Michelson interferometer within the inner of two thermally insulated foam boxes. By creating an air gap between the two insulation boxes and with the use of resistive heating pads, in the arrangement shown in Figure 4.8, and a small 12 V electric fan, warm temperature stabilised air can circulate evenly around the inner of the two boxes.

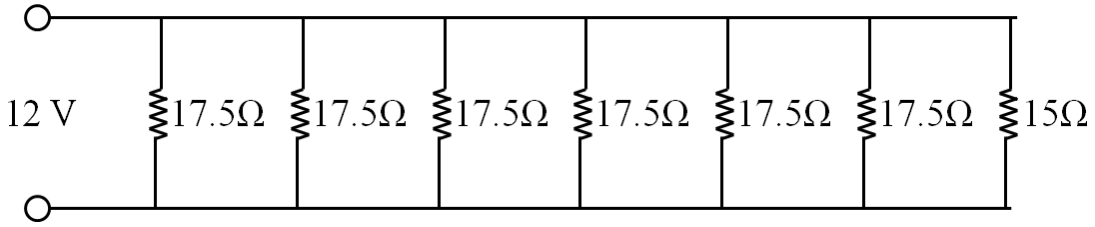

Figure 4.8: Schematic of the resistor arrangement used in the heat pads for controlling the temperature of Michelson interferometer.

Using such an arrangement should limit the temperature changes within the inner isolation box due to changes in temperature of the surrounding area. A secondary technique of placing a large thermal mass within the inner isolation box will also mitigate the effects of temperature changes.

As a means of controlling the temperature to which the resistive heating pads are driven to, a CAL9000 temperature controller is used. This unit operates through measurement of the current temperature via a PT100 sensor, and passing a current through the resistive heating pads depending on the temperature difference between the measured value and the desired value controllable via the unit.

As previously stated, it is important to limit the effects of temperature changes to the Michelson interferometer, or to ensure that any temperature alterations will be distributed equally over the two fibre arms of the Michelson interferometer. This is carried out as a means of reducing unwanted changes in the measurable OPL which may result in inaccurate measurements of the differential path length of interest. Figure 4.9 shows the measured temperature at three separate positions within the inner isolation box, which housed the Michelson interferometer, and the surrounding laboratory temperature over a period of 3 days.

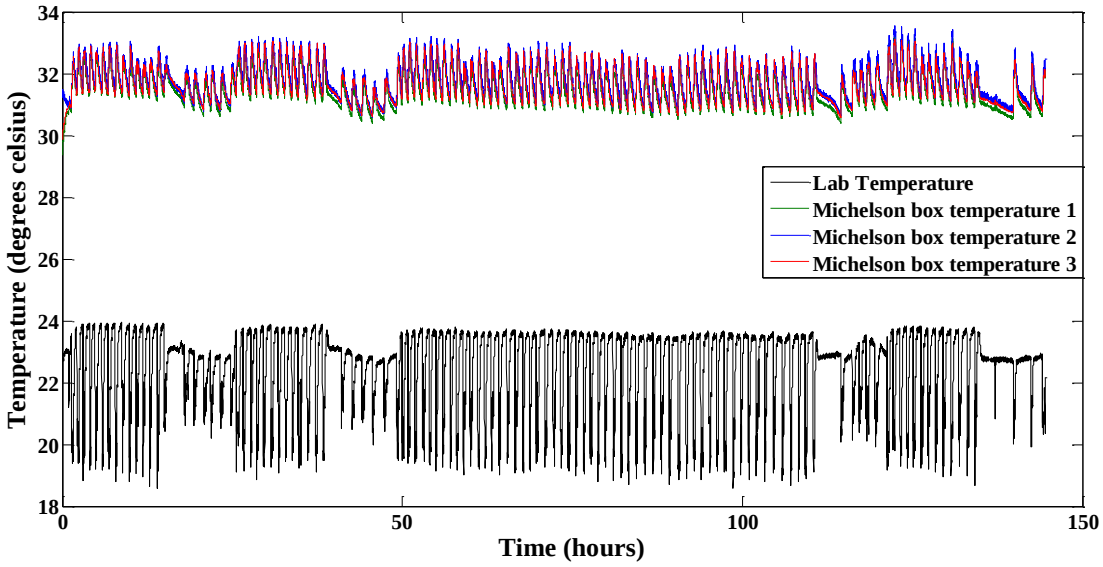

Figure 4.9: Measured temperature of the Michelson box at three separate locations, and the surrounding laboratory to demonstrate temperature stabilisation.

As in can be seen from the data in Figure 4.9, even with the measures taken to temperature control the air surrounding the Michelson interferometer, the temperature changes within the lab still have an effect of the temperature changes which occur within the inner isolation box. This, due to the thermal expansion of both the fibre fused silica and the piezoelectric tube material, could result in changes in the optical path length between the two Michelson interferometer arms. It is, however, also observable from this data that the temperature variation within the Michelson interferometer box changes equally at all three measurable locations. This suggests that although a constant temperature could not be achieved, the temperature change is equally distributed surrounding the reference Michelson interferometer, and therefore any expansion in fibre length as a result of this change will be equal over both arms.

4.2.2. Tandem Fabry-Perot's

In section 4.2 the full configuration for a sensing system to measure the differential length of two individual Fabry-Perot cavities was described. This was then followed with a detailed description of the arrangement and application of the Michelson interferometer and how this was implemented as a reference measurement.

In this section, the remainder of the sensing configuration after the light has propagated through the Michelson interferometer will be discussed. The Fabry-Perot cavities and their arrangement will be examined, as will the limitations behind the measurable lengths and the analysis in determining the differential length required.

Tandem Fabrication

In order to measure the differential length between two individual Fabry-Perot cavities, it would be possible to simply measure each cavity separately and obtain the difference. In taking the measurement in this way, there are introduced uncertainties in both individual measurements, with the overall error in measurement a result of the two separate error measurements being taken. As a means of removing this double error and allowing the measurement to be dependent of one single error uncertainty, the two Fabry-Perot cavities can be arranged in tandem with one another. In this instance, the light will propagate through one cavity first, before propagating through the second. In doing so this creates a third measurable cavity, the length of which is the difference in lengths of the individual two.

One method, and probably the simplest, for connecting the Fabry-Perot cavities in a tandem arrangement, is to use two 50:50 2×2 couplers as shown in Figure 4.10.

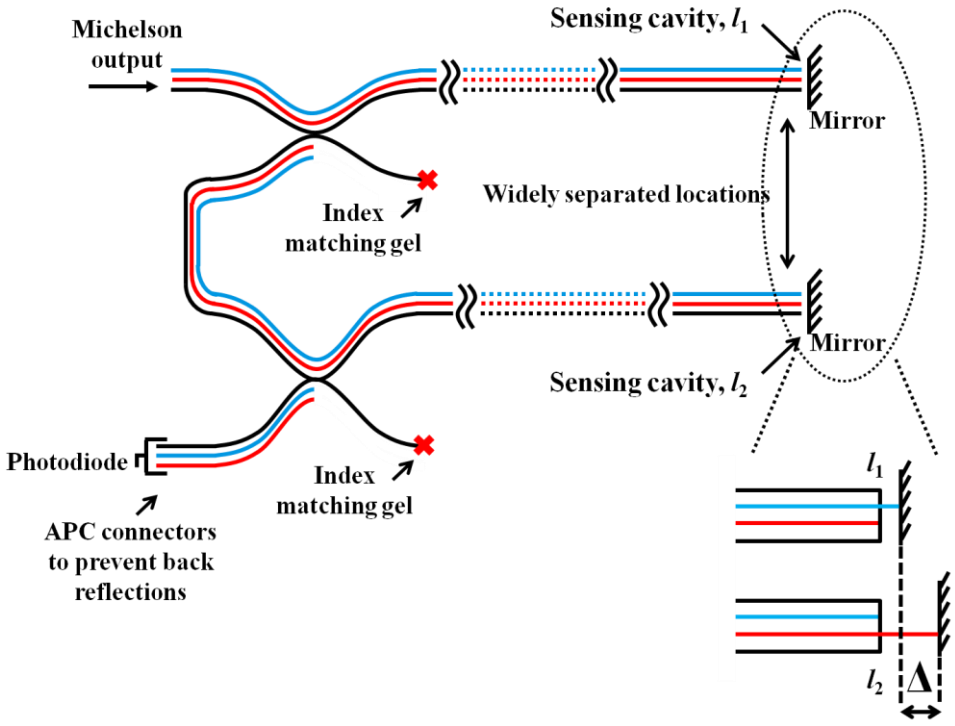

Figure 4.10: Schematic of the tandem arrangement of the Fabry-Perot sensing cavities using two 50:50 2×2 couplers. The black line shows the optical fibre leads with the blue and red lines tracing the two possible paths through which the light can propagate. The insert shows the interactions of the two light paths with the individual Fabry-Perot sensing cavities and the differential length, Δ, to be measured.

Upon exiting the reference Michelson interferometer, the broadband light is split via the first 2×2 coupler sending half the power to the first sensing cavity, l_1, and half down the unused coupler arm.

Index matching gel, a substance having a refractive index similar to that of fused silica, is applied to the fibre end of the unused coupler arm to eliminate any Fresnel or scattered reflections that may occur from the fibre end. The elimination of any such reflections is a necessity as this could result in the generation of additional unwanted cavities, detectable through the scanning Michelson interferometer, and could cause anomalies in the desirable length measurement.

After reflection via sensing cavity l_1, the propagating light travels back via the first coupler and through the second. Similarly with the first coupler, the light is equally split along the two coupler arms, half interacting with sensing cavity l_2, and half through

the unused coupler arm and removed from the system with the use of index matching gel.

The resulting interference fringes from the light interactions with the two sensing cavities are detectable via an InGaAs photodiode.

The component configuration described above and as shown in Figure 4.10 is the simplest arrangement for connecting two Fabry-Perot cavities in tandem with one another. It is however not the most convenient method due to the high signal loss experienced. The 2×2, 50:50 couplers, combined in such a way, along with the index matching gel to remove the signal and prevent any back-reflections from the two unused coupler arms means that at most only 6.25% of the light entering through the Michelson interferometer is detectable via the InGaAs photodiode assuming perfect reflectivity of the mirrors in the Fabry-Perot cavities and maximum re-coupling of the light into the optical fibres at the two Fabry-Perot cavities, which is known not to be the case. This is also not taking into consideration the insertion losses of the optical couplers.

One approach to improve the signal strength detectable and to reduce or even eliminate any light lost or removed from the system, would be in replacing the existing 2×2 couplers with 3-port circulators.

Replacing the 2×2 coupler with a 3-port circulator removes the unnecessary unused arm in which 50% of the light was being lost out of the system. The 3-port circulator also allows almost all the light, taking into account the component isolation loss, to propagate to the sensing cavities, and the reflected light to propagate throughout the remainder of the system.

The configuration using two 3-port circulators dramatically improves the detectable signal strength and thus reduces the noise level in order to more accurately determine, as will be described later, the centre of the interference fringes. A further improvement to this arrangement would be to replace the two 3-port circulators with one single 4-port circulator, shown by the final sensing configuration in Figure 4.11.

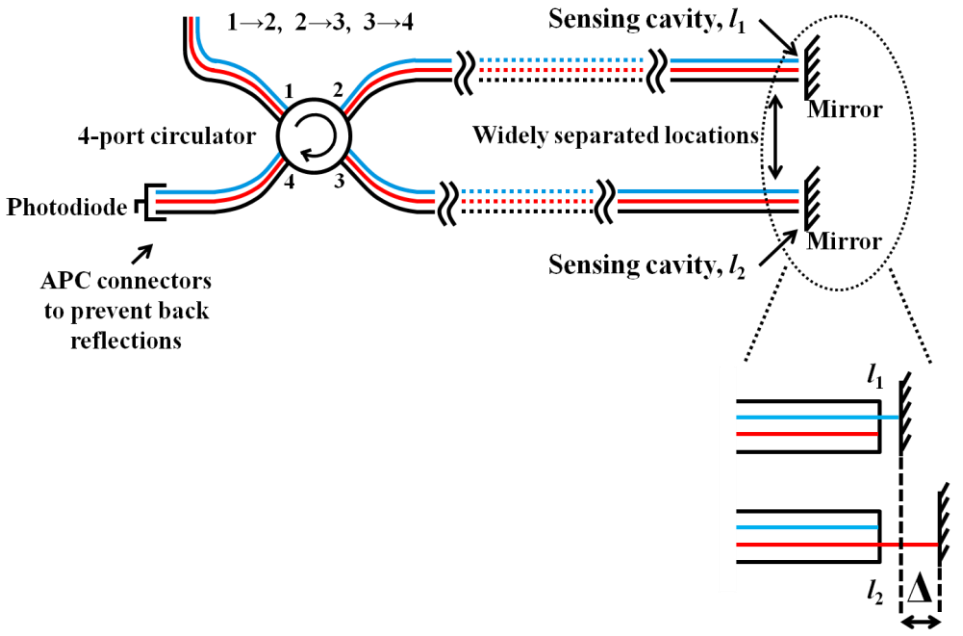

Figure 4.11: Schematic of the final sensing arrangement of the tandem Fabry-Perot cavities using a 4-port circulator. The black line shows the optical fibre leads with the blue and red lines tracing the two possible paths through which the light can propagate. The insert shows the interactions of the two light paths with the individual sensing cavities and the differential length, Δ, to be measured.

In using this circulator there will be the removal of unnecessary insertion losses that would be present when using the arrangement consisting of the 3-port circulators, however there will still be insertion losses in the new arrangement. As well as eliminating these insertion losses, the sensing section of the system is now only reliant on one single component as oppose to two, removing the need for fibre splices between components which may incur losses.

A typical optical circulator consists of micro optical components operating in a similar fashion to that of an optical isolator. The reflectivity within this micro optic system is minimised with the use of anti-reflective coatings preventing the formation of OPL's within the coherence length of the light source being used. In many cases the optical components include a Faraday rotator in which light travelling in one direction through the rotator has its polarisation rotated in one particular direction. Therefore it can be arranged such that light propagating into one of the circulator ports will only be transmitted to the adjacent port; for example in Figure 4.11, light travelling into the circulator via the port 1 fibre will only transmit via the port 2 fibre. This has the

advantage over an optical coupler as the full propagating signal is transmitted to the Fabry-Perot sensing cavities sequentially without any power splitting ratio. The circulator also acts as a form of optical isolator preventing any reflections transmitting back through the system.

As shown by the red and blue coloured traces, both propagating light paths interact with the two sensing cavities l_1 and l_2, resulting in the generation of the differential path length of interest, Δ.

A burst of interference fringes will occur when the OPL difference between the two arms of the Michelson reference interferometer is equal to the OPL difference between the two Fabry-Perot cavities, Δ. This however is not the only condition in which interference fringes can occur. Interference fringes can result from an equal OPL difference between any two optical lengths that are matched to within the coherence length of the light source being used. This will therefore lead to limitations in the initial arrangement of the Fabry-Perot sensing cavities.

In order to determine the length difference of the two Fabry-Perot sensing cavities, the length change in the Michelson reference interferometer from the position where fringes are generated due to equal arm lengths to the position where fringes are generated due to the Michelson interferometer arm mismatch being equal to the modulus difference in cavity length is calculated. It is therefore important that the interference fringe packets from the two events do not overlap in such a way as to interfere and cause deformations in the fringe packet envelope, resulting in errors in the determination of the central fringe position. To reduce or eliminate the effects of superimposing interference fringes, the minimum differential length of the two sensing cavities must be greater than the coherence length of the broadband light source being used, in this instance, 27.02 μm.

The Fabry-Perot cavity length is also limited by the scanning range of the piezo fibre stretcher. As stated above, interference fringes are observed when the mismatch in length of the Michelson interferometer arms is matched within the coherence length of the source to any other OPL within the system configuration. To prevent interference fringes from being observed when the Michelson interferometer arm mismatch is equal in length to one of the individual sensing cavities, the length of the smallest Fabry-Perot cavity must be made greater than the scanning range of the piezo fibre stretcher.

Table 4.3 details the initial length parameters which have to be adhered to as a means of avoiding unwanted interference fringe superimposition due to the Fabry-Perot cavity limitations in terms of the light source coherence length.

Michelson scanning range: y Light source coherence length: l_c Maximum differential length: Δl_{max}	$l_{1(initial)} = y + l_c$	$l_{2(initial)} = l_{1(initial)} + \Delta l_{max} + l_c$

Table 4.3: General Fabry-Perot initial cavity lengths, l_1 and l_2, due to the limitations set by the coherence length, l_c, of the light source to be used, the scanning range of the Michelson interferometer, y, and the maximum differential length, Δl_{max}.

These limitations have a drawback on the system power being observed via the InGaAs photodiode, as the greater the cavity length of the Fabry-Perot's, the less light there will be coupled back into the fibre end due to the light spread effect from the fibre end, as described in Chapter 3.

An approach to improve the coupling ratio between the fibre and the Fabry-Perot cavity would be to use a gradient-index (GRIN) lens on the fibre end. This type of lens would collimate the beam exiting the fibre and provide nearly full coupling into the fibre from the reflected beam. This technique was tested however introduced additional cavities into the system which were detectable through the Michelson reference interferometer and interfered with the desired length measurement.

4.3. Conclusion

An all optical fibre arrangement has been designed and constructed based on literature reviews in order to provide an ideal solution of measuring differential length to solve to problem set at the beginning of this research. The system is based on two Fabry-Perot sensing cavities arranged in tandem with one another, probed by a reference interferometer in the form of a Michelson.

As a means of scanning the Michelson interferometer to induce an OPL change, a piezo fibre stretcher was used. This was constructed "in-house" through manual winding of a suspended fibre length around a piezo ceramic tube. With a mass attached to the fibre end to create a continuous applied strain, slow rotation of the piezo ceramic tube allowed for a compact and even distribution of the optical fibre along its 25 mm length. Due to the long lengths required in the Michelson interferometer arms, to allow for significant coiling around the piezo material, measuring these to within the coherence length of the broadband light source used proved difficult. This was carried out however using interference measurement techniques in the form of FSR measurements, and also with the use of mechanical tools such as an LVDT, to accurately measure the lengths to within the coherence length of 27.02 μm.

An approach for application of a silver coating to the fibre end substrate of the Michelson interferometer arms was introduced. This procedure was to increase the fibre end reflectivity from the already existing Fresnel reflection of 3.6% to > 97.5%. Achieving this increased the signal output of the Michelson interferometer and improved the signal strength propagating through the remained of the system.

The arrangement of the tandem Fabry-Perot interferometer sensing cavities was carried out using a 4-port circulator. This approach was selected over alternatives involving 2×2 couplers and 3-port circulators as a means of removing unnecessary component isolation losses and additional splice losses which would reduce the signal strength and thus reduce the measurement quality.

There is however limitations in the cavity lengths of the Fabry-Perot interferometers arising due to the conditions by which interference fringes will be observed as a result of the broadband light source used for interrogation purposes. Length limitations of the Fabry-Perot cavities, set by the broadband source coherence length, are detailed in Table 4.3.

Environmental stability surrounding the Michelson interferometer was described and a method of stabilisation was implemented. The results demonstrated that although temperature stabilisation to within >1°C could not be achieved due to the temperature variation of the laboratory, this is not a critical aspect, provided that the temperature variation surrounding the Michelson is, over time, equal at all positions. This was demonstrated by recording the temperature at separate locations of the Michelson interferometer.

Temperature stability surrounding the Michelson interferometer is necessary during the process of an OPL change within the system, performed by scanning the voltage through the piezo fibre stretcher, to prevent unwanted thermal expansion of the fibre. It should be noted however that with the inclusion of a separate reference measurement, from which the change in OPL in determined, details of which will be provided in Chapter 5, temperature stability is not as essential due to the unlikely situation of such a rapid change in the surrounding environment during the scan time of 10 seconds.

4.4. References

1. Valis T, Tapanes E, Liu K, Measures RM. Passive-quadrature demodulated localized-Michelson fiber-optic strain sensor embedded in composite materials. Lightwave Technology, Journal of. 1991;9(4):535-44.
2. Jing Z, Hao S, Ruohui W, Dan S, Tuan G, Zhongyao F, et al. Simultaneous Measurement of Refractive Index and Temperature Using a Michelson Fiber Interferometer With a Hi-Bi Fiber Probe. Sensors Journal, IEEE. 2013;13(6):2061-5.
3. Smith LM, Dobson CC. Absolute displacement measurements using modulation of the spectrum of white light in a Michelson interferometer. Applied Optics. 1989;28(16):3339-42.
4. Corning inc. SMF 28e Optical Fiber Product Information. In: Incorporated C, editor. 2002.
5. Thorlabs, Inc Protected Silver Mirror 1999-2015. Available from: http://www.thorlabs.de/newgrouppage9.cfm?objectgroup_id=903.
6. Hardy N. Thin Film Deposition By Thermal Evaporation: Essential Basics. Semicore Equipment, Inc.2013.
7. Nuffield Foundation A Giant Silver Mirror 2011. Available from: http://www.nuffieldfoundation.org/practical-chemistry/giant-silver-mirror.
8. Morgan Advanced Materials plc Piezoelectric Ceramics- Electro Ceramic Solutions. 2013.
9. Applied Kilovolts Ltd High Voltage (HV) Power Supplies 2015. Available from: http://www.exelis-ps.com/high_voltage.cfm.
10. Ghosh G. Handbook of Thermo-optic Coefficients of Optical Materials with Applications: Academic Press; 1998.

Chapter 5: Differential Length Analysis

5.1. Introduction

The problem set for the topic of this research was the development of a sensing arrangement for the differential measurement of two widely separated, independent lengths. A potential solution to this using an all fibre optic configuration with the measurement being made based on interferometric techniques was considered. In Chapter 4, the elements of such a fibre optic sensor capable of measuring the differential length of two Fabry-Perot cavities arranged in tandem were described.

Chapter 4 began by showing the full sensing arrangement, and then investigated each individual section which would have an effect on how the measurement would be made. The final sensing configuration was chosen due to the benefits of observing just the cavity differential and not the two separate cavities individually. The system would also have the benefit of insensitivity on the optical fibre interconnecting leads due environmental effects such as temperature and pressure, due to the tandem arrangement of the cavities.

In this chapter, the system characterisation with respect to the operational light sources being used will be discussed. Here the measurement techniques that have been described in previous chapters will be implemented and results given. This chapter will also consider the analysis techniques as a process of determining accurate measurements. Finally, methods in which the sensing configuration could be refined will be discussed with particular attention on noise within the sensing arrangement.

5.2. Light Sources

In the previous chapter, an optical fibre arrangement, as shown in Figure 4.1, was described as a method of deriving the differential length of two Fabry-Perot cavity lengths, when at widely separated locations, in differing environments.

In order to make such a measurement with the accuracy required, two separate light sources are to be used, with the arrangement utilising the properties of interference effects for each individual source. A broadband light source is used as a means of

providing the locations between which the desirable differential length of the sensing cavities is to be measured. An additional light source in the form of a DFB laser is used as a reference, through which the differential length measurement can be deduced through a process of fringe counting analysis, as will be discussed in subsections of section 5.2.2.

5.2.1. Low coherence light source

Light will experience interference effects and create fringe patterns when the interfering path lengths are matched to within the coherence length of the source. For the case of a broadband light source, the coherence length can be extremely small, down in the orders of microns, making it ideal for use in the measurement of the short lengths that will be investigated in this project.

For the investigation carried out of a sensing system used for the measurement of differential length one light source considered was an EBS30 Series Broadband Light Source, centred at 1572.3 nm, supplied by Exalos (1). The spectral profile of this particular light source is shown in Figure 5.1, measured using an Advantest OSA model Q8384. This particular OSA operates using a monochromator and diffraction grating arrangement, as described in section 2.5.3, to scan through the desired wavelength range.

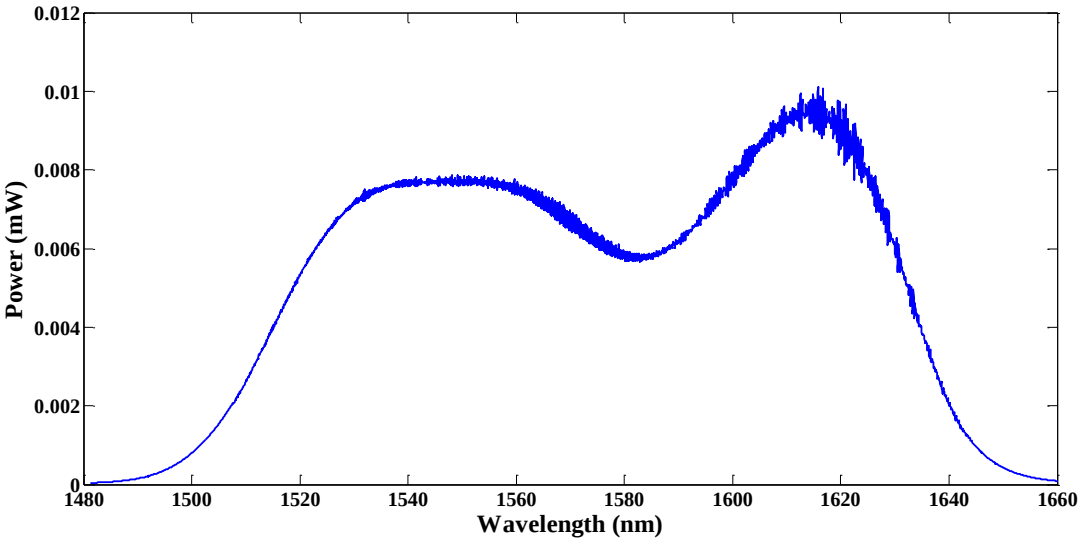

Figure 5.1: Spectral profile of an EBS30 Series Broadband light source centred at 1572.3 nm, measured using an Advantest OSA model Q8384.

As can be seen from the figure above this broadband light source, which has a -3dB band width of 117.6 nm, does not have a typical Gaussian profile since this source is in fact composed of two separate broadband sources at differing central positions, coupled together at the output. Although this light source does have a large spectral width and thus the resulting interference pattern generated would be narrow due to the short coherence length of 14.32 µm ± 0.076 µm, the envelope will result in the interference fringes shown in Figure 5.2. The coherence length was calculated using equation 3.22 with the error determined due to the variation of 0.60 nm in the measured -3dB band width. Figure 5.2 was obtained by illuminating the Michelson interferometer with this light source and scanning one of the arms through the position of zero OPL difference by increasing the voltage applied across the piezo fibre stretcher, monitoring the output intensity via an InGaAs photo-diode. The effect of a non-Gaussian profile on interference fringes has been previously reported (2). Due to the shape profile of the resulting interference fringes locating the central position of the fringe packet can be a difficult task.

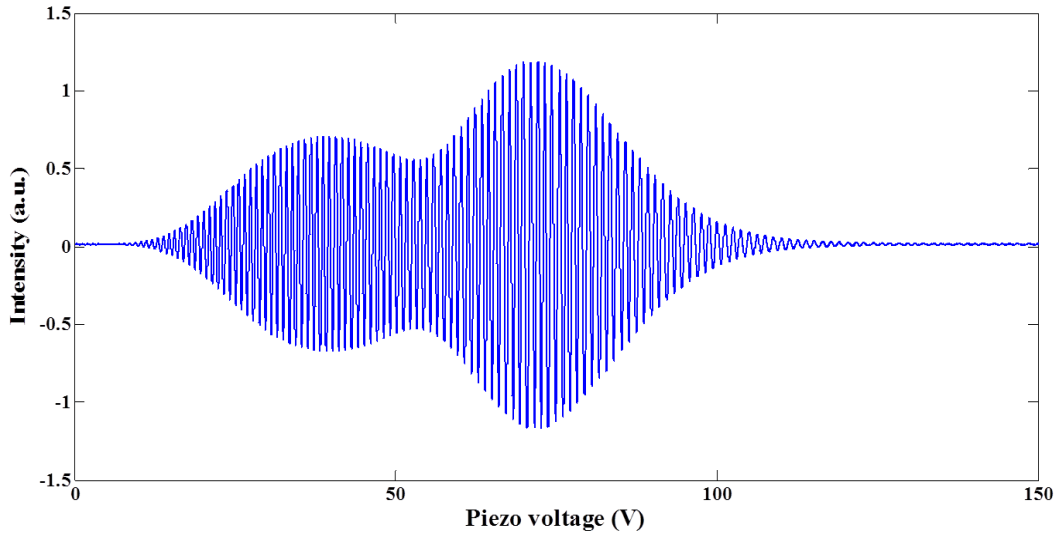

Figure 5.2: Effect of a non Gaussian spectral envelope of interference fringes during the scanning of optical path length. The interference pattern obtained is through illuminating the Michelson interferometer with the non-Gaussian light source and monitoring the intensity output via an InGaAs photo-diode whilst scanning one of the interferometer arms through the position of zero OPL difference via an increased voltage change across the piezo fibre stretcher.

With the existence of side lobes in the interference pattern, the Fabry-Perot cavity lengths could be affected, as overlap of the differential cavity length fringes and the Michelson interferometer reference fringes could superimpose. If it is desirable to use a multi-source broadband light source, methods such as the use of a tailor made fibre Bragg grating could be used to provide a near Gaussian spectrum. This however would incur additional charges. It was for these reasons that the remainder of the investigation would be carried out using a SLED light source, again provided by Exalos (1), centred at 1542.8 nm with the spectral profile illustrated in Figure 5.3. This spectrum was measured using an Advantest OSA model Q8384.

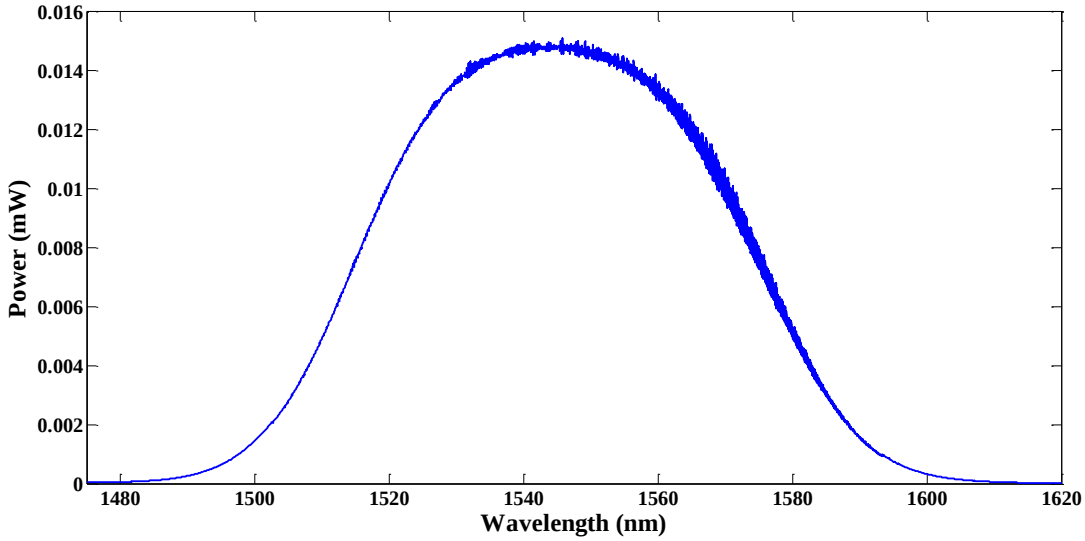

Figure 5.3: Spectral profile of the Exalos supplied broadband light source used for research centred at 1542.8 nm, measured using an Advantest OSA model Q8384.

With a -3dB band width of 60.0 nm, this particular light source will experience interference effects when the optical path lengths of the measurand in question are matched to within the coherence length, measured within the fibre core, of 27.02 µm ± 0.31 µm. The coherence length was calculated using equation 3.22 with the error determined due to the variation of 0.70 nm in the measured -3dB band width.

The coherence length of the source can also be determined through measurement of the resulting interference fringes during a scan of the Michelson interferometer. Interference fringes are generated when the OPL's of the two interferometer arms are matched within the coherence length, hence by measuring the change in OPL across these fringes, the coherence length is found to be half this value. To verify this the change in OPL over one of the interference fringe sets of Figure 5.4 was measured using a laser reference source and a fringe counting technique that will be discussed later in the chapter. Following this method the coherence length of the source was measured to be 26.52 µm ± 0.89 µm. This corresponds to the value obtained through calculation within the measurement error, found due to the error in determining fringes unobtainable due to system noise.

The broadband light source is used in the sensing configuration as a method of determining the location at which the optical path length between the two arms of the Michelson interferometer is equal to zero, and the location at which the mismatch in the

Michelson interferometer arm length is equal to the differential length of the two Fabry-Perot cavities. It is the length change, as a consequence of the fibre expansion due to the voltage applied through the piezo fibre stretcher, of the scanning Michelson interferometer between these two locations that determines the desired differential length. For that reason, the resulting interference pattern, shown in Figure 5.4, as a consequence of the system arrangement and the differential length, must be analysed as to the conditions from which it arises.

Figure 5.4 shows the plot of the measured intensity versus the applied voltage to the piezo fibre stretcher. As the voltage through the piezo ceramic increases this induces an OPL change in the Michelson interferometer due to stretching of one of the fibre arms, whilst the other arm remains constant. The length change that occurs due to the expansion of the piezo ceramic, and the subsequent expansion of the optical fibre length coiled around it, cannot be determined through the expansion properties of the ceramic material as a consequence of nonlinear effects with voltage, hysteresis with expansion, and the external force of the coiled fibre length acting against the ceramic. Determination of the change in the optical fibre length, between the two measurement locations of interest, will be found through use of the additional DFB laser light source propagating through the Michelson interferometer, analysing the interference effects of such light. Further details of which will be provided in section 5.2.2.

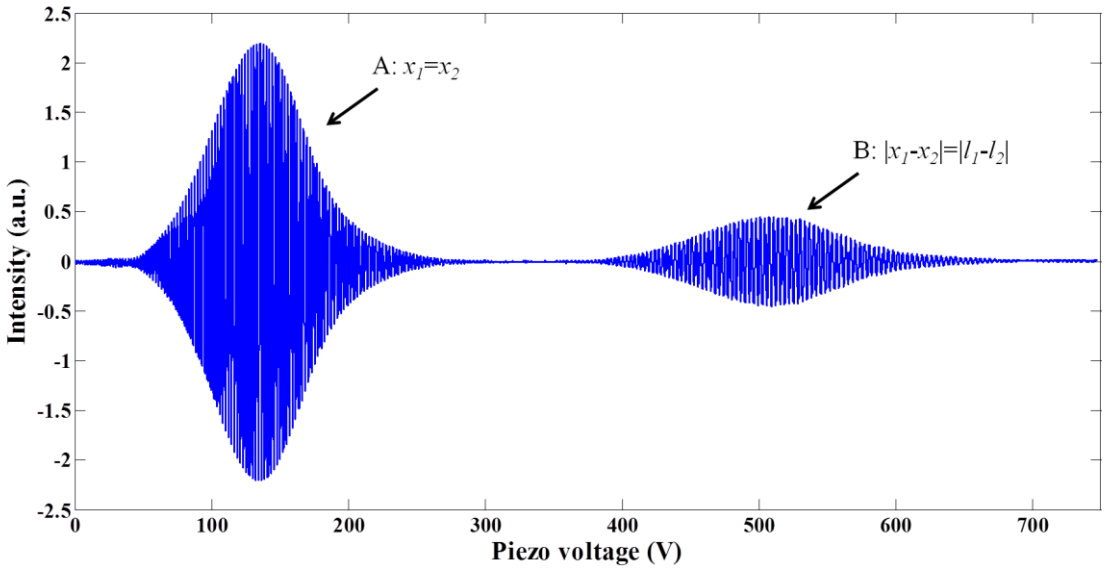

Figure 5.4: Interference fringes due to the characteristics of the Exalos broadband light source from the complete sensing configuration. The intensity is plotted against the applied voltage through the piezo fibre stretcher which induces an OPL change, the length of which will be determined through interference analysis of the additional 1310 nm DFB laser source. With reference to Figure 4.1, interference fringe packet A results due to equal optical path lengths of the scanning Michelson interferometer ($x_1=x_2$), and interference fringe packet B results from the modulus of the differential of the Michelson interferometer arms being equal to the modulus of the differential of the two Fabry-Perot sensing cavities ($|x_1-x_2|=|l_1-l_2|$).

Figure 5.4 shows the interference pattern, measured via an InGaAs photodiode at the output of the system, as a consequence of two Fabry-Perot cavities arranged in tandem with a connecting Michelson interferometer illuminated with a broadband light source. In order to provide a changing OPL one of the Michelson interferometer arm lengths is increased due to the increasing voltage through the piezo fibre stretcher. With reference to Figure 4.1, the first set of interference fringes, A, of Figure 5.4, results when the optical path lengths of the two Michelson interferometer arms, x_1 and x_2, are equal. Keeping one arm constant, interference effects are observed when the OPL of the changing fibre arm matches that of the stationary one within the coherence length of the broadband source used. In order to account for any external factors which may affect the change in OPL, both fibre lengths of the Michelson interferometer arms are

positioned within a stable environment, or an environment in which both fibre lengths will experience the same effects.

It is at the position of equal OPL's of the two Michelson interferometer arms that the start of the reference measurement for determining the final differential length is made. In order to always have this start reference measurement it is imperative that the initial length of the stationary fibre arm of the Michelson interferometer is made slightly longer than that of the scanning interferometer arm, such that when the arm length is increased, a matched OPL between the two will always be achieved.

The secondary set of interference fringes, B, is a result of a matched OPL between the modulus of the differential length of the Michelson interferometer arms, $|x_1-x_2|$, and the modulus of the differential length of the two Fabry-Perot sensing cavities, $|l_1-l_2|$. It is at this position where the reference measurement will end, with the desired differential length of the two sensing cavities being determined by the optical length change of the Michelson interferometer arm between the two reference positions determined through interference analysis of the DFB laser source.

Low coherent interference fringe analysis

In order to determine the length by which the fibre arm of the Michelson interferometer has been expanded due to the piezo fibre stretcher, between the two reference positions found by the interference fringe packets, the central position of each fringe packet must be located.

In Chapter 3, when discussing the theory behind the formation of interference fringes when using a broadband light source, techniques for determining the central position of the individual fringe packets were discussed. One of these techniques involved finding the position of maximum intensity, the point at which the OPL's of the interferometer are equal. As described, however, the maximum intensity, particularly when using a light source with a spectral width up to 100's of nm's, may be difficult to deduce due to the closeness of adjacent fringes and the effects of noise within the system. Using this method may result in an offset between the maximum peak intensity and the desired fringe packet centre, as was illustrated in Figure 3.15.

As a means of obtaining an accurate estimation of the central position and in order to remove the uncertainty as a result of noise, the Hilbert Transform is employed. The Hilbert transform (3), as described in Chapter 3, is a technique that can be used in signal processing to extract, in the case of this research, the corresponding envelope of an interferogram signal. By applying the Hilbert transform, using a VI module within the Labview computer language, to the resulting interference signal shown in Figure 5.4, the signal envelope, as illustrated in Figure 5.5, can be obtained. The first envelope peak at position A corresponds to the interference fringes resulting from the matched OPL between the two arms of the reference Michelson interferometer. The secondary envelope peak at B corresponds to the matched OPL between the modulus of the differential length of the two Michelson interferometer arms and the modulus of the differential length of the two Fabry-Perot cavities.

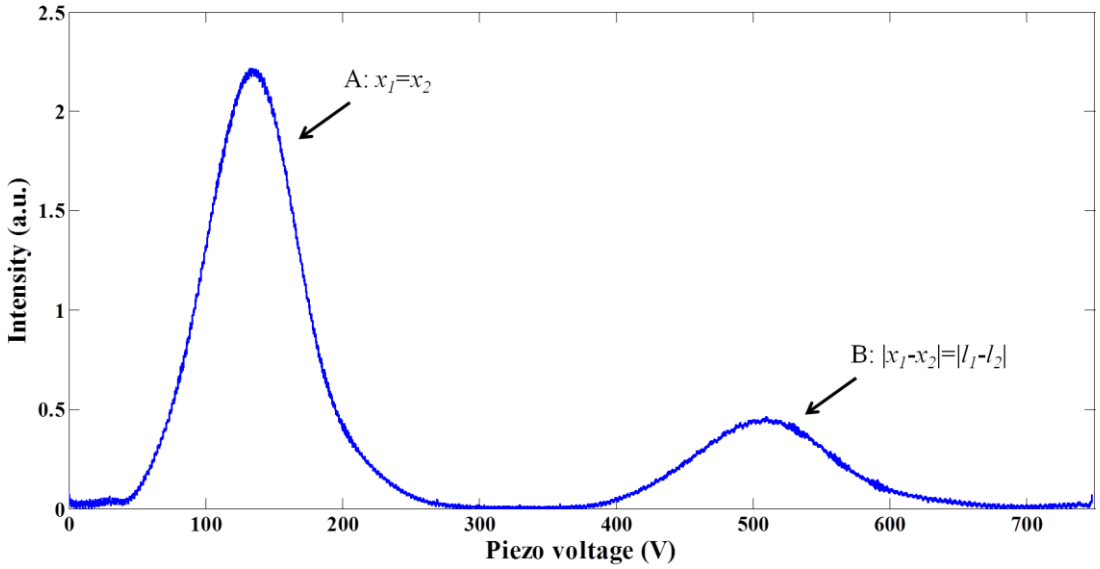

Figure 5.5: Signal envelope of interference fringes shown in Figure 5.4, generated as a result of the interaction of the 1550 nm broadband light source with the sensing system, found through use of the Hilbert transform.

It is from the signal envelope that the central position of the interference packets can be deduced. Using a 'peak finding' technique applied to each of the envelope curves from the two sets of interference fringes, the central positions can be found and used for determining the differential length of the two cavities.

The peak detector used for the data analysis is a VI module within the LabView programming language, which can be used to find the location, amplitude, and second derivative of peaks within a section of processed signal data (4). The peak detector VI function is based on an algorithm that fits a quadratic polynomial to sequential groups of data points, specified by a given width. The purpose of such a given width is to remove the detection of unwanted peaks being located where noise spikes may exist within the signal under analysis. For each peak a quadratic fit is applied to consecutive data points, the number of which being greater than the width value, above a specified threshold value. If the number of data points above the specified threshold does not exceed the width value, the fit is not applied and no peak is detected. The peak location of the polynomial, the position where the derivative is equal to zero, is calculated via the VI.

When recovering the peak positions of the two interference fringe packet envelopes, given by the corresponding optical path lengths of the sensing configuration, it was found that over a period of time, due to effects of noise, that the determined peak would shift, however within the measured data there existed areas whereby no data would be recovered. This effect, which has been previously investigated, is referred to as the 'zone of avoidance'.

In a previous experiment to investigate this phenomenon, the peak find VI was used to calibrate the wavelength stability of an OSA monitoring a single wavelength line of a hydrogen cyanide (HCN) gas cell.

These 'zone of avoidance' bands are a consequence of the peak width parameter used in the peak find routine. If the width is set to a high value compared to the actual width of the peak, then the quality of the fit is degraded. To combat this problem the data over which the polynomial fit is applied is interpolated prior to running the peak find routine. Interpolation of the data does not improve on the inherent accuracy of the interrogation technique however it does eliminate the discontinuity. Figure 5.6 shows the recovered wavelength line of the HCN gas cell where, (a) no interpolation of the data is carried out, and (b) interpolation is carried out on the data.

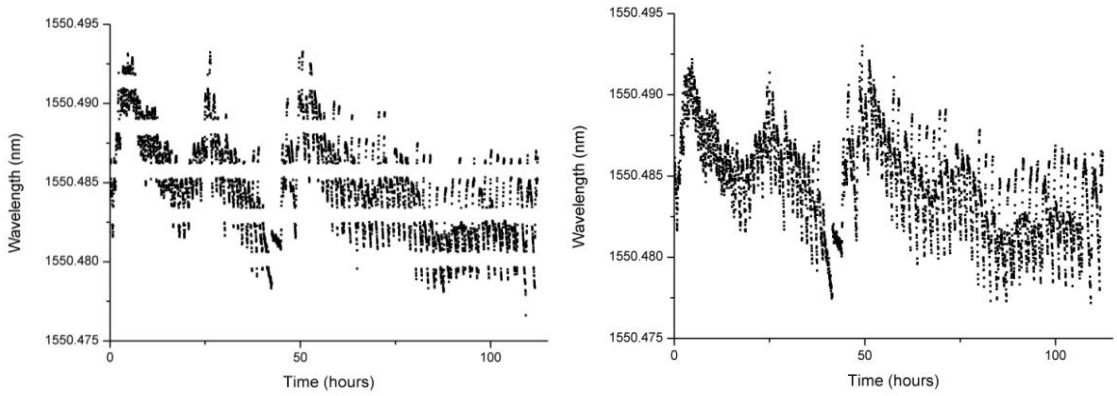

(a) (b)

Figure 5.6: Recovered wavelength peak of a HCN gas cell found using the peak find VI within the Labview computer program. Figure (a) shows the recovered wavelength with areas of no data, referred to as the 'zone of avoidance', due to no interpolation of the signal prior to the peak find algorithm. Figure (b) shows the same data, however with interpolation being carried out, and thus no 'zone of avoidance' areas.

With a routine in place to accurately determine the peak position of the interference fringe packet envelopes and thus the central positions of said fringe packets, the range over which the differential length to be measured can be determined due to the reference interference fringes as a result of the Michelson interferometer matched arm lengths, and the measurement interference fringes as a result of the optical path length equality between the differential length of the Michelson interferometer arm lengths due to the changing path length of one arm and the differential length of the two Fabry-Perot sensing cavities.

5.2.2. Reference measurement

Having secured a procedure using a broadband light source to determine the reference positions between which a differential length of two Fabry-Perot sensing cavities can be derived, taking advantage of the effects of interference, it is important to develop a technique for accurately measuring the length change between these two positions.

When the two Fabry-Perot micro cavities are kept stable, the interference effects observed are as a result of the scanning Michelson interferometer through which one of the fibre arm optical path lengths in increased due to a piezo fibre stretcher. Matching OPL's in the Michelson interferometer and matching differential lengths in the Michelson interferometer with the differential in the sensing cavities supply the positions between which the change in OPL should be measured. This in turn will provide the differential length required of the sensing Fabry-Perot's.

With the overall measurement accuracy dependant on the accuracy with which the reference measurement can be made, it is imperative that the mechanics of the piezo fibre stretcher are known.

In order to provide a suitably large range over which measurements can be made approximately 10 meters of fibre are coiled around a piezo-electric tube 25 mm in length with an outer diameter of 38 mm. Without any fibre coiled around the piezo tube, the expansion due to applied voltage could be determined using equation 3.27, knowing the piezo material properties. This equation cannot be used however when the fibre length is wound due to the external restriction the ~ 83 turns of fibre will introduce. Even if equation 3.27 could be adapted to compensate for the additional force of the fibre, given that the exact fibre length is not known due to expansion of the fibre that may have resulted during the winding procedure as a consequence of a constant applied strain, and that a fibre length of 10 meters is simply an approximation, methods have to be deployed as a means of calibrating the fibre length increase.

Piezo ramp voltage

One method of determining by how much the coiled fibre length increases with applied voltage would be by measuring the differential length of the two Michelson interferometer arms, through a means of the FSR measurement technique described in section 2.5.5, when no voltage is applied to the piezo material and when the maximum voltage is applied. The length change from these measurements can then be determined and fibre expansion per applied voltage can be calculated. When using this approach, it is important to note that in the initial state of the Michelson interferometer the fibre arm to be expanded is set to a slightly shorter length than that of the stationary arm to allow the expandable arm to pass through the position of equal arm length.

This is a suitable technique for determining the fibre expansion per applied voltage assuming that the piezo stretcher expansion is linear with applied voltage. Studies have shown however that this is not the case (5). Figure 5.7, which shows a curve for the change in OPL against the change piezo voltage, verifies the non-linear fibre expansion with applied voltage for the piezo fibre stretcher used for this research.

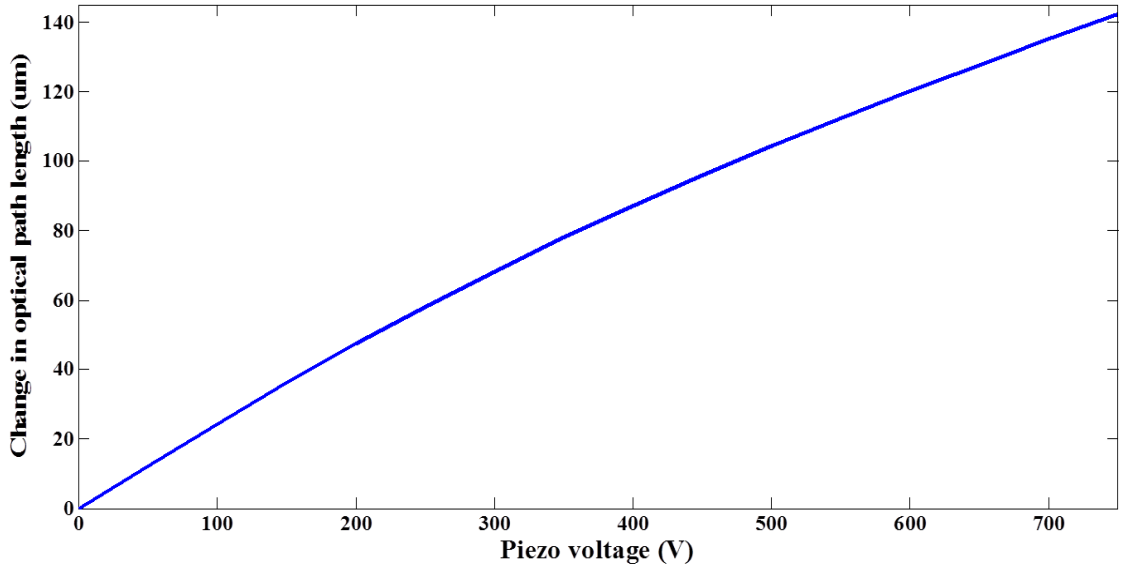

Figure 5.7: Change in the OPL of the fibre arm of the Michelson interferometer due to the expansion of the piezo fibre stretcher with applied voltage. The length change of the fibre is calculated through monitoring the interference fringe effects that are emitted via the Michelson interferometer when illuminated with a DFB laser source whilst the OPL is changing due to the piezo voltage.

The length change of the fibre was calculated using the fringe counting technique which will be discussed in the following sections as a means of determining the differential length desired, utilising the interference effects that will be observed due to a changing OPL within a Michelson interferometer when illuminated with a DFB laser.

Figure 5.7 shows that the OPL of the fibre changes more rapidly at the start of the voltage ramp when compared to the length change at the end of the voltage ramp. It is for this reason that an alternative method is employed as a means of characterising the reference Michelson interferometer.

Laser reference source

As a result of the nonlinear expansion of the piezo stretcher with applied voltage an alternative approach for measuring the change in optical path length was implemented.

With the implementation of a secondary light source in the form of a single wavelength laser, the change in optical length of the Michelson interferometer arm can be monitored whilst voltage is applied through the piezo stretcher to induce expansion. Figure 5.8 shows the monitoring arrangement used of the Michelson interferometer with the use of WDM's to introduce and extract the laser signal.

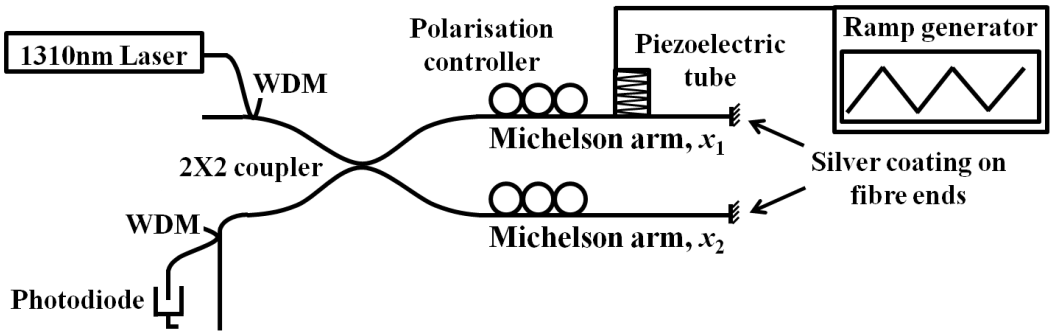

Figure 5.8: Schematic of the arrangement of the Michelson interferometer with the incorporated 1310 nm DFB laser source used for monitoring the OPL change during the piezoelectric tube expansion.

In Chapter 3 the theory behind the interference effects that are observed when illuminating a Michelson interferometer with a light source of single wavelength were discussed. If monitoring the output via an InGaAs photodiode, interference effects are not observable when the interferometer is in a stationary state. Only when the OPL of one of the interferometer arms is changing are interference effects detected in the form of fringes shown in Figure 5.9. This therefore provides an ideal solution for determination of the length change of the optical fibre between the two reference positions due to the expansion effects of the piezo stretcher through the number of interference fringes witnessed.

Figure 5.9 shows a decrease in intensity as the voltage through the piezo fibre stretcher, and subsequently the fibre length of the interferometer arm, is increased. The change in the monitored output intensity comes as a result of the change in the polarisation state of

the propagating light within the Michelson interferometer due to the changing fibre length. This was verified as alterations to the Michelson polarisation controllers, as a means of altering the polarisation state, resulted in differing output intensities for a changing OPL.

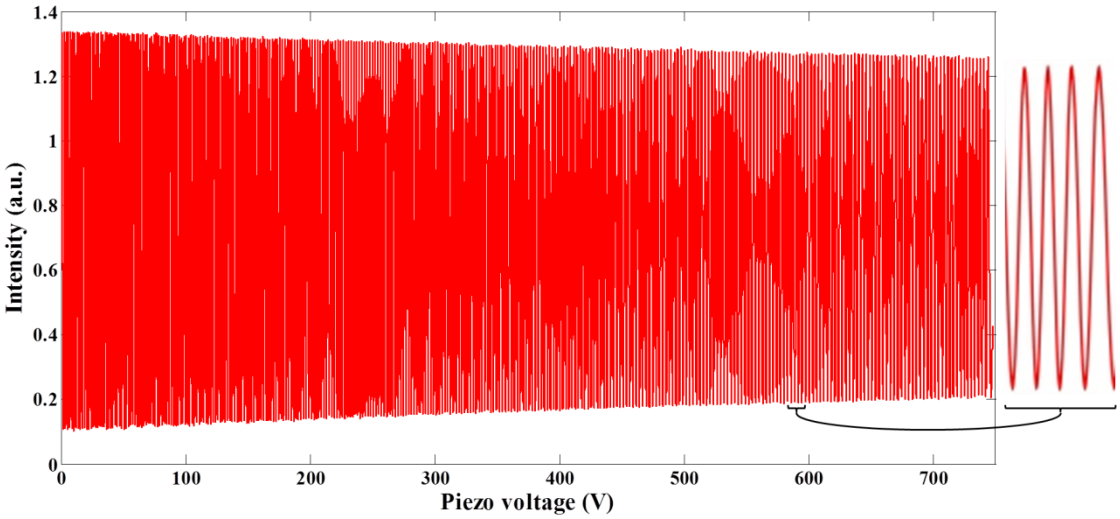

Figure 5.9: Interference fringes as a result of the 1310 nm DFB laser source during expansion of the piezoelectric fibre stretcher when the voltage is gradually increased.

Whilst illuminated with a DFB laser the Michelson interferometer arm is expanded due to applied voltage to the piezo fibre stretcher, altering the OPL within that arm, whilst keeping the secondary interferometer arm length stable. The DFB laser used has an operating wavelength of 1308.17 nm with a wavelength stability of 1.3 pm as was monitored via a Burleigh WA-7600 multi wavelength meter. Figure 5.9 shows the detected interference fringes monitored via an InGaAs detector whilst the applied voltage to the piezo fibre stretcher is ramped at a constant rate from an initial value of zero to the maximum value of 750 V.

Figure 5.7 shows the effects of nonlinearity in piezo expansion with applied voltage. The length change in the fibre with applied voltage through the piezo material was calculated by observing the number of interference fringes over a given voltage range and using the fringe counting technique as will be described in the following section. On closer inspection of the interference fringe spacing at different stages of equal applied voltage, as illustrated in Figure 5.10 (a), (b), and (c), it can be seen that the

fringe spacing increases from when the voltage is first applied (Figure 5.10 (a)) to when the voltage approaches the maximum (Figure 5.10 (c)).

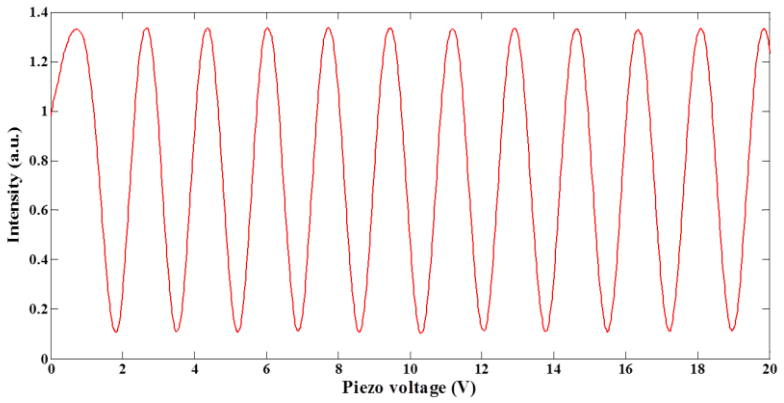

(a)

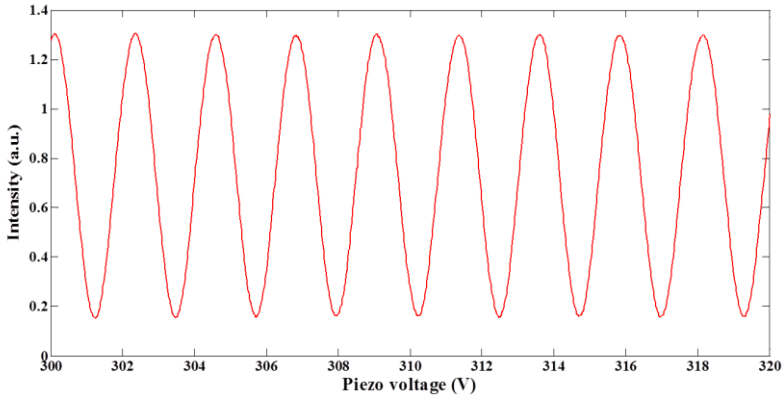

(b)

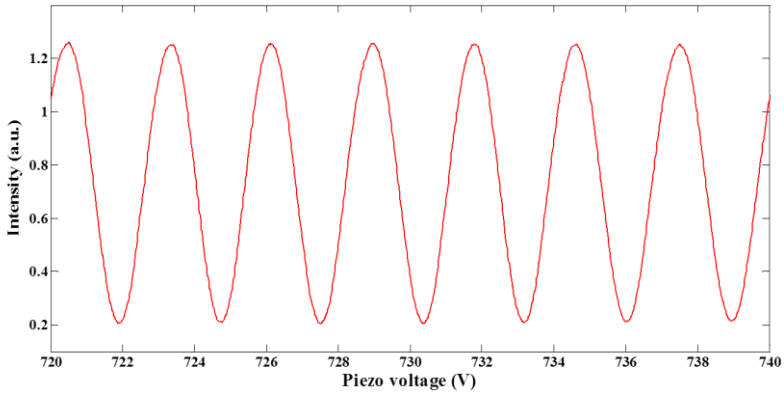

(c)

Figure 5.10: (a) Interference fringes due to voltage increase from 0-20 V. (b) Interference fringes due to voltage increase from 300-320 V. (c) Interference fringes due to voltage increase from 720-740 V. Increased spacing between adjacent fringes as the voltage is increased confirms the nonlinear expansion of the piezo material with applied voltage.

As has been demonstrated, by using a laser light source to illuminate the Michelson interferometer, length changes can be monitored through the analysis of the generated interference fringes, removing the uncertainty introduced by the nonlinear expansion of the piezo fibre stretcher material with applied voltage. This additional calibration measurement also removes the necessity of having to temperature stabilise the Michelson interferometer as the change in the optical path due to the scanning piezo fibre stretcher will occur more rapidly than temperature drifts surrounding the system.

By extracting the resultant interference fringes generated via the 1310 nm DFB laser within the Michelson interferometer due to OPL changes in one of the interferometer arms and performing a fringe counting technique to precisely determine the number of interference fringes, the desired differential length between the two sensing cavities can be found.

Fringe counting technique

Accurate determination of the number of interference fringes occurring as a result of the laser light source within the Michelson interferometer is essential for obtaining the optical length change taking place between the two broadband light source reference positions from the interaction between the Michelson interferometer and the Fabry-Perot sensing cavities.

A process has been developed and deployed within the system to determine the exact number of fringes as a means of making a final length measurement. Before this procedure is applied the d.c. offset of the interference fringes is removed by taking the average fringe intensity and subtracting, to provide a zero crossing point for each fringe, such that the number of zero crossing points within the data set can be established using a Labview sub VI. This VI operates by analysing the data, point by point, to establish whether the current data value is of the opposite sign, i.e. positive or negative, of the previous data value. For each change in sign value the VI records a zero crossing position.

Interpolation and smoothing of the data set prior to this stage is pivotal. Smoothing, through a process of averaging, of the data set removes the effects of noise, preventing the detection of zero crossings at positions where noise spikes may exist. Interpolation is also essential as due to the VI analysing the data point by point, it is important to

determine the data point at which the position at which the zero crossing occurs, as close to the value of zero as possible. This is particularly essential as the positions of first and last zero crossing must be recognised.

Having scanned the interference fringe data set, and determined the number of zero crossing positions, the following equation, knowing that each zero crossing is equal to half a fringe, can be used for calculating the resultant number of interference fringes, *m*, between the first and last zero crossing positions

$$m = \frac{(N-1)}{2} \tag{5.1}$$

Where *N* is the number of zero crossing positions. The subtraction of one from the number of zero crossing positions is to take into account the first zero crossing position which does not have a complete half fringe before it.

Although this approach provides the number of interference fringes whereby a complete fringe crosses the zero axis, in order to accurately measure the full length change monitored via the number of interference fringes occurring, the partial fringes between the first data point in the series and the first zero crossing, and the last zero crossing and the last data point in the series must be considered.

In order to find what fraction of a fringe exists at the start of the data series, shown in Figure 5.11 (a), the number of data points in the first complete interference fringe, from the first zero crossing to the third, is counted. This value is then compared to the number of data points in the first small fraction is order to provide a ratio of that to a complete fringe. A similar approach is used to calculate what fraction of a fringe exists at the end of the data series, illustrated in Figure 5.11 (b). In this instance however, the ratio is found when comparing the number of data points in the small fraction to that of the last complete interference fringe, from the third last zero crossing to the last.

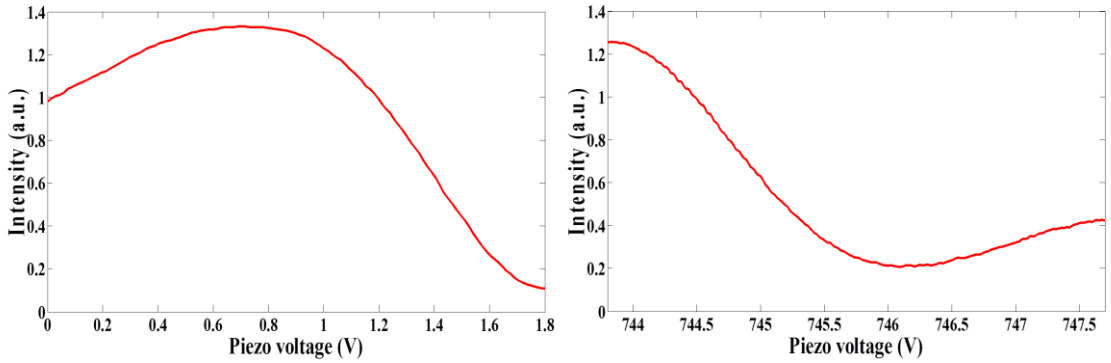

Figure 5.11: (a) Fraction of fringe at start from the first data point in the extracted set to the first zero crossing position, (b) Fraction of fringe at end from the last zero crossing position to the final data point in the extracted set.

As a result of the closely spaced fringes at the start of the optical scan compared to the slightly wider spaced fringes at the end, due to the nonlinear expansion of the piezo fibre stretcher, there will be a greater number of data points in the first complete fringe compared to the last. It is for this reason that when calculating the fringe fraction at the start and end of the data set it is not a viable solution to simply consider the average number of data points for each fringe in the complete series, and why the number of data points per fringe is calculated separately for the beginning and the end.

Implementing the above protocol to find the precise number of fringes between the measurement positions and applying this to the equation below, the optical path length change, Δd, and thus the differential length between the two Fabry-Perot sensing cavities can be calculated.

$$\Delta d = \frac{m\lambda}{2n} \tag{5.2}$$

Where λ is the wavelength of the DFB laser source, 1310 nm, n is the refractive index of the optical fibre, and m is the number of interference fringes counted.

The use of a separate light source and the implementation of the above mentioned fringe counting technique, provides a stable approach to characterising the optical length change of the Michelson interferometer arm due to the piezo fibre stretcher.

With the scan rate of the Michelson interferometer less than the time resolution of the InGaAs photo diode, 30,000 data points over the full scanning range can be captured. Through data analysis, in which the captured data is interpolated to provide 300,000 data positions over the scan range consisting of ~319.7 interference fringes providing 938.38 data points per fringe, the above fringe counting technique could be used to determine the number of interference fringes to within $1/938.38^{th}$ of a fringe. This corresponds to a length of 0.48 nm either side of the extracted data. As will be detailed in section 5.4 however, this is simply one parameter in calculating the Fabry-Perot differential length. The accuracy of determining the peak location of the broadband fringe envelopes due to the noise within the system, must be taken into consideration. Variations in the recovered peak position subsequently determines the length over which the reference fringes are calculated.

5.3. Differential Length Measurements

Having described so far an arrangement for making differential measurements of two independent sensing cavities and a procedure by which the system can be characterised to provide accurate results, the capture and analysis of data can be made.

5.3.1. System arrangement

With the reference scanning Michelson interferometer encased within a temperature stabilised environment to reduce the effects of optical path length change due to external factors, the Fabry-Perot sensing cavities, formed using the Fresnel reflections from the end surface of the optical fibre and a reflective mirror surface, are arranged in such a manner as to also prevent the effects of temperature drift from altering the fixed optical path length. Through positioning both optical fibres on the same mounting block and using the same reflective mirror, as shown in Figure 5.12, temperature or other environmental changes causing the mounting block to expand or contract will have an equal effect on the position of both fibre positions. This will therefore not alter the differential length of interest.

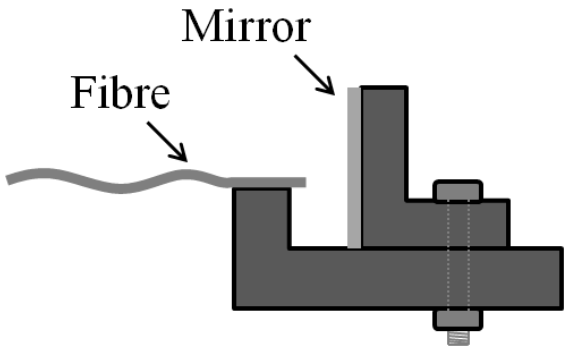

Figure 5.12: Fabry-Perot sensing cavity mounting positions to allow for minimum differential length changes due to environmental effects.

In Chapter 4 it was stated that due to the manner in which interference effects take place with the use of a broadband light source, there are certain limitations that have to be taken into consideration with the Fabry-Perot optical cavity lengths. Individual cavities of short length may be observable when monitoring the system output if matched to within the coherence length of the scanning Michelson interferometer, and for that reason must be longer than the overall differential length of the two. The differential length must also, however, be greater than the coherence length of the source. If closely matched, overlap of interference fringes may result, providing inaccurate measurements due to superimposition of the fringes. It is for these reasons, and in order to determine if the length determined is that desired, that the individual sensing cavity lengths must be known prior to recording measurements.

Using a micrometer optical stage to position the optical fibre, the arrangement shown in Figure 5.13 consisting of a 3-port circulator and an OSA is illuminated with a broadband light source. The OSA used in this instance was an Advantest OSA model Q8384 which operates using a monochromator and diffraction grating arrangement, as described in section 2.5.3. Using the OSA to monitor the reflected intensity pattern, similar to that shown in Figure 2.20, from the fixed Fabry-Perot cavity over the wavelength range of the broadband light source, the cavity length can be determined using the FSR measurement technique as described in section 2.5.5. Once at a suitable length, meeting the criteria of the length limitations set out in section 4.2.2, the fibre is adhered to the mounting block using a fast setting adhesive. A final length calculation for each of the cavities is made to allow for any shifts in position during the adhesive hardening period, thus providing a known differential length. Through fusion splicing,

the individual Fabry-Perot cavities are connected to the optical fibre interconnecting leads of the tandem sensing configuration.

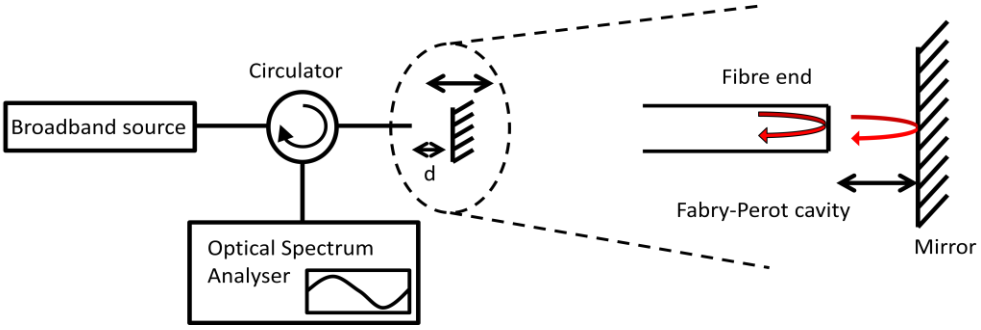

Figure 5.13: Configuration for determining and setting the individual Fabry-Perot cavity lengths. Individual lengths are monitored via the free spectral range measurement technique.

A signal generator unit, used to feed the high voltage amplifier which in turn provides the voltage to the piezoelectric material for expansion of the optical fibre, is programmed to produce a periodic, symmetric triangular waveform, with a maximum applied voltage to provide significant fibre expansion in order to monitor the interference fringe patterns.

Illuminating the full sensing configuration with the 1550 nm broadband light source, and using WDM's for the introduction and extracting of the 1310 nm DFB laser into and out from the Michelson reference interferometer, InGaAs photo diodes provide intensity monitoring of each light source via the separate outputs within the system as a means of observing the effects of interference as the piezo fibre stretcher is scanned from its initial position of zero voltage through to the maximum applied.

For a differential length between the two Fabry-Perot sensing cavities of 82.571 µm the resultant interference fringe effects, due to a changing optical path length as the piezo voltage is gradually increased, are illustrated in Figures 5.4 and 5.9, resulting from the characteristics of the 1550 nm broadband light source and the 1310 nm DFB laser source respectively.

Repeated scans over a periodic time frame of the piezo fibre stretcher provide raw data on which analysis is carried out to provide differential length measurements.

5.3.2. Data analysis

Capture of the intensity signals of the two separate light sources producing the interference patterns is through two InGaAs photo diodes. An analogue to digital converter transfers the raw data captured via the detectors to a Labview computer program in order for analysis to take place.

The program is initially set to recover the intensity measurements of the 1550 nm light source interference fringes, the 1310 nm DFB laser source interference fringes, and also the voltage level applied to the piezo fibre stretcher during the forward scan of the Michelson interferometer. 30,000 data points over the full range of the piezo scan for each of the three parameters are recovered.

Before investigation into the data can begin the d.c. offset of the interference fringe intensities recorded for both sets of light sources is removed. It is from here that the procedure is carried out to find the central positions of the broadband light source interference fringe packets, due to the effects of light interaction with the Michelson interferometer and the differential of the Fabry-Perot sensing cavities, extract the corresponding data obtained via the interference effects of the DFB laser source with the Michelson interferometer during the optical path length change from the piezo fibre stretcher, and calculate the relative number of interference fringes within that selection of data.

With a known differential length between the two Fabry-Perot cavities of 82.571 μm, the same that was used in the generation of the interference fringes shown in Figure 5.4, and having removed the d.c. offset, the Hilbert transform is carried out on the broadband light source interference fringe data set as a means of obtaining the fringe envelope shape, illustrated in Figure 5.5, to which a peak finding algorithm will be applied in order to determine the central fringe packet locations.

Interpolation of the data is performed prior to the peak find algorithm being carried out. The interpolation of the data set at this stage is to provide additional data points between the already existing data positions to improve the accuracy with which the peak position will be determined and remove the consequence of a zone of avoidance, as mentioned in section 5.2.1, due to the properties of the Labview peak finding VI. Equal interpolation must be performed on all three sets of data due to the data extraction of the DFB laser

interference fringes between the two reference positions determined via the peak values of the fringe envelopes.

Having obtained the peak position of the two fringe packet envelopes due to the interference pattern of the broadband light source as a result of the interactions within the sensing configuration, the corresponding data, between these two positions, of the laser interference fringes due to the changing optical path length of the Michelson interferometer is extracted from the full captured set as demonstrated in Figure 5.14.

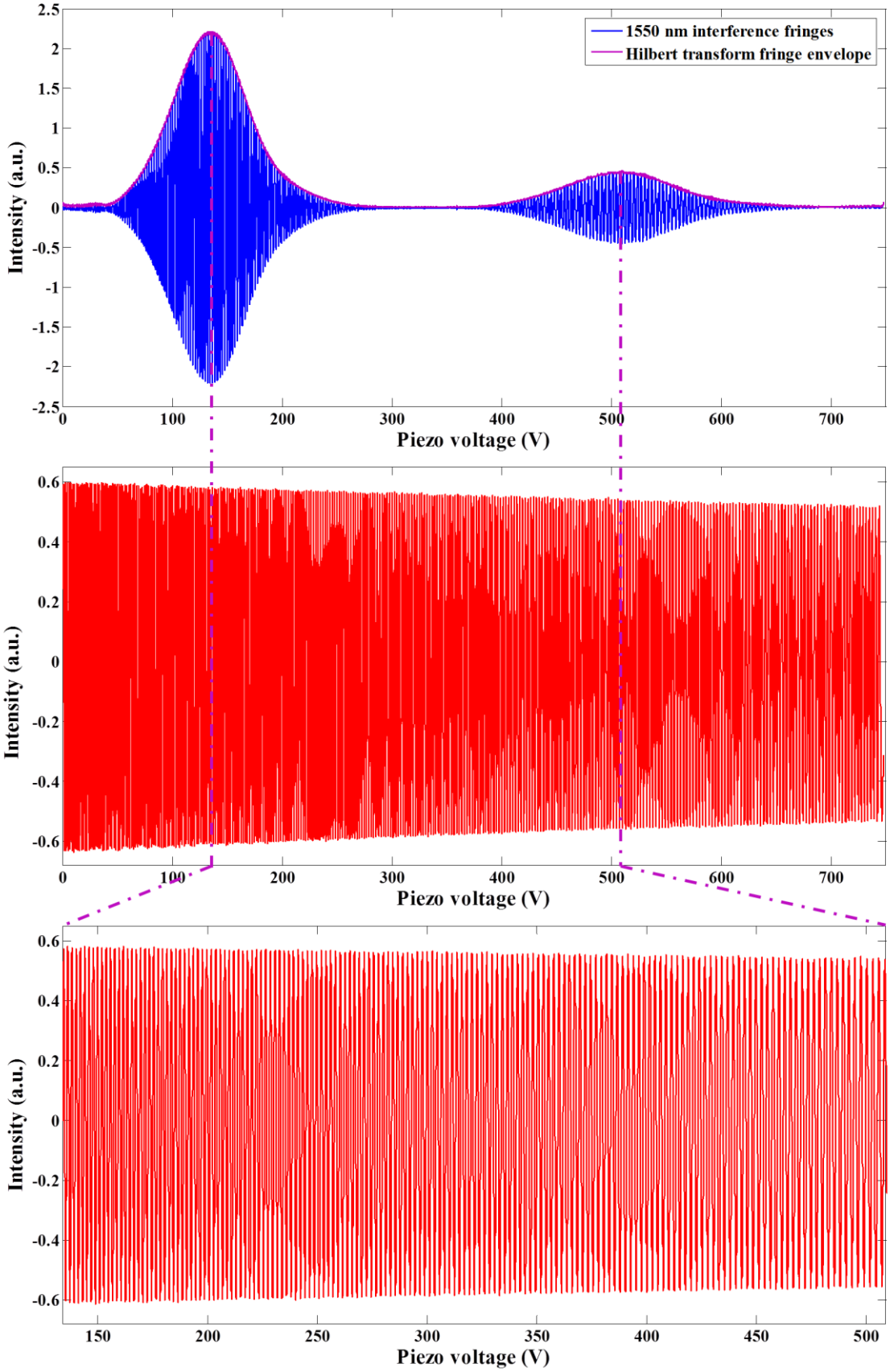

Figure 5.14: 1310 nm fringe extraction between the two peak positions of the 1550 nm fringe envelopes.

It is to these extracted fringes that the previously mentioned fringe counting technique is applied as a means of determining the change in optical path length required to obtain an equal differential length between the two fibre arms of the Michelson interferometer and the differential length between the two Fabry-Perot sensing cavities, from the position where both arms of the Michelson interferometer are of equal length. The change in optical path length, which is therefore also the desired differential length of the two sensing cavities, is found using equation 5.2.

Repeated differential lengths of the two Fabry-Perot cavities over a period of time, as shown in Figure 5.15, can be recorded and saved for additional analysis if required.

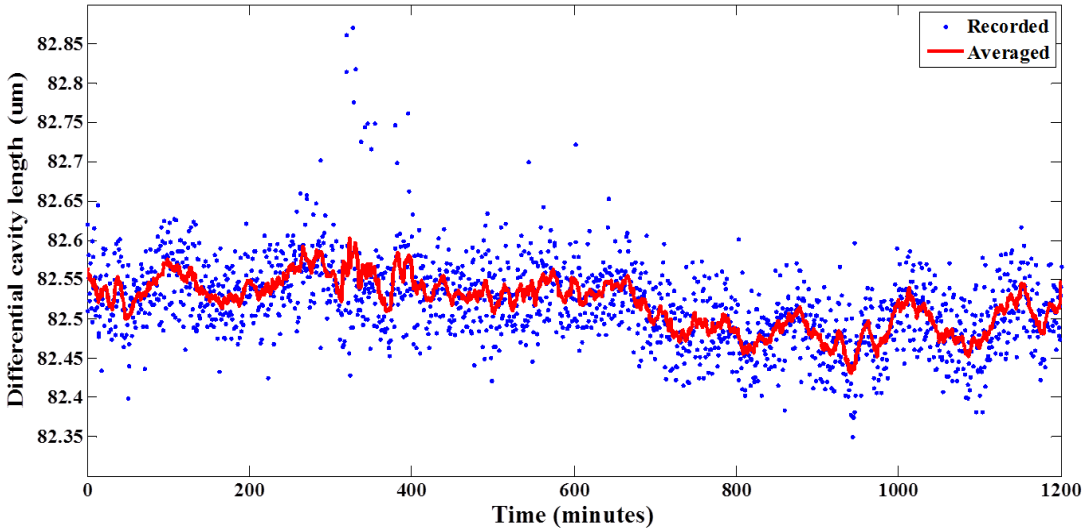

Figure 5.15: Fabry-Perot differential length measurements recovered using the sensing configuration illustrated in Figure 4.1, and the data analysis techniques described in this chapter.

When the recorded results were analysed, the average differential cavity length of the 1818 repeated measurements was measured as 82.539 µm ± 0.041 µm (± 1σ), demonstrating a procedure for successful measurement of differential length. Fluctuations in the measured differential length could be as a result of temperature drifts in the surrounding environment of the sensing cavities, or the instability of the optical fibre mounting structure at the sensing cavities.

Based on the arrangement used to obtain the above results, the differential length range over which measurements can be taken is 88.435 μm. This is calculated from the scanning range of the Michelson interferometer due to the expansion of the optical fibre arm length coiled around the piezoelectric ceramic tube, and the maximum voltage applied across the piezo material poles. The coherence length of the light source and thus the width of the resulting interference fringes must also be taken into consideration. It is therefore during the diaphragm development stage, as will be reviewed in Chapter 6, that the measurement range has to be used in order to establish a suitable design such that the central deflection will exceed the maximum differential length when the maximum specified pressure, based on the guidelines provided in Table 4.1, is applied.

Knowing the range over which the differential length can be made is useful in developing a suitable deformable diaphragm which can deal with the pressure range guidelines, however the noise of the system, detailed in Figure 5.15 must also be considered. Although it is possible to design a diaphragm with deformation characteristics that will meet the guidelines for the maximum pressure range, it may not be suitable in providing the minimum deflection required, resulting from the system noise, for measuring the differential pressure resolution of 1 Pa. Both the noise, in terms of the minimum deflection required for 1 Pa pressure, and the Michelson interferometer scanning range, in terms of the required pressure range, must be taken into account when developing the sensing diaphragm.

5.4. System Resolution and Noise

From the previous section, the uncertainty in the determined differential length, through obtaining the standard deviation of the repeated measurements, was found to be 41 nm. In order to establish the system resolution the parameters that contribute to the measurement have to be taken into consideration and the effects of noise on these parameters.

5.4.1. Resolution

Contributing factors to the noise effects within the system may include optical noise from the different light sources, and from digital noise due to the InGaAs detectors, the cabling in the connections of the analogue-to-digital converter unit, and the analogue-to-digital card itself. Possibly the main contributing factor to the uncertainty in the measurement accuracy lies in the determination of the central locations of the broadband light interference fringe packets, through use of the Hilbert transform for envelope detection and through the Labview peak finding routine.

As a result of the power lost of the broadband light source throughout the system and due to the coupling of light at the fibre interface of the Fabry-Perot sensing cavities, noise within the detected interference fringe signal can affect data analysis, thus influencing the location at which the peak of the fringe packet envelope is identified. Figure 5.16 shows a magnified view of one of the fringe packet envelope peaks, found through application of the Hilbert transform on the interference pattern, illustrating the signal scatter due to the effects of noise.

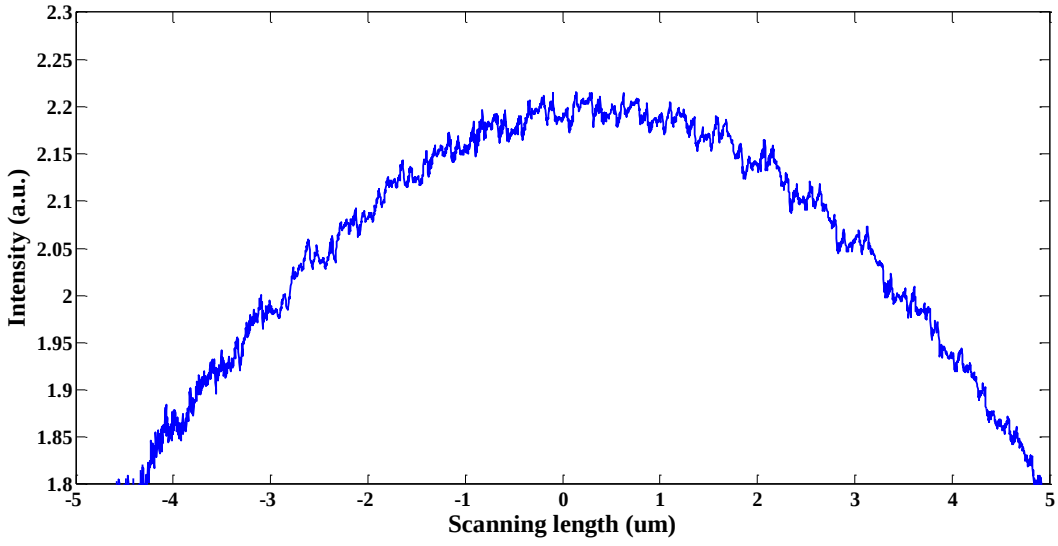

Figure 5.16: Envelope peak showing noise within the system.

The process through which the peak find routine determines the peak location is through the application of a curve fitting function to the data selected. The VI performs a least-square quadratic fit on a window consisting of the number of data points specified.

Due to all the data points being taken into account for fitting the most appropriate curve to the set, the influence of noise can result in varied shifts in the position of the fitted curve and in turn result in a shift in the identified peak position from the actual peak position. As the location of the two low coherent peaks is carried forward as part of the data processing and used as the reference positions for the extraction and analysis of the DFB laser interference fringes, shifts in the identified peak location will result in different differential lengths being determined via the system for repeated measurements of a given known length.

The level of noise as detected at the output of the InGaAs photo diode for the interference fringes generated via the broadband light source is 0.005 V. This is partly due to the signal loss through the system, electrical noise generated through the detector, due to the gain settings required in order to detect the output signal, and the bit resolution of the analogue-to-digital converter.

As a means of predicting the system resolution with the current arrangement, the variation in the recovered peak location of the two broadband interference fringe envelopes, as a result of the system noise, is determined. A method of obtaining this variation is through a system model based on experimental parameters. With a noise level of 0.005 V applied to a simulated interference fringe pattern as would be generated with the 1550 nm broadband light source and interrogation arrangement used, repeated scans were carried out in order to observe the spread in the recovered peak locations of the two interference packets.

Based on the fringe counting technique detailed in section 5.2.2 in which a change from one data position to the next corresponds to a length change of 0.48 nm, it was found through taking the standard deviation that the variation in the recovered peak location at the position of equal path length of the two Michelson interferometer arms corresponds to a length change of 5.68 nm. Taking the standard deviation of the variation in the recover peak location at the position where the OPL differential of the two Michelson interferometer arms is equal to the OPL differential of the two Fabry-Perot sensing cavities corresponds to a length change of 26.84 nm. Combination of these two errors results in a potential length variation of 27.43 nm.

It is clear that the noise effects in the recovered peak location of the fringe envelop is the main contributing factor to the system performance. It can therefore be noted that with the current arrangement the system resolution would be 27.43 nm.

The calculated system resolution of 27.43 nm is less than the calculated measurement uncertainty of 41.00 nm indicating that something within the system during the measurement process was not stable. One possibility for this is the stability of the Fabry-Perot cavity lengths. Due to the mounting of the optical fibre, as illustrated in Figure 5.12, small variation in the cavity length could result due to slight changes in the surrounding environment.

5.4.2. Noise reduction techniques

The previous section discussed the system resolution based on the effects of noise on the recovered interference fringes. Methods such as filtering can be introduced after the intensity signal is detected as a means of improving the signal to noise ratio prior to data analysis.

The interference fringes of interest, resulting from the system interactions of the broadband light source, occur at a lower frequency than the high frequency noise interactions which may cause shifts in the signal during analysis. An approach for removal of these high frequency anomalies would be to introduce a resistor-capacitor (RC) circuit in the form of a low pass filter after the capture of data.

A low pass filter can be a combination of capacitance, inductance or resistance intended to produce high attenuation above a specific frequency with little or no attenuation below that frequency. The frequency at which the transition occurs is called the "cut-off" frequency. A simple passive RC low pass filter consists of a single resistor and capacitor as shown in Figure 5.17. The arrangement shown below is generally known as a "first-order filter" as it consists of only one reactive component, the capacitor (6).

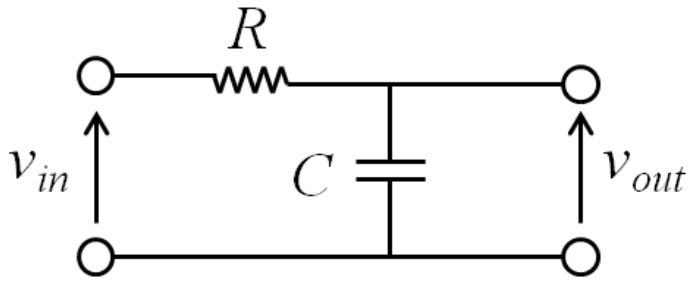

Figure 5.17: Schematic of a first order low pass filter RC circuit.

When developing a low pass filter it is important to consider how the signal output changes in terms of intensity and phase for a given "cut-off" frequency as the signal frequency changes.

The frequency response curve of an RC circuit illustrates that for signals of low frequency the input passes directly to the output until it reaches the "cut-off" frequency. At frequencies beyond this point the response of the circuit decreases giving a negative slope of -6dB/Octave.

At the "cut-off" frequency the output signal is at 70.7% of the input signal. It is for this reason that the selected "cut-off" frequency is beyond the frequency value of the fringes of interest as not to attenuate the usable signal. The "cut-off" frequency must also be considered due to the -45° phase change of the signal that occurs at this point. Equations 5.3 and 5.4 calculate the "cut-off" frequency and the phase shift respectively of given values of resistance and capacitance.

$$f_c = \frac{1}{2\pi RC} \tag{5.3}$$

$$\varphi = -\arctan(2\pi fRC) \tag{5.4}$$

For the purposes of this thesis whereby the interference signal of interest that will be used in the determination of the central fringe packet positions occur at an average frequency of 43.1 Hz, a low pass RC filter with a "cut-off" frequency of 100 Hz was constructed and used.

The application of this filter can be applied to two separate ways. The first approach would be to use a hardware circuit forming a first order low pass filter composed of a 100 kΩ resistor and an 0.1 μF capacitor, connected to the output of the InGaAs detector before reading the data into the Labview program via the analogue to digital unit. The second method would be to apply the filtering after the analogue to digital unit via a filtering VI within the Labview program. This approach has the advantage that the "cut-off" frequency can be easily changed to view the measurement effects for differing values. There is the additional benefit using the Labview filter in that any electrical

noise brought about by the analogue to digital unit or the connecting cabling will also be removed from the interference signal before analysis takes place.

When repeated scans of a known differential length were carried out using the differential length measurement system, incorporating the RC filtering system, the results unfortunately did not reap any benefits. This could possibly be due to the effects to the signal which are a consequence of the RC circuit. Alternatively the signal, even with the high frequency noise removed, may still contain noise jitter such that when the curve fitting process is carried out, the changes to the data point positions could still be a factor in the recovered peak position.

As has been discussed, high frequency noise within a low frequency signal can be reduced/removed with the use of a low pass RC circuit. The introduction of such a sub-system however has been show to slightly alter the initial input signal as a result of the "cut-off" frequency used, whether through reduction in the signal strength, or through phase shifts. A second approach considered as a method of reducing the effects of noise prior to data analysis is through application of the wavelet transform.

The wavelet transform is a multiresolution analysis technique for obtaining the time-frequency representation of a signal. The continuous wavelet transform (CWT), defined by equation 5.5, is computed by changing the analysis window, shifting the window in time, multiplying by the signal, and integrating over all times (7).

$$CWT_{\tau}^{\Psi}(\tau, s) = \frac{1}{\sqrt{|s|}} \int x(t) \Psi^{*}\left(\frac{t-\tau}{s}\right) dt \tag{5.5}$$

Where $x(t)$ is the input signal, τ is the translation, s is the scale, and $\Psi(t)$ is the transforming function, known as the mother wavelet, given by

$$\Psi_{\tau,s} = \frac{1}{\sqrt{s}} \Psi\left(\frac{t-\tau}{s}\right) \tag{5.6}$$

Discrete wavelet transform (DWT) coefficients are usually sampled from the CWT on a dyadic grid. Choosing parameters of translation $\tau = n.2^m$, and scale $s = 2^m$, it is possible to define the mother wavelet in DWT as

$$\Psi_{m,n}(t) = \frac{1}{\sqrt{2^m}} \Psi\left(\frac{t - n.2^m}{2^m} \right) \tag{5.7}$$

DWT analyses the signal through decomposing it into its coarse and detailed information which is accomplished by using successive high and low pass filtering operations, repeated for further decomposition of the low pass filtered signals.

The wavelet transform method can be used to produce much higher noise removal quality than conventional methods. The DWT also ensures zero-time shifts of the initial input signal, retaining the details of the original signal after the denoising procedure is carried out.

The use of the wavelet transform is applied within the Labview program after the capture of data before further analysis is performed.

Previously, as with the noise reduction technique of the low pass RC filter, the overall differential length measurements, when repeated over a period of time, did not alter with the introduction of the wavelet transform.

As with the RC circuit, the original problem seems to stem from the light source and the power loss throughout the system. It is therefore recommended that as a process of improving the overall measurement accuracy, a broadband light source with a higher output power rating could be used. Additionally, due to the optical power lost in the Fabry-Perot cavities, improvements to the light re-coupling at these locations would increase the signal strength at the output, thus improving the signal to noise ratio of the configuration.

5.5. Environmental Effects

Separation of the sensing cavities is an important aspect that was taken into consideration during the development of the overall sensor configuration. This is

largely due to the environmental effects that may have an impact on the overall determined differential length. As was discussed in section 4.1, separation distances in the order of tens of meters could result in large temperature or air pressure changes in the surrounding environment from one sensor location to the other. It is for this reason that the sensing configuration is constructed in such a way that environmental factors will not have an effect of the interconnecting fibre leads used in the tandem arrangement of the Fabry-Perot cavities, and thus disrupt the differential length of interest.

The nature of the differential length measurement system is such that effects of temperature and/or strain on the interconnecting fibre leads, from the reference Michelson interferometer to the InGaAs detector via the sensing cavities, will not cause any anomalies on the overall calculated cavity length difference due to the common optical path followed between the sensor heads. The only OPL's which have an effect on the differential length measurement are those of the two Fabry-Perot cavities.

Verification of the interconnecting fibre lead immunity to environmental factors was tested by increasing the temperature of 2 meters of connecting optical fibre lead to sensing cavity l_2 during a measurement period. The results of this are displayed in Figure 5.18.

As a means of determining if any outside surrounding factors had an influence of the measurements being recorded, the Fabry-Perot sensing cavities were placed, along with the scanning Michelson interferometer, into a temperature stabilised environment. The interconnecting leads however, were kept exposed. In reality this would not be the case due to the large temperature variations which may exist between the two sensing locations, however in order to deduce if the interconnecting leads would influence the measured length, the two Fabry-Perot cavities had to remain constant.

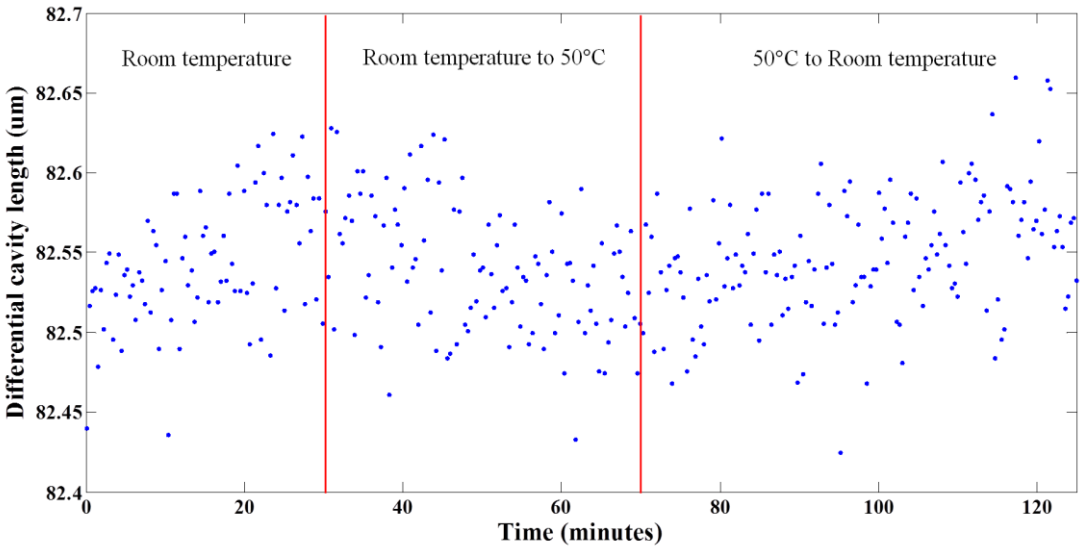

Figure 5.18: Differential length measured during increase in fibre temperature.

After 30 minutes of recording the differential length of two Fabry-Perot sensing cavities, the interconnecting fibre length was heated, via a hotplate, to a temperature around 50°C where it remained for a period of 45 minutes. The fibre length was then returned to room temperature (~ 21°C) for the remainder of the scan. Figure 5.18, which display's the period during which the fibre temperature was altered, demonstrates that no change in the recorded differential length is noticeable due to the change in the surrounding environment.

5.6. Discussion

In the previous chapter, the design of a measurement system used for determining the differential length of two Fabry-Perot cavities was discussed. Following on from the design, this chapter focussed on how the system was used in obtaining the raw data and how data analysis was carried out as a means of calculating the desired differential length of interest.

A broadband light source, centred at 1550 nm, is used as a means of interacting the Michelson interferometer with the differential lengths of the Fabry-Perot sensing cavities in order to provide locations over which a length measurement could be taken. The particular source chosen had a Gaussian type spectral profile with a -3dB bandwidth of 60.0 nm, producing interference fringes with an envelope matching that of

the source spectrum. Alternative light sources could have been used in which the bandwidth was greater and would therefore generate a narrower burst of interference fringes than that generated of this study. Issues arise in such situations however, due to the use of multiple SLED sources. Multi source broadband SLED systems may have a non-Gaussian profile with the resultant interference fringe envelope matching this. This is an issue as superimposition of fringes may occur for closely matched optical path lengths. Tailor made fibre Bragg gratings can be used in these circumstances when a near Gaussian profile is required however such a component will come at an additional cost, and is such why use of the 60.0 nm bandwidth source was continued.

A DFB laser light source at 1310 nm, with a wavelength stability of 1.3 pm, provides a reference measurement of the OPL change of the scanning interferometer. Due to the non-linearity of the piezo material expansion with the applied voltage, the resulting interference fringes provide an accurate determination as the change in optical path length between the two locations of the central fringe packet positions. When using a technique to calculate the number of interference fringes between these positions, this in turn can then be used to calculate the change in path length, and thus the differential optical path length of the two sensing micro cavities.

Noise reduction techniques through the use of low pass filtering and wavelet transforming are introduced as a solution for reduction of electrical and optical noise within the system and for improved measurement resolution. The measurement system however did not reap the benefits of these methods with the possibility that signal loss throughout the configuration has a greater effect on the recovered interference fringes. Further techniques for improvement may result in the use of a light source with a higher operating output power, or with improved re-coupling of light into the optical fibre within the Fabry-Perot cavities. These solutions will be discussed further in Chapter 7.

5.7. Conclusion

Within this chapter it has been demonstrated that the sensing configuration, described in Chapter 4 and illustrated in Figure 4.1, is a suitable procedure for the determination of the differential length of two separate Fabry-Perot cavities.

A broadband light source is utilised for determining the position at which the optical path length mismatch of a Michelson interferometer, connected to the tandem

arrangement of the Fabry-Perot cavities, is equal to the optical path length mismatch of the two sensing cavities. The broadband light source also provides a reference position when the OPL's of the Michelson interferometer arms are equal in length. These positions are found due to the interference effects observed when the OPL's are matched to within 27.02 μm ± 0.31 μm, the coherence length of the source. The coherence length was calculated using equation 3.22 with the error determined due to the variation of 0.70 nm in the measured -3dB band width.

As a means of providing accurate length change measurements of the scanning Michelson interferometer a DFB laser source is used, the interference fringes of which are monitored using a fringe counting technique for determination of the optical path length change between subsequent broadband interference fringe bursts. The use of a laser source to analyse the change in path length eliminates the uncertainty in the length change as a result of the nonlinear relationship between the piezo fibre stretcher expansion and the applied voltage.

Measured differential lengths of two Fabry-Perot cavities have been made with standard deviation of 41.00 nm. The system resolution was also calculated based on the noise effects in the system on the recovered interference fringe envelope locations, over which the differential length is determined. As a consequence of contributing noise factors a system resolution was calculated to be 27.43 nm. This value is less than that of the measurement uncertainty with a possible solution being the instability of the mounted optical fibres during the measurement process.

It was also demonstrated within this chapter that due to the configuration of the sensing system, environmental effects such as temperature and air pressure on the interconnecting optical fibre leads between the two sensing cavities do not have an influence on the measured signal. A temperature increase up to 50°C on two meters of interconnecting fibre showed no change on the measured differential length within the noise of the system.

5.7. References

1. Exalos Broadband Light Sources 2003-2014. Available from: http://www.exalos.com/broadband-light-sources/.

2. Jansz P, Richardson S, Wild G, Hinckley S. Modeling of low coherence interferometry using broadband multi-Gaussian light sources. Photonic Sensors. 2012;2(3):247-58.
3. Hahn SL. Hilbert Transforms in Signal Processing: Artech House; 1996.
4. National Instruments Corporation Peak Detector VI 2015. Available from: http://zone.ni.com/reference/en-XX/help/371361J-01/lvanls/peak_detector/.
5. Devasia S, Eleftheriou E, Moheimani SOR. A Survey of Control Issues in Nanopositioning. Control Systems Technology, IEEE Transactions on. 2007;15(5):802-23.
6. Basic Electronics Tutorials Passive Low Pass Filter 1999-2015. Available from: http://www.electronics-tutorials.ws/filter/filter_2.html.
7. Matz V, Kreidl M, Šmíd R. Signal-to-Noise Ratio Improvement based on the Discrete Wavelet Transform in Ultrasonic Defectoscopy. Acta Polytechnica. 2004;44(4):61-6.

Chapter 6: Sensor Applications

6.1. Introduction

In Chapter 1 the requirement for this research was set out for the development of an interrogation technology for measuring the differential pressure of two individual sensors at two widely separate locations. As a means of achieving this goal, a technology was designed that would measure the length of two separate Fabry-Perot cavities which act as individual pressure sensors and directly measure the difference in length of these two cavities. The difference in length is proportional to the difference in pressure. The benefit of measuring only the difference in length is that any common offset, i.e. a background pressure is eliminated from the measurement. Such a differential measurement can potentially achieve a much higher sensitivity in measuring pressure differences in the presence of a large common background pressures compared to two individual absolute pressure measurements.

From Chapter 2, in which a review of different sensing configurations was carried out, it was decided that conventional techniques, based on electrical methods, had limitations in terms of resolution over specified ranges because they measure the absolute pressure unless the pressures are 'piped' to a common differential pressure measurement head. This can cause significant deviations in the in the transmitted pressures if the piped lengths are in the order of meters.

A suitable alternative approach to these would be through the use of an optical fibre sensing configuration, in particular, an interferometric configuration. The sensing system utilises the properties of both low and high coherence interferometry to provide a solution for the differential measurement of two Fabry-Perot cavities arranged in tandem with each other.

A change in the OPL of a Fabry-Perot cavity, due to an external force acting on one of the reflective surfaces, can be monitored to calculate the pressure applied to induce such a change if the mechanical and material properties of the reflective surface are known.

This chapter considers the arrangement of a Fabry-Perot cavity using a deformable diaphragm as the reflective surface, which when applied with pressure will result in an OPL change, as a suitable sensor head configuration. The chapter investigates the

different materials which could be used for constructing a suitable sensing diaphragm and the mechanical properties of such a deformable surface for different geometries.

The chapter concludes by considering the optimised conditions and construction of a sensing diaphragm which could be integrated into the interrogation configuration for future measurements of pressure.

6.2. Sensor Configuration

In Chapter 2 during a brief introduction to pressure sensing, it was described that for many optical fibre pressure sensing configurations, a diaphragm is a common tool for pressure sensing. Such a method usually involves the formation of a Fabry-Perot cavity using the fibre end as one cavity reflective surface and the diaphragm as the secondary reflective surface, illustrated in Figure 2.1. Changes in the cavity length result from deformation of the diaphragm material due to external pressure acting upon it. This technique utilises interferometry and was the basis of the research carried out throughout this thesis.

6.2.1. Diaphragm design

Within Chapter 3, section 3.8, the theoretical characteristics of a circular deformable diaphragm were covered. This theoretical analysis reviewed the deformation properties for a given circular flat diaphragm when exposed to external pressures. From this review it was understood that the main characteristics which affect the performance of a pressure diaphragm are the thickness, radius, and material.

Design of diaphragm sensors is extremely important to achieve the required range and resolution of linear deflections. Although it is possible to calibrate nonlinear effects out of the system, hence the maximum linear pressure is not the maximum operating pressure, for simplistic reasons it is desirable to operate within the linear range. High sensitivity is achievable through a thin diaphragm capable of maximising the deflection due to the applied pressure, however, if the deflection is too large, nonlinear effects come into play (1). For that reason the maximum deflection should be small, usually no more than 30% of the material thickness (2). By controlling the diaphragm thickness it

is possible to selectively alter the sensitivity, frequency response, and burst pressure of the diaphragm.

The theory within Chapter 3 details the deformation characteristics of a flat circular diaphragm. Having been used on numerous occasions for the measurement of pressure (3, 4) it was decided that such a configuration would be used in the design of the differential measurement system. Alternative diaphragm constructions are also a possibility however. One such alternative option would be a corrugated deformable diaphragm.

Research has been carried out into the design of corrugated diaphragms (2, 5) and has demonstrated that with the introduction of corrugations into the diaphragm structure, as illustrated in Figure 6.1, the linearity of the diaphragm can be increased considerably.

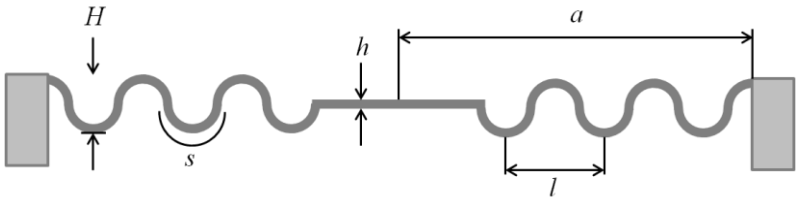

Figure 6.1: Corrugated diaphragm design.

For a corrugated diaphragm the load-deflection relation is given by

$$\frac{Pa^4}{Eh^4} = A_p\left(\frac{y}{h}\right) + B_p\left(\frac{y}{h}\right)^3 \tag{6.1}$$

Where

$$A_p = \frac{2(q+1)(q+3)}{3\left(1-\frac{\mu^2}{q^2}\right)}$$

$$B_p = 32\frac{(1-\mu^2)}{(q^2-9)}\left[\frac{1}{6}-\frac{(3-\mu)}{(q-\mu)(q+3)}\right] \tag{6.2}$$

Where q is the corrugation quality factor defined, for sinusoidal corrugations as

$$q^2 = \frac{s}{l}\left(1+1.5\left(\frac{H}{h}\right)^2\right) \tag{6.3}$$

From Figure 6.1, H is the corrugation depth, l is the corrugation spatial period, and s is the corrugation arc length.

Although there is a lot more details which have to be considered when using corrugated diaphragm, such as the design and dimensions of the corrugations, it has been demonstrated that this approach can result in greater deflection with applied pressure. Figure 6.2, taken from "The design, fabrication, and testing of corrugated silicon nitride diaphragms" by P. R. Scheeper (6), shows the difference in deflection lengths between a circular flat diaphragm and a circular corrugated diaphragm of the same material and dimensions.

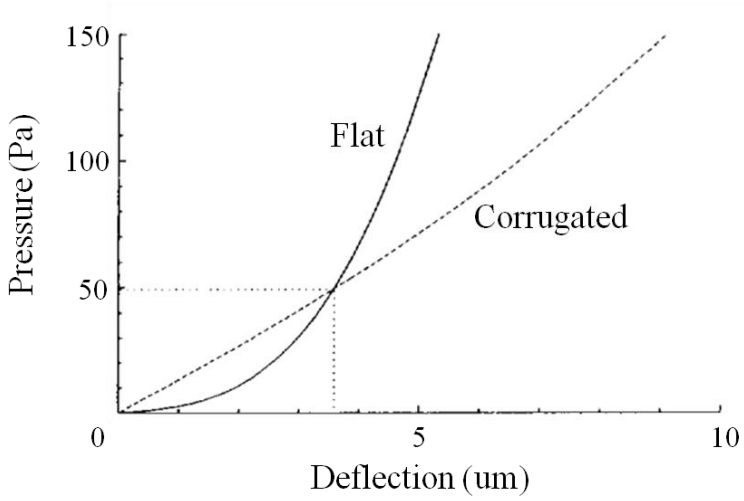

Figure 6.2: Response curves for diaphragm deflection vs. applied pressure for flat and corrugated diaphragms. (6)

Although it has been shown that with the use of a corrugated diaphragm over that of a flat diaphragm the linear range of deflection is greater for a given pressure, there are many design considerations which have to be taken into account, such as the number, depth, and spatial period of the corrugations. Each of these factors contributes to the diaphragm deflection parameters and so further investigations into this technology would have to be considered.

It is also due to the complex procedures in the formations of corrugations within a material surface that for the design configuration of the differential sensor a flat circular diaphragm will be considered. The remainder of this chapter will focus on the equations provided in Chapter 3 for the design of a suitable sensing diaphragm.

6.2.2. Diaphragm material

Optimisation of the expressions given in the Chapter 3 for the deformation properties of a flat circular diaphragm is not an easy task in order to maximise the sensing range, resolution, and resonant frequency, as conflicting requirements arise.

Before optimisation of the diaphragm dimensions are performed, it is first necessary to consider the material of which the diaphragm will consist of.

There are many different material types which could be considered for use as a deformable diaphragm. It is important however to take into consideration the material properties to determine whether said material would be suitable under the conditions to which the differential measurement system will be exposed. Polymer materials have been used in the formation of a deformable diaphragm (7). The diaphragm can be thinned down to a few microns and is thus suitable for mass production. However, for under water measurement applications, the polymer must be kept in water for a long period of time to stabilize before it can be used, due to its tendency to absorb water. Meanwhile, due to the porous cellar structure of the polymer, the diaphragm cannot be fabricated too thin and is not suitable for long term pressure measurement.

Fused silica is also a material which has been demonstrated in the use of deformable diaphragms in the measurement of pressure (4). Due to matched thermal expansion coefficients between the diaphragm and the optical fibre they have an outstanding thermal performance, with a wide range of working temperatures and temperature stability. Fused silica suffers however, when compared with metal materials, due to the relatively low maximum tensile strength. With the large operating pressure range of this research, it has been determined, due to the achievable system resolution of the measurement configuration in its current form, that the maximum operating pressure of a fused silica diaphragm would be close to the maximum operating pressure of the measurement range.

Silicon is considered as a diaphragm material due to the existing vast knowledge of the material and the ease of material machining. It also has desirable mechanical properties which are an important aspect to consider, as single crystal silicon is elastic (up to its fracture point), is lighter than aluminium, and has a modulus of elasticity similar to stainless steel. The deflection of silicon results in virtually no hysteresis and hence almost no energy dissipation (8). Metals can also be used as a diaphragm material as they exhibit high reliability however can be limited due to their high stiffness.

Table 6.1 details the material properties of silicon which will be used in calculating, using the equations provided in section 3.8, in particular equation 3.29, the required diaphragm thickness and radius which will be suitable of use in a pressure sensing system for differential measurements to achieve the goals of this research.

Density	ρ	2329	kg m^{-3}
Young's modulus	E	129.5 x 10^9	Pa
Poisson's ratio	μ	0.28	
Max tensile stress	σ_m	3400 x 10^6	Pa

Table 6.1: Material properties of silicon.

6.2.3. Diaphragm housing

In section 6.3, the equations provided in Chapter 3 of the theoretical analysis for diaphragm deformation will be used to design the optimum diaphragm configuration which would be suitable for use in the current differential measurement system to provide a differential pressure. Prior to this the final construction of a sensor head will be discussed taking into consideration the varying temperature which may occur in the surrounding sensor environment.

As was discussed in Chapter 4 it is important to consider the varying temperature of the surrounding environment between the two sensing locations due to the potentially large separation of the cavities. Table 4.1 detailed guide specifications of the sensing system which had an operating temperature range of 15 – 200 °C. In Chapter 5 it was demonstrated that due to the configuration of the overall sensor system the optical fibre downleads to the Fabry-Perot cavities from the scanning Michelson interferometer are virtually immune to changes in the surrounding environment. It is still important however to consider the effect of temperature changes at the location of the sensor heads. As previously stated, techniques for temperature monitoring are out with the scope of this research, however one approach to compensate for this varying effect would be through material design of the sensor head arrangement.

Figure 6.3 shows one such configuration of a sensor head illustrating the positions of the optical fibre and deformable diaphragm, along with the direction of applied pressure.

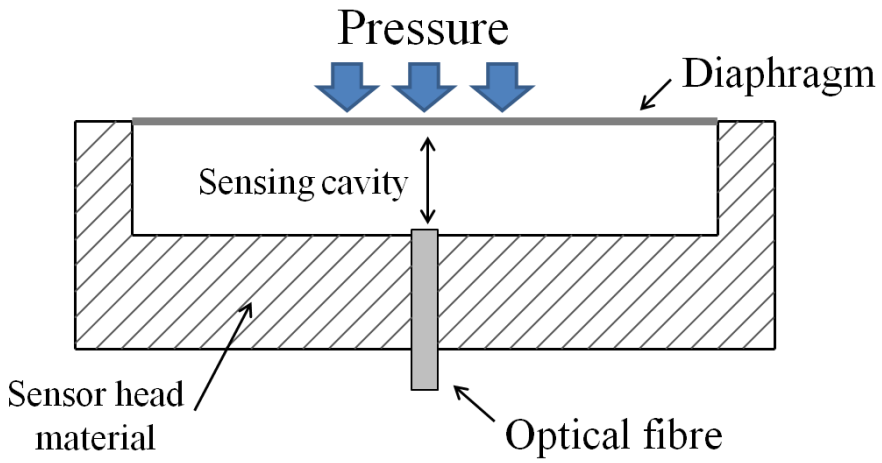

Figure 6.3: Schematic of a possible configuration for the pressure sensing head of the differential measurement system.

Through the use of a single material for housing the optical fibre along with the deformable sensing diaphragm and with knowledge of the thermal expansion coefficient of said material, temperature monitoring at the sensing location, possibly through the use of FBG's, can be used to calculate any expansion or contraction which may result from changes in the surrounding temperature. Expansion or contraction of the housing material may cause subtle changes in the cavity length which, when dealing with nanometer measurements, could disrupt the desired measurements. With knowledge of the material properties and temperature monitoring, such changes could be compensated for in both sensing locations.

6.3. Sensor Optimisation

From the previous chapter the measurement resolution by which a differential length could be determined using the optical fibre sensing configuration, illustrated and described in Chapters 4 and 5, was calculated as 27.43 nm. This calculated resolution based on the system noise in terms of the electronics and the optical light source differs from the measured uncertainty of 41 nm. As was discussed in Chapter 5 this difference could be as a result of the instability of the mounted optical fibres during the measurement process.

For application in a pressure sensing arrangement where the optical fibre will have a more stable surrounding the measurement resolution of 27.43 nm, along with the dynamic range over with pressure is to be applied, is a requirement for the determination of the diaphragm deflection for the maximum exerted pressure.

For a pressure sensing system in which a measurement resolution of 1 Pa is required over a dynamic range of 100 kPa, for measurement using the researched differential measurement configuration, a diaphragm deflection of 2.74 mm would be required.

Having determined the pressure range over which, ideally, linear measurements are to be made and the diaphragm deflection required for such measurements, the diaphragm thickness and radius can be calculated, through rearranging equation 3.29, for a silicon diaphragm using the properties detailed in table 6.1.

The thickness of a deformable diaphragm has been described in terms deflections within the linear range. It was described that in order to keep within the kept linear range, the deflection be no more than 30% of the diaphragm thickness, thus $h=y_{max}/0.3$. For the given deflection above, this would require a diaphragm thickness of 9.13 mm.

With a diaphragm thickness of 9.13 mm, the diaphragm radius for the required pressure resolution of 1 Pa can be found though rearrangement of equation 3.29. Using the length resolution of 27.43 nm as the deflection, $y(0)$, 1 Pa of the exerted pressure, P, and the material characteristic of silicon, a diaphragm radius of 0.35 m is calculated. This in turn corresponds to a burst pressure, P_m, as calculated using equation 3.30, of 4.94 MPa.

As would be expected, in order to achieve a large diaphragm deflection of 2.74 mm, due to the length resolution determined via the fibre sensing configuration, a diaphragm of large thickness and radius is required for measurements of pressure detectable within the linear range. A diaphragm of this proportion is, however, out of the question.

As it can been seen, the main issue of requiring a diaphragm of such large dimensions is a result of the differential length measurement resolution obtained for the researched sensing configuration. A measurement resolution of 27.43 nm is unfortunately too great a number and, in fact, this should ideally be a factor of ten, if not more, smaller. If a length resolution of 1 nm could be achieved such a diaphragm would only require a deflection of 100 μm for linear measurements within the specified pressure range. Using the same calculations as those used above for a 27.43 nm length resolution, the diaphragm dimensions would be reduced to a thickness of 333.33 μm and a radius of

12.91 mm. The maximum burst pressure would remain the same due to the scaling of the diaphragm dimensions. Although these dimensions are still fairly large when compared to other optical fibre sensing configurations (9), this would be a more realistic fabrication and would in fact generate a measurement system with a higher pressure resolution for the given pressure range. Such a diaphragm performance when compared to a similar sensor based on a MEMS technique (1), would again produce a greater pressure resolution over the given pressure range required.

An alternative approach in which a diaphragm with more realistic dimensions could be used, whilst keeping the current differential length measurement resolution, would be one in which the diaphragm deflection, within the measurement range, is greater than 30% of the thickness. At this point the deflection is no longer linear with applied pressure. In doing so the dimensions could be dramatically reduced from the linear region dimensions, provided the maximum burst pressure is not exceeded. This approach would however require correction data for measurements made outside of the linear region due to the lower deflection at higher pressures, illustrated in Figure 6.4.

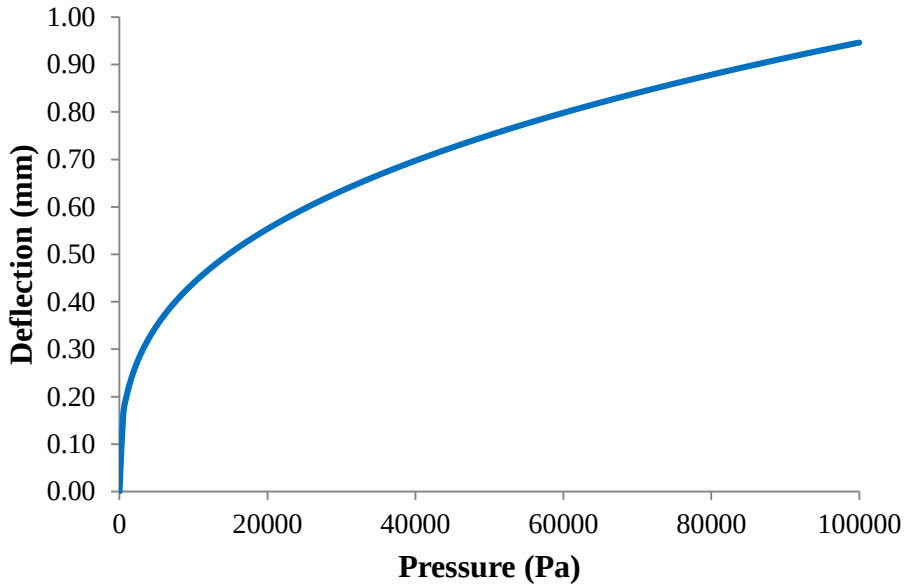

Figure 6.4: Response curve for the diaphragm deflection vs. the applied pressure.

When moving out of the linear measurement region there are consequences that need to be addressed. Outwith the linear region there is a need to measure the absolute pressure

in order to determine the local slope of the sensitivity with applied pressure, shown in Figure 6.5, due to this changing as a function of the absolute pressure. As the differential pressure is small, hence the 1 Pa resolution, the sensitivity response in the upper pressure region, 100 kPa ± 10 kPa, has changed relative to atmospheric pressure, however is still quite similar in the two different regions.

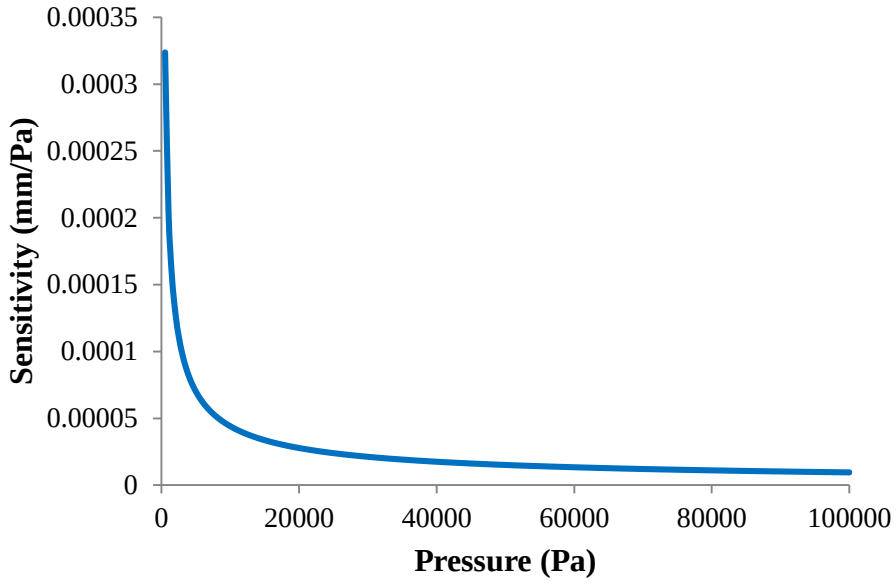

Figure 6.5: Response curve for the diaphragm sensitivity vs. the applied pressure.

At the higher pressure ranges the sensitivity is lower, and also changes in a given pressure region, 100 kPa ± 10 kPa. In this region, if the absolute pressure is known as the sum or average of both of these, the common mode deflection can be used. Although this is not linear, it would be the same in both arms due to both being in the 100 kPa pressure range.

Figures 6.4 and 6.5 show the central deflection and sensitivity of a silicon diaphragm, for applied pressures up to 100 kPa. The diaphragm dimensions in this case are 250 μm and 26.32 mm for the thickness and radius respectively, keeping the maximum applied pressure below the burst pressure of 638.93 kPa. This diaphragm, when compared to the previous thickness and radius of 9.13 mm and 0.35 m, has dimensions of a more realistic design. As a consequence of the nonlinear deflection at the central position, however, the deflection at 100 kPa is not suitable of use with the differential length

interrogation technology with the resolution of 27.43 nm. Increasing the diaphragm dimensions will subsequently increase the deflection range however this leads back to the original issue of a large diaphragm.

For applications in differential pressure measurement, the differential length interrogation system could be used with the current length resolution if alternative diaphragm characteristics are employed.

6.4. Conclusion

This chapter has described the pressure application in which the optical fibre differential length measurement system, researched throughout this thesis, could be utilised. Differential pressure measurements can provide a useful technique for the determination of liquid flow within a pipe work series for the understanding of how particular geometries change the fluid flow rate.

In order to make such pressure measurements using the constructed configuration in which length measurements are made, the characteristics of a deformable diaphragm, described in Chapter 3, have to be understood. A diaphragm, when subjected to an external force, will bend, with the maximum deflection occurring at the centre. If this deflection, in terms of length, can be measured and the properties of the diaphragm are known, the exerted pressure to cause such a deflection can be calculated.

Within this chapter the characteristic of a deformable diaphragm have been used for the determination of a suitable sensing configuration in which the differential length measurement system could be use for the determination of a differential pressure measurement. Investigation of diaphragm materials and designs was covered in the text, along with a schematic of a sensor head housing for pressure measurements.

Although out with the scope of this research, a basic solution to account for temperature changes in the surrounding environment was described. This solution is based on fabricating the sensor head at the sensing location using one single material with a known thermal expansion coefficient, within which the optical fibre and pressure sensing diaphragm will be located.

For simplicity the diaphragm deflection, within the measurement range of interest, should be kept within the linear range. This however is not a necessity as correction data can to used to counteract measurements made outside of the linear regime.

For use in the form of a pressure sensing system, where a measurement resolution of 1 Pa is required, the fibre optic differential length measurement configuration, having a differential length resolution of 27.43 nm, would require a diaphragm with a central deflection of 2.74 mm for applied pressures up to 100 kPa. In keeping the measurements within the linear range, this would require a diaphragm 9.13 mm thick with a 0.35 m radius, if constructed using Silicon material. As can be imagined, this is simply not plausible.

When verified against diaphragms of similar material properties as that which have been used in this arrangement (10), it is due to the high length resolution of the measurement system achievable, and the pressure resolution required over the large range, that such large diaphragm dimensions are necessary. It is however possible with such a design to achieve the desired measurements of the guidelines set in Chapter 4, table 4.1.

Reduction of the diaphragm dimensions to more realistic values of 250.00 μm and 26.32 mm, for the thickness and radius respectively, can be made, however this would now be operating in the nonlinear measurement range to which additional analysis would be required.

This may also not provide the required deflection necessary to measure differential lengths using the differential length sensing configuration. Alternative diaphragm designs may have to be considered such as a corrugated design.

A reduction in the differential length measurement resolution from the current value of 27.43 nm would also result in a diaphragm with smaller dimensions being fabricated in which measurements would be within the linear regime, removing the need for additional analysis. Possible methods through which the differential length resolution can be reduced will be discussed in Chapter 7.

6.5. References

1. Wang X, Li B, Russo O, Roman H, Chin K, Farmer K. Diaphragm design guidelines and an optical pressure sensor based on MEMS technique. Microelectronics Journal. 2006:50-6.

2. Di Giovanni M. Flat and Corrugated Diaphragm Design Handbook. New York: Marcel Dekker; 1982.
3. Cibula E, Pevec S, Lenardic B, Pinet E, Donlagic D. Miniature all-glass robust pressure sensor. Optics Express. 2009:5098-106.
4. Wang W, Wu N, Tian Y, Niezrecki C, Wang X. Miniature all-silica optical fiber pressure sensor with an ultrathin uniform diaphragm. Optics Express. 2010;18(9):9006-14.
5. Van Mullem CJ, Gabriel KJ, Fujita H, editors. Large deflection performance of surface micromachined corrugated diaphragms. Solid-State Sensors and Actuators, 1991 Digest of Technical Papers, TRANSDUCERS '91, 1991 International Conference on; 1991 24-27 June 1991.
6. Scheeper PR, Olthuis W, Bergveld P. The design, fabrication, and testing of corrugated silicon nitride diaphragms. Journal of Microelectromechanical Systems. 1994;3(1):36-42.
7. Cibula E, Đonlagi D. Miniature fiber-optic pressure sensor with a polymer diaphragm. Applied Optics. 2005;44(14):2736-44.
8. Hasikin K, Soin N, Ibrahim F. Modeling of a Polyimide Diaphragm for an Optical Pulse Pressure Sensor. 2009 International Conference For Technical Postgraduates (Techpos 2009). 2009:34-8.
9. MacPherson WN, Kilpatrick JM, Barton JS, Jones JDC. Miniature fiber optic pressure sensor for turbomachinery applications. Review of Scientific Instruments. 1999;70(3):1868-74.
10. Totsu K, Haga Y, Esashi M. Ultra-miniature fiber-optic pressure sensor using white light interferometry. Journal of Micromechanics and Microengineering. 2005:71-5.

Chapter 7: Conclusions and Future Work

7.1. Introduction

The work contained in this thesis was concerned with the application of fibre optics and interferometry techniques for the development of a measurement system used in the determination of the differential length of two widely separate, individual Fabry-Perot micro cavities. With the design of such a system, an application, in the form of a pressure sensor, which could utilise the measurement principles of the researched sensing configuration, was considered.

The final conclusions of the research will be offered in this chapter with an assessment and analysis of the final system provided. Finally possible improvements and various suggestions for direction of further work are noted.

7.2. Summary

The outline of the research was set in Chapter 1 to develop an interferometric interrogation technology for problems of differential length measurement, which could be applied in industrial pressure measurements. The measurement technique, based on properties of low and high coherence interferometry, would provide a differential length between two widely separate, individual locations. The interconnecting optical leads to the sensing locations would also be ideally insensitive to surrounding environmental effects.

A review of conventional sensing techniques that might provide differential measurements was carried out in Chapter 2 in order to confirm that current systems available would not provide a suitable solution to achieving the required goals of this project. Chapter 2 continued by investigating different optical fibres currently available along with possible measurement techniques that can be employed within them. Examples of optical fibre sensor systems were shown. This provided numerous measurement methods from which the most suitable and practical method was selected.

Having selected a suitable fibre optic based approach in order to meet the requirements of the measurement system, a theoretical investigation into the working components of

the system was carried on in Chapter 3. Detailed analysis of the Michelson interferometer and Fabry-Perot etalons were discussed, and how such systems can be used for optical metrology. Light sources in the form of both low and high coherent sources were detailed and the conditions under which interference effects can arise. The properties of these light sources and how each can be utilised within the sensing configuration to provide differing results were also considered. Finally in Chapter 3 the theory of deformable diaphragms for the purpose of pressure measurements was discussed.

In Chapter 4 the full differential length sensing configuration was described, with an in-depth analysis of the individual aspects that make up the system. This was followed in Chapter 5 with a discussion on the data analysis and performance of the full optical arrangement for the measurements of differential length, taking into consideration the noise within the system.

Procedures to accurately determine differential length measurements were shown in Chapter 5, along with an investigation into the effect of environmental factors acting on the optical fibre interconnecting leads between measurement locations.

Finally in Chapter 6, having reviewed the theoretical analysis of a deformable diaphragms in Chapter 3, a possible design for a final pressure sensing configuration into industrial applications was presented.

7.3. Conclusions

The purpose of the research behind this thesis was for the development of an interrogation technology which could be applied to the problem of differential length measurement which may exist in pressure measurements. The desired differential length measurement would be made between two individual sensing components at widely separate locations. An optical fibre system was developed based on the principles of interferometry. Several different light sources were utilised in the system to achieve the required measurements to determine the single measurand of a difference in length.

The differential length of two Fabry-Perot cavities, arranged in tandem, was measured using a scanning Michelson interferometer and a broadband light source. Interference

fringes where observed when the optical path length difference of the two Michelson interferometer arms were equal to the differential length of the Fabry-Perot cavities. Through monitoring the change in the optical path length of the Michelson interferometer the desired length is obtained.

Due to the system configuration and the chosen components, the output signal level of the broadband source is relatively low and as such introduces optical noise into the system. With the use of a higher output source, and through improved coupling techniques in the Fabry-Perot cavities as will be discussed in the following section, the signal strength detectable via the InGaAs photodiodes would be improved, allowing a more accurate data analysis with less influence by measurement noise.

A laser source, used to illuminate the Michelson interferometer, provides a reference measurement to which the differential length is determined, as a result of the formation of high coherent interference fringes during the optical path scanning process of the piezo fibre stretcher.

Utilising techniques such as the Hilbert transform, as a means of obtaining the broadband interference fringe envelope, a peak detector function in Labview, to determine the central locations of the interference envelope, and a fringe counting routine, as a procedure for calculating the high coherent fringes during the Michelson scan, an accurate determination of the optical length change can be found. With use of the fringe counting technique, interference fringes can be determined to within $1/1750^{th}$ of a fringe.

Using the data analysis methods employed the differential length of two Fabry-Perot cavities can be determined with a measurement resolution of 27.43 nm.

Although the designed configuration has been proven for making differential measurements, with further analysis showing that environmental factors on the fibre interconnecting leads between the sensing locations having negligible effect on the overall measurement accuracy, the recovered resolution is higher than what would have liked to have been achieved and a reduction in this would be preferred before incorporation into applications involving length measurement.

One application in which such a measurement system could be incorporated is in the use of pressure measurement. In an ideal pressure system one might wish to determine the differential pressure up to 100 kPa with a resolution of 1 Pa, something that can

prove to be difficult with current measurement techniques. Using the configured system, in which the length resolution is 27.43 nm, in order to measure up to 100 kPa a deformable diaphragm with a central deflection of 2.74 mm would be required. For this deflection, and in keeping the measurements within the linear range, a diaphragm 9.13 mm thick with a radius of 0.35 m would need to be fabricated. As it can be imagined, this is not a possible scenario.

An approach for reducing these diaphragm dimensions to more realistic dimensions of 250.00 µm and 26.32 mm for the thickness and radius respectively, would be to record measurements in the nonlinear regime. Linear measurements are ideal for simplistic means as when you move to the nonlinear regime correction data is required to compensate for the change in deflection with applied pressure. Out with the linear region there is also a need to obtain the absolute pressure in order to determine the local slope of the diaphragm sensitivity in the upper pressure regions, 100 kPa ± 10 kPa. At the higher pressure ranges the sensitivity is lower, and also changes in a given pressure region. In this region, if the absolute pressure is known as the sum or average of both of these, the common mode deflection can be used. Although this is not linear, it would be the same in both arms due to both being in the 100 kPa pressure range.

Alternatively, if it is desirable to have a functioning diaphragm in which the measurements within the pressure range of interest are linear, a means of reducing the differential length resolution of the optical fibre researched arrangement could be implemented. With a reduction in the length resolution, the diaphragm deflection and dimensions would not be required to be as high as the current value. With a length resolution reduced to 1 nm, a diaphragm for measurements of pressure up to 100 kPa would require a central deflection of only 100 µm. Such a diaphragm would not only benefit from a smaller fabrication size, 333.33 µm thickness and 12.91 mm radius, it would also have a linear deflection with applied pressure within the measurement range of interest.

It is hoped that with further improvements to the system, as will be discussed in the following section, the differential length measurement resolution, achieved using the constructed optical fibre arrangement, can be reduced, preferably by a factor of ten if not more.

7.4. Contribution of This Work Beyond the State of the Art

In Chapter 2, in which a review was carried out on current conventional and optical sensing techniques, it was clear that there existed a gap for the development of a measurement system in which differential pressure, through a means of determining a differential length, could be calculated between two independent and widely separated sensing locations. As described in the discussion carried out in section 2.6, many existing sensor configurations suffer from a lack of high resolution measurements over large pressure ranges, or in some instances, the sensing components are located at some distance from the point of interest and require tubing to carry the pressure to the sensing head. Such systems suffer from environmental factors surrounding the tubing and may result in changes in the desired pressure level.

In this thesis, research has been carried out to demonstrate a technique using low coherence interferometry in which the differential length of two Fabry-Perot cavities can be determined without knowledge of the separate cavity lengths, thus reducing the measurement uncertainty. Using a tandem arrangement of the sensing cavities and a scanning Michelson interferometer, desired high resolution measurements can be made at large pressures due to the common background pressure which both sensing locations will experience. Only small changes in the deflection of pressure sensing diaphragms are of interest.

It has also been demonstrated within this work that due to the design configuration of the overall sensing system, environmental effects such as changes in temperature and pressure surrounding the downlead optical fibre will not influence the measured differential. This is as a result of the common optical path length between the two sensor locations.

7.5. Future Work

Upon completion of this experimental study several areas of further work can be identified. The main requirement of the current interrogation system is to improve the output power measureable as a means of improving the signal to noise ratio. Further work would be with the implementation of the system into a pipe work system for measurements of differential pressure.

7.5.1. Broadband light source

Further to a change in optical power of the broadband light source, a source with a larger spectral profile would also add improvements to the system. Due to the coherence length of the current source there are limitations regarding the initial optical path lengths of the tandem Fabry-Perot sensing cavities. A broader spectral profile would provide a shorter coherence length over which interference effects take place. This would therefore allow for shorter initial cavity lengths, which in turn would improve the fibre coupling at the Fabry-Perot interface. A broader spectral profile would also reduce the width of the interference fringe packets resulting from the interactions of the Michelson interferometer and the sensing cavities, making peak detection a simpler procedure. The source profile however would ideally have to be a uniform Gaussian shape. A non-consistent envelope profile may create later problems during the data analysis procedures (1).

The use of a light source with an increased spectral width raises the question over the operating bandwidths of the optical components within the interrogation system. With component bandwidths ranging from 20 nm for the WDM's to 40 nm of the 4-port optical circulator, it is important to determine whether or not they would be suitable for use with a high band width spectral light source and the implications involved.

7.5.2. Michelson interferometer

Possible changes in the probing Michelson interferometer would include the substitution of the current piezo fibre stretcher with one of a larger diameter. With the current piezo tube diameter of 38 mm, large numbers of fibre turns could be resulting in signal losses due to bend effects, particularly at 1550 nm wavelengths. At this wavelength attenuation around a 50 mm tube is ≤ 0.10 dB for 100 turns, and even greater at ≤ 0.50 dB around a tube 32 mm in diameter (2). With the introduction of a piezo tube with a diameter greater than 60 mm bend losses would be negligible. The use of a fibre stretcher with a thicker piezo material would also allow for a greater voltage application, resulting in further expansion and the advantage of using shorter fibre lengths

As a consequence of the current fibre length of the Michelson interferometer arms and the large number of coils around the piezo fibre stretcher, birefringence is introduced

into the system which has to be altered using polarisation controllers. The polarisation controllers have a limited effect however, and changes in the polarisation can arise during expansion of the fibre length. With shorter interferometer arm lengths, polarisation maintaining fibre could be introduced to maintain the polarisation state of the light during the expansion process.

7.5.3. Fabry-Perot cavities

Fibre coupling of light at the Fabry-Perot cavity interface remains one of the leading sources of signal loss within the system. This could be improved through shorter cavity lengths. Alternatively, the addition of a collimating lens (GRIN lens) on the fibre end would improve the coupling ratio of the light. This approach was considered and tested, as mentioned in section 4.2.2, however as a result of the GRIN lens structure additional interference effects were observed which had an impact on the interference fringes of interest. Further investigations into this could be carried out with different lenses, for example micro lenses, being used or collimation techniques in the form of modifying the end shape of the fibre.

7.5.4. Improved data analysis

The current measurement resolution could also be improved through an averaging process of the measured differential length. Recording an average of the differential length under investigation could result in a reduction in the resolution. This however would only be a possibility if the data processing rate was to increase. An improvement in data analysis could increase the recorded number of length measurements, providing additional sampling data at a greater rate. This can be achieved through the use of data processing cards or even graphics cards with increased sampling rates compared to the current situation.

7.5.5. Pressure sensing measurement

As a possible application of the constructed interrogation system in the measurement of differential pressure, future measurements could be made using deformable diaphragms

as the reflecting surface of the Fabry-Perot cavities, with the possibility of performing measurements when exposed to a liquid pressure.

Having determined the design parameters of a sensing diaphragm capable of measuring differential pressures, utilising the researched length measurement procedure, up to 100 kPa, fabrication of such a diaphragm could be made. With the construction of a sensor head containing the aforementioned sensing diaphragm, a known pressure in the form of liquid or gas could be exerted to determine whether through measurement of the differential length, the applied pressure could be calculated.

Further investigation into suitable diaphragm designs could be made to find a solution to reducing the current diaphragm dimensions based on the measurement capability of the differential length measurement system.

7.6. References

1. Jansz P, Richardson S, Wild G, Hinckley S. Modeling of low coherence interferometry using broadband multi-Gaussian light sources. Photonic Sensors. 2012;2(3):247-58.
2. Incorporated C. Corning SMF 28e Optical Fiber Product Information. In: Incorporated C, editor. 2014.